

Somatic cell-derived extracellular vesicles and phenotypic outcomes in the next generation

Doctoral thesis

to obtain a doctorate (PhD)

from the Faculty of Medicine

of the University of Bonn

Emma Louise Salt

from Darmstadt, Germany

2023

Written with authorization of the Faculty of Medicine of the University of Bonn

First reviewer: Priv.-Doz. Dr. Dan Ehninger

Second reviewer: Prof. Dr. Alexander Pfeifer

Day of oral examination: 05.05.2023

From the German Centre for Neurodegenerative Diseases (DZNE e.V.)

Directors: Prof. Pierluigi Nicotera, MD PhD (Scientific Director and Chairman of the Executive Board) and Dr. Sabine Helling-Moegen, LL.M. (Administrative Director)

Table of Contents

List of abbreviations	7
1. Introduction	9
1.1 Soma to germline communication challenges the ‘Weismann Barrier’	9
1.2 Paternal physiological and psychological conditions lead to phenotypic changes in the next generations	9
1.2.1 Evidence of paternal effects from human cohort studies	9
1.2.2 Evidence of paternal effects from mammalian models	10
1.2.3 Evidence of paternal effects from <i>Drosophila melanogaster</i>	11
1.2.4 Potential mechanisms causing paternal intergenerational effects	12
1.3 Extracellular vesicles as intercellular communicators in health and disease	13
1.4 Extracellular vesicles released from somatic cells of the male reproductive tract are essential for sperm maturation	15
1.5 Study purpose	18
2. Materials and Methods	19
2.1 Analysing candidate mouse models with decreased EVs within epididymal fluid	19
2.1.1 Mouse lines	19
2.1.2 Isolation of EVs from mouse epididymal fluid using ultracentrifugation	20
2.1.3 Nanoparticle tracking analysis of UC-EVs	20
2.2 Analysis of protein components of UC isolated epididymal EVs	21
2.2.1 Protein extraction	21
2.2.2 Western Blot	21
2.2.3 Mass spectrometry analysis of UC isolated epididymal EVs	22
2.3 Analysis of RNA content within UC isolated epididymal EVs	23

2.3.1	RNase pre-treatment and RNA extraction from UC isolated epididymal EVs	23
2.3.2	Total RNA sequencing from UC isolated epididymal EVs	23
2.4	Analysis of <i>Drosophila Melanogaster</i> model system of inhibited secretion of EVs from SCs within the AG and their offspring under paternal dietary interventions	24
2.4.1	Establishment of a <i>Drosophila Melanogaster</i> model system with decreased secretion of EVs from SCs within AG	24
2.4.2	Imaging of the AG within the male <i>Drosophila melanogaster</i> reproductive tract	26
2.4.3	Quantification of CD63-GFP puncta within the <i>Drosophila melanogaster</i> AG lumen	26
2.4.4	Food preparation and dietary exposures of male F0	27
2.4.5	F1 Generation	27
2.4.6	Fecundity analysis	27
2.5	Metabolic analysis of <i>Drosophila Melanogaster</i> F0 models and their F1 offspring	28
2.5.1	Body weight measurement of male F0 flies and their F1 offspring	28
2.5.2	Triglyceride measurement of male F0 flies and their F1 offspring	28
2.5.3	Lifespan analysis of male F0 and F1 offspring	29
2.5.4	RNA isolation and mRNA sequencing of F1 offspring	29
2.6	Gene ontology analysis	30
2.7	Statistical analysis	30
2.8	Reagents and consumables	30
3.	Results	33
3.1	Evaluation of candidate mouse lines as <i>in vivo</i> loss of function models for EVs secreted by the epididymis into the epididymal fluid	33

3.1.1	Characterisation of EVs isolated from epididymal fluid using ultracentrifugation	33
3.1.2	NTA-based size characterisation of epididymis-derived UC-EVs from mouse lines carrying mutations within the EV biogenesis or secretion pathway	36
3.1.3	Characterisation of epididymis-derived UC-EV RNA content of the candidate mouse lines carrying mutations within the EV biogenesis or secretion pathway	38
3.2	Establishment of an <i>in vivo</i> loss of function model for EVs secreted by somatic cells within the male reproductive tract in <i>Drosophila melanogaster</i>	40
3.2.1	<i>Drosophila melanogaster</i> lines expressing RNAs in the secondary cells of the accessory gland under <i>dve-Gal4</i> control	40
3.2.2	Body composition and fecundity analysis of male <i>Drosophila melanogaster</i> lines expressing RNAs under <i>dve-Gal4</i> control and exposed to dietary interventions	43
3.3	<i>In vivo</i> analysis of the impact of EVs secreted by somatic cells of the reproductive tract on offspring phenotypic outcome in <i>Drosophila melanogaster</i>	46
3.3.1	Body composition analysis of F1 offspring derived from F0 male <i>Drosophila melanogaster</i> expressing RNAi under <i>dve-Gal4</i> control exposed to dietary interventions	46
3.3.2	Lifespan analysis of F1 offspring from male F0 expressing RNAi under <i>dve-Gal4</i> control exposed to dietary interventions	50
3.3.3	Gene expression analysis of young and older adult F1 offspring from male F0 expressing <i>Hrs-RNAi</i> under <i>dve-Gal4</i> control	52

3.3.4	Gene expression analysis of older adult male F1 offspring from male F0 expressing <i>Rab11-RNAi</i> under <i>dve-Gal4</i> control exposed to HSD and HFD	55
4.	Discussion	58
4.1	Generation of an <i>in vivo</i> mouse model with inhibited secretion of EVs from the somatic cells of the male reproductive tract	59
4.1.1	Establishment of the EV isolation method using ultracentrifugation	60
4.1.2	Characterisation of three candidate transgenic mouse lines as <i>in vivo</i> models with inhibited secretion of EVs from the epididymis	61
4.2	Investigation of the impact of EVs secreted by somatic cells of the male reproductive tract on the phenotypic outcome of the next generation in <i>Drosophila melanogaster</i>	63
4.2.1	CD63-GFP is used as a marker for EVs secreted by SCs in the <i>Drosophila melanogaster</i> AG lumen	64
4.2.2	F0 body composition and fecundity are not changed by the expression of RNAi lines under <i>dve-Gal4</i> control, but by dietary exposures	67
4.2.3	Sex-specific phenotypic changes are observed in the offspring from male flies expressing RNAis under <i>dve-Gal4</i> control exposed to dietary interventions	68
4.3	Conclusion	73
5.	Abstract	74
6.	List of figures	75
7.	List of tables	76
8.	References	77

List of abbreviations

AG	Accessory gland
ANOVA	Analysis Of Variance
DAPI	4',6-diamidino-2-phenylindole
DEG	Differentially expressed genes
DTT	Dithiothreitol
EV	Extracellular vesicle
FDR	False discovery rate
HEPES	Hydroxyethyl piperazineethanesulfonic acid
HFD	High fat diet
HSD	High sugar diet
KO	Knockout
MVB	Multivesicular bodies
NaCl	Sodium chloride
ND	Normal diet
NTA	Nanoparticle tracking analysis
PBS	Phosphate buffered saline
PBST	Phosphate-Buffered Saline/Tween
PFA	Paraformaldehyd
Rab27DKO	Rab27a ash/ash; Rab27b -/-
Rab35-control	Rab35 fl/+ ; Cdh16-cre -/-
Rab35-het	Rab35 fl/+ ; Cdh16-cre -/+
RNA	Ribonucleic acid
RNAi	RNA interference
SCs	Secondary cells
SD	Standard deviation
SDS	Sodium dodecyl sulfate

TAG	Triglyceride
TEMED	Tetramethylethylenediamine
UC	Ultracentrifugation
UC-EV	Epididymal EVs isolated by UC
WT	Wildtype

1. Introduction

1.1 Soma to germline communication challenges the 'Weismann Barrier'

With the present awareness that our diet, lifestyle choices, physiological and psychological state have an impact on our health, the question whether our choices and experiences affect our children and if so, what those molecular mechanisms are, remains unclear. Since the first theories of inheritance by scientists such as Charles Darwin (Darwin, 1859), not our life experiences but simply natural selection by our environment have been considered the impacting factor on our children. In accordance with the hypothesis of the 'Weismann barrier' (Weismann, 1893), no heritable information can be passed on from somatic cells to the germ cells, meaning that the phenotypic fate of our descendants comes from the luck of the Mendelian genetic draw given to us by our ancestors. With accumulating research on human pathologies and their risk factors, the once discarded Lamarckian theory of the inheritance of acquired characteristics, suggesting that experiences during our lifetime have an effect on our descendants, needs to be investigated more closely. These changes to the next generation due to parental exposure are defined as 'intergenerational effects' (or 'transgenerational effects', if they pass onto multiple generations). Currently, societies' focus is mostly on the mother's impact on the developmental health of her child, by for example her age, lifestyle choices and physical and mental health at conception, *in utero* or lactation periods, whilst paternal contribution is mainly disregarded. However, there is a growing body of evidence that a father's experiences, choices and health can lead to changes in the phenotypic outcomes of his offspring (Crean and Bonduriansky, 2014).

1.2 Paternal physiological and psychological conditions lead to phenotypic changes in the next generations

1.2.1 Evidence of paternal effects from human cohort studies

In humans, multiple studies have shown that (grand-) paternal nutrition at various time points in life have an effect on their descendants (Dimofski et al., 2021). From datasets gathered from the historical events such as 'Dutch Winter' in 1944, the Swedish village Överkalix and other cohort studies, variable food intake *in utero* or pre-puberty can lead to increased risk of obesity, diabetes, cardiovascular disorders and cancer with an

overall decreased lifespan in the next generations (Kaati et al., 2002, Pembrey et al., 2006, Vågerö et al., 2018, Veenendaal et al., 2013). Other paternal factors such as diabetes, smoking, age, stress and trauma have been shown to increase the risk of obesity, metabolic and neuropsychiatric disorders in the next generation (Dashorst et al., 2019, Denomme et al., 2020, Gao et al., 2021, Golding et al., 2022, Kanmiki et al., 2022, Kawai et al., 2018, Kong et al., 2021, Merrill et al., 2021, Polga et al., 2022). While of significant importance, within human studies factors such as time point of paternal exposures, genetic diversity, environmental changes, nurture and grooming cannot always be controlled for. With animal models, paternal intergenerational effects and their mechanisms can be studied in more standardised conditions, controlling for most external and internal variables.

1.2.2 Evidence of paternal effects from mammalian models

Rodent models replicate many of the findings from human data in paternal dietary intervention studies (Dimofski et al., 2021). For example, the offspring of male rodents exposed to a Western diet, containing a high sugar and high fat content, show many phenotypic changes ranging from increased body weight, altered gut microbiome and behavioural changes (Bodden et al., 2022), as well as changes in glucose and insulin response in rats (César et al., 2022) and increased rates of obesity and risk of metabolic diseases in mice (Grandjean et al., 2015, Raad et al., 2021). A paternal high fat diet (HFD) leads to various intergenerational effects depending on the study and diet regimes, ranging from increased susceptibility to cancer (da Cruz et al., 2019), impaired choline metabolism and decreased sperm counts in their grandsons (Crisóstomo et al., 2022). Similar experiments describe a susceptibility to developing obesity and diabetes (Huypens et al., 2016) with an impaired insulin secretion, insulin resistance and glucose tolerance in the offspring of HFD exposed mice (Fullston et al., 2015, Ng et al., 2010). In contrast, one study found no changes to body weight of the F1 from paternal HFD in mice, but a cognitive impairment instead (Zhou et al., 2018). Changes to paternal protein intake also cause metabolic changes in the next generation, including positive changes to the gut microbiome, reduced fat mass and improved insulin sensitivity compared to HFD under paternal high protein diet and changes to cholesterol and lipid metabolism under low protein diet (Carone et al., 2010, Chleilat et al., 2021). Additionally, offspring

from male mice given a high methyl diet show decreased cognitive function in hippocampus-dependent learning and memory (Ryan et al., 2018).

Other non-dietary factors also show intergenerational effects. For example, old age of male mice leads to a reduced lifespan in their offspring (Xie et al., 2018), while paternal exercise has been shown to have protective effects on their offspring if exposed to HFD (de Sousa Neto et al., 2020, Salomão et al., 2021). Experiencing environmental extremes such as cold can increase the formation of brown fat and neurogenesis leading to improved metabolic health in the next generation (Sun et al., 2018). Psychological stressors such as fear and trauma on the fathers cause altered metabolism and behaviours in their offspring. These behaviours range from altered exploration, stress response and sensitivity to paternally exposed odours (Dias and Ressler, 2013, Dietz et al., 2011, Gapp et al., 2014, Morgan and Bale, 2011, Rodgers et al., 2013, Zheng et al., 2021), stemming for instance from altered functional connectivity and signalling in the offspring's brain (Bohacek et al., 2015, Bohacek and Mansuy, 2015, Razoux et al., 2017).

1.2.3 Evidence of paternal effects from *Drosophila melanogaster*

Rodents, such as mice or rats, are not the only model organism used in intergenerational studies. Invertebrate species such as *Drosophila melanogaster* are a useful model system because of the fly's shortness of lifespan (~60 days for males and ~80 days for females), short reproductive cycle (10 days from egg to full fly adult) and most importantly ~75 % of genes related to human diseases have orthologues in the fly (Eickelberg et al., 2022). For this reason, *Drosophila melanogaster* is commonly used in the research fields of developmental biology, genetics and medicine, for example in the study of metabolic diseases (reviewed by Chatterjee and Perrimon, 2021, Eickelberg et al., 2022, Gálíková and Klepsatel, 2018, Gray et al., 2021, Musselman and Kühnlein, 2018). Under dietary extremes such as HFD or high sugar diets (HSD), flies experience diverse impacts on their health outcome similar to humans, for example their body weight, fat mass (assessed primarily with the triglyceride (TAG) content), lifespan and reproductive capacity (Eickelberg et al., 2022, Musselman et al., 2011).

In the last decade, paternal intergenerational studies carried out in *Drosophila melanogaster* have reflected the phenotypic patterns seen in humans and rodent models

(Camilleri-Carter et al., 2019). Paternal HFD, consisting commonly of different coconut oil concentrations, has been shown to increase body weight, TAG content and lead to cardiomyopathy in the next generation (Dew-Budd et al., 2016, Guida et al., 2019). As sugar is a more natural food source than fat in the diet of a fly, more studies have been carried out investigating paternal HSD with varying sugar amounts and exposure time points. Öst et al. (2014) demonstrated that the paternal intake of a diet containing 30 % sucrose, leads to an increase in TAG content, body weight, lipid droplet sizes and food intake in male offspring if exposed to an obesogenic diet, with no changes to their glucose or trehalose amounts (Öst et al., 2014). Other studies using other dietary regimes and high sugar concentrations have shown decreased amounts of TAG or only increased amounts in male offspring in one generation (Emborski and Mikheyev, 2019, Teltumbade et al., 2020). Similar to mice, high protein intake in *Drosophila melanogaster* fathers leads to advantages in the next generation with altered genes involved in the immune response, metabolism and reproduction (Zajitschek et al., 2017). Other non-dietary factors, such as stress and environment have also been shown to alter the offspring's metabolism and behaviours (Dasgupta et al., 2019, Seong et al., 2020).

It is important to note here that the study of paternal effects is highly complex, not only due to the diversity and range of exposures in multiple animal models, but also as similarly examined paternal exposures do not result in exactly the same changes in the offspring (Emborski and Mikheyev, 2019, Teltumbade et al., 2020) or the phenotypic outcomes are sex-specific in the next generation (Dew-Budd et al., 2016, Emborski and Mikheyev, 2019, Gong et al., 2021, Huypens et al., 2016, Ng et al., 2010, Pembrey et al., 2006, Vågerö et al., 2018). Furthermore, factors such as at what time point in a father's life and for how long exposures take place need to be considered (Fennell et al., 2020, Schellong et al., 2020).

1.2.4 Potential mechanisms causing paternal intergenerational effects

While the phenotypic changes, their duration and effect size on the next generation vary from study to study, many papers have identified a range of mechanisms, including epigenetic changes to the sperm that contribute to the intergenerational effects (Champroux et al., 2018, Fitz-James and Cavalli, 2022, Ghai and Kader, 2022). These epigenetic changes consist of DNA methylation changes, histone modifications,

chromatin remodelling or varying non-coding RNA species, depending on the focus of the study, and correlate with the phenotypic outcomes of F1 (Champroux et al., 2018, Fitz-James and Cavalli, 2022, Ghai and Kader, 2022). This is of interest as sperm is transcriptionally inactive, with highly compacted chromatin and with most DNA methylation erased during meiotic division (Teves and Roldan, 2022). Notably, the sperm non-coding RNA content has been shown to dynamically change throughout a father's experience. A study by Nätt et al. (2019) demonstrated that just 1 week of high sugar diet in humans changes the sperm RNA profile by upregulating tRNA-derived small RNAs (tsRNAs). Many studies have shown that in fact just the non-coding RNA (for example miRNA and tsRNA) of sperm from male mice exposed to either chronic stress or a HFD are sufficient to induce the metabolic and behavioural changes in the next generation (Chen et al., 2016, Gapp et al., 2014, Grandjean et al., 2015, Rodgers et al., 2015, Zhang et al., 2018). The mechanism how paternal physiological or environmental conditions overcome the 'Weismann barrier' (Weismann, 1893) and how these sperm epigenetic changes occur remains to be elucidated. One recognised hypothesis is that sperm gains information of the paternal condition from extracellular vesicles (EVs) secreted by somatic cells (Conine and Rando, 2022, Eaton et al., 2015, Smythies et al., 2014).

1.3 Extracellular vesicles as intercellular communicators in health and disease

EVs are small membrane bound particles that are secreted from nearly every cell and found in all biological fluids, such as blood, cerebral spinal fluid, urine, breastmilk and seminal fluid (Kalluri and LeBleu, 2020, Kalra et al., 2016, Maas et al., 2017). They are currently classified into three main categories, based on their size and biogenesis pathways: exosomes, microvesicles and apoptotic bodies. Exosomes are the smallest group with a diameter of 30 - 150 nm and are generated through the formation of intracellular multivesicular bodies (MVB) containing intraluminal vesicles (ILVs), which are later released by exocytosis. Microvesicles are 150 - 500 nm in diameter and are released directly through ectocytosis (budding off the plasma membrane), while apoptotic bodies are the largest category (500 – 5000 nm in diameter) and are released when the cell undergoes apoptosis (Colombo et al., 2013, Colombo et al., 2014).

Currently, the literature describes many different biogenesis and secretion pathways for EVs involving a complex and diverse array of proteins, such as Ras-related GTPase (e.g. RAB11) and endosomal sorting complexes required for transport (ESCRT) proteins such as HRS; tetraspanins (e.g. CD63, CD9), as well as other lipids and molecules that are cell type and organism dependent (Blanc and Vidal, 2018, Colombo et al., 2013, Colombo et al., 2014, Kalluri and LeBleu, 2020, Kalra et al., 2016). EVs carry various cargos including DNA, proteins and various RNA species. Many mechanisms of how this cargo is loaded into EVs have been described in the literature (Chen et al., 2021, Villarroya-Beltri et al., 2014), with some reporting that cargo such as some RNAs can be loaded specifically into EVs under various mechanisms such as the binding and later loading of miRNA carrying a specific sequence known as the EXOmotif into exosomes by ribonucleoprotein A2B1 (hnRNPA2B1) (Garcia-Martin et al., 2022, Janas et al., 2015, Ragusa et al., 2017, Villarroya-Beltri et al., 2013). Based on current consensus in the research field, EVs function as messengers between cells, even at long distances, as these small vesicles once secreted by one cell can be picked up by another and cause physiological changes in the accepting cell (Alvarez-Erviti et al., 2011, Maas et al., 2017, Meldolesi, 2018, Raposo and Stahl, 2019). These changes depend on what the EV cargo is or what components the EVs are made of (Kalluri and LeBleu, 2020, Valadi et al., 2007). Therefore, EVs have been shown to play a role in physiological beneficial processes like wound healing/regeneration (Lin et al., 2022, Ma et al., 2022, Sahoo and Losordo, 2014). Due to their ability to be released by one cell and be picked up by another, their roles in pathologies such as cancer (Becker et al., 2016), obesity (Brandao et al., 2022) and neurodegeneration (Busatto et al., 2021, Kalluri and LeBleu, 2020, Meldolesi, 2021, Rastogi et al., 2021) have been becoming increasingly evident. This has made using EVs as a diagnostic marker for diseases like stroke (Qi et al., 2021) and cancer (Beylerli et al., 2022) become a topic of interest for researchers. EVs biogenesis, secretion and function are studied in nearly all model systems using a variety of methods, including rodent models, cell culture models and even invertebrates such as *Drosophila melanogaster* (Beckett et al., 2013, Beer and Wehman, 2017, Fan et al., 2020, Gross et al., 2012, van Niel and Théry, 2020). With the multitude of bodily fluids, cell types and model organisms currently used in the study of EVs, heterogeneity and complexity are prevalent in this field of research. Attempts to standardise the field, at

least in terms of isolation and analytical methods, are being made by guidelines set from the International Society of Extracellular Vesicles (Théry et al., 2018). These include the minimum characterisation steps required to identify and describe EVs from a given biological cells source, such as characterisation of the EV size and protein composition (Théry et al., 2018).

1.4 Extracellular vesicles released from somatic cells of the male reproductive tract are essential for sperm maturation

When discussing the mechanisms of how epigenetic changes are transmitted to sperm, EVs are good candidates due to their evident function as a messenger between cells (as discussed above). The previously mentioned 'Weismann barrier' is only a theoretical barrier (Cornwall, 2009, Eaton et al., 2015) as no structure separates germ cells from the surrounding somatic cells throughout their production, maturation and transit. These somatic cells of the reproductive tract are hypothesised to release EVs with specific cargo (i.e. small non-coding RNA species) that fuse with sperm causing phenotypic changes to the offspring.

Within the male reproductive tract, spermatogenesis takes place in the testis. In mammals, immature sperm then travels through a tissue known as the epididymis for 2 - 4 days in humans and 10 - 14 days in mice to reach the vas deference (Cornwall, 2009). The epididymis is segmented into different regions: caput (head), corpus (body) and cauda (tail). During its travel through the epididymis, sperm maturation takes place with sperm gaining its full functionality and motility, with both its protein and RNA composition changing along the way (Cornwall, 2009).

EVs secreted from different tissues within the reproductive tract have been found in seminal and epididymal fluid (reviewed by Simon et al., 2018, Sullivan and Saez, 2013). They are differentiated by their source cell, with EVs secreted from the prostate (named prostatasomes) found mostly in the seminal fluid and EVs secreted from the epithelium of the epididymis (named epididymosomes) identified in the epididymal fluid (Simon et al., 2018, Sullivan and Saez, 2013). Epididymosomes are very heterogeneous in their protein components and contain known EV proteins, such as CD9 and Flotillin-1 (FLOT1) (Frenette et al., 2006, Paul et al., 2021, Sullivan, 2015). The different epididymal regions produce different small RNAs profiles packaged in EVs (Belleannée

et al., 2013, Nixon et al., 2019) that can also fuse and deliver their RNA cargo to other downstream epididymal segments (Belleannée et al., 2013).

Both human and animal studies have investigated the role of EVs from somatic cells in regard to post-testicular sperm maturation (Machtinger et al., 2016). *In vitro* and *ex vivo* co-incubation studies have shown that epididymosomes can firstly fuse with sperm (Al-Dossary et al., 2015, Zhou et al., 2019) and secondly can transmit various proteins that are essential for sperm functionality in cattle and mice, such as ADAM7 and SPAM1, (Frenette et al., 2006, Griffiths et al., 2008, Martin-DeLeon, 2015, Nixon et al., 2019, Oh et al., 2009, Park et al., 2011, Schwarz et al., 2013, Suryawanshi et al., 2012) and small non-coding RNA species (Reilly et al., 2016, Sharma et al., 2018). During its epididymal transit, the small RNA profile of sperm changes and correlates with that of the different segments of the mouse epididymal tissue (Nixon et al., 2019, Nixon et al., 2015, Sharma et al., 2016, Twenter et al., 2020). Furthermore, EVs released by the epididymal epithelium have been shown to carry a cargo of small RNA species (e.g. tRNA fragments) that match the RNA species gained by sperm (Nixon et al., 2019, Reilly et al., 2016, Sharma et al., 2016, Trigg et al., 2021). Foot et al. (2021) demonstrated in an *in vivo* study using *Arrdc4*^{-/-} mice, that if EVs are not released by the epididymis, sperm maturation does not take place. Other evidence of sperm and EVs interacting is shown in the *in vivo* study by Sharma et al. (2018), where a traceable RNA was expressed in the cauda epididymis and later found in the sperm.

While mammalian models dominate the literature, EVs within the reproductive tract have also been studied in *Drosophila melanogaster*. Spermatogenesis takes place in the testes similar to mammals. While a structure equivalent to the epididymis does not exist, the male fly has an organ named the accessory gland (AG), which is similar to the male prostate in that it produces most of the seminal fluid and seminal fluid proteins (SFPs) essential for sperm health (Beer and Wehman, 2017). At the tip of the AG, approximately 40 cells named secondary cells (SCs) produce a specific set of SFPs, including some required for sperm-binding and female post mating behaviour (Gligorov et al., 2013, Minami et al., 2012, Sitnik et al., 2016). Corrigan et al. (2014) labelled EVs by expressing CD63-GFP in SCs and showed that BMP-signalling drives EV secretion in SCs. These EVs are released into the AG lumen and, upon mating, are transported to the female reproductive tract, where they interact with sperm (Corrigan et al., 2014).

Notably, the inhibition of known EV biogenesis pathways using RNAi (e.g. *Hrs-RNAi*) leads to a decreased secretion of EVs labelled with CD63-GFP into the AG lumen (Corrigan et al., 2014). Additionally, this depletion of EVs from SCs causes no changes to their fecundity, but an increased remating behaviour in their female partners (Corrigan et al., 2014). The suppression of the BMP pathway and hence, the inhibited release of products (including EVs) from SCs have been shown to disrupt sperm storage in females and change the seminal fluid proteome composition (Hopkins et al., 2019).

The fact that EVs from somatic cells are essential for sperm maturation is evident from the growing amount of published research, but what roles EVs play on the offspring phenotypic outcome still remains to be elucidated. While paternal exposures such as stress lead to changes in the content of EVs secreted by the epididymis in mice (Alshanbayeva et al., 2021), there is currently only one study that has investigated EVs from somatic cells as the mediators of phenotypic changes in the offspring (Chan et al., 2020). Chan et al. (2020) collected EVs from mouse distal caput epididymal epithelial (DC2) cells after treatment with corticosterone. These EVs were incubated with caput epididymal sperm, which produced offspring with altered neurodevelopment and adult stress reactivity (Chan et al., 2020).

It is important to emphasise that the data cited above is mostly from *in vitro* and only a few *in vivo* experiments, meaning that concluding EVs as a mediator of intergenerational effects is currently not possible. To address the question, whether EVs released from somatic cell sources within the male reproductive tract lead to changes in the phenotypic outcome of the next generation, *in vivo* studies need to be carried out.

1.5 Study purpose

The purpose of this thesis is to establish an *in vivo* model system with an inhibited secretion of EVs from somatic cells within the male reproductive tract. With this model, we aim to investigate the involvement of EVs in the phenotypic outcome of the next generation. Our approach is to generate a model in mice and in *Drosophila melanogaster*, by inhibiting the EV biogenesis in epithelial cells of the epididymis and SCs of the AG, respectively. These models will be exposed to paternal interventions and transcriptomics and phenotypic analyses will be carried out on their offspring. With this investigation, we will address the following questions:

1. Does the inhibited secretion of EVs from a somatic cell source of the reproductive tract lead to changes in the offspring's phenotypic outcome?
2. After paternal dietary exposure, are paternal intergenerational effects mediated by somatic cell-derived EVs?

2. Materials and Methods

2.1 Analysing candidate mouse models with decreased EVs within epididymal fluid

2.1.1 Mouse lines

All mice were housed on a 12 h light/dark cycle with ad libitum food and water access under pathogen-free conditions. The local and federal animal welfare regulations were followed. To identify a mammalian *in vivo* model with decreased number of EVs within the epididymal fluid, three transgenic mouse lines with mutations in genes involved in the biogenesis or secretion pathway of EVs were evaluated. The following candidates were analysed in this thesis: 'Cdh16-cre/Rab35-flox', 'Rab27' and 'Sytl4' (Tab. 1). For the Cdh16-cre/Rab35-flox line, *Rab35 fl/+;Cdh16-cre -/+* mice (named hereafter 'Rab35-het') have a conditional knockout of *Rab35* in the kidney and in the epididymis. The control mice for this genotype were *Rab35 fl/+;Cdh16-cre -/-* litter mates (referred to as 'Rab35-control'). For the Rab27 line, *Rab27a ash/ash;Rab27b -/-* have a global double knockout of *Rab27a* and *Rab27b* (named hereafter 'Rab27DKO'). Age matched C57BL/6J wildtype mice (referenced as 'WT') acted as their control. Within the Sytl4 line, *Sytl4ko/wt* mice exhibit a global heterozygous knockdown of *Sytl4*. *Sytl4wt/wt* litter mates were used as their control.

Tab. 1: Genotype, strain, sex and age of the lines analysed as candidate models of mice with decreased amount of EVs within the epididymal fluid.

Line	Genotype	Strain	Sex; Age [Months]	Named in thesis
Cdh16-cre/ Rab35-flox	<i>Rab35 fl/+;</i> <i>Cdh16-cre -/+</i>	C57BL/6J (25%), C57BL/6N (75%)	Male; 3	Rab35-het
Cdh16-cre/ Rab35-flox	<i>Rab35 fl/+;</i> <i>Cdh16-cre -/-</i>	C57BL/6J (25%), C57BL/6N (75%)	Male; 3	Rab35-control
Rab27	<i>Rab27a ash/ash;</i> <i>Rab27b -/-</i>	C57BL/6J	Male; 4	Rab27DKO
wt	C57BL/6J	C57BL/6J	Male; 4	WT
Sytl4	<i>Sytl4ko/wt</i>	C57BL/6Ncrl	Male; 3	Sytl4 ko/wt
Sytl4	<i>Sytl4wt/wt</i>	C57BL/6Ncrl	Male; 3	Sytl4 wt/wt

2.1.2 Isolation of EVs from mouse epididymal fluid using ultracentrifugation

Mice were sacrificed using an overdose of isoflurane and blood was drained from the abdominal inferior vena cava using a needle. The right and left epididymis were dissected and placed separately into Eppendorf tubes filled with 1 ml sterile filtered PBS. After cutting the tissue 5 times, the tubes were placed at 37 °C for 45 min under gentle shaking on a thermomixer to allow the epididymal fluid containing sperm and EVs to flow out into the PBS. This PBS and epididymal fluid mixture was transferred to a new tube whilst the remaining epididymal tissue was frozen in liquid nitrogen and stored at -80 °C until further processed. The epididymal supernatant was centrifuged at 1000 x g for 8 min at 4 °C to pellet the sperm. The supernatant was centrifuged at 2000 x g for 10 min at 4 °C and then again at 10,000 x g for 30 min at 4 °C to pellet cell debris. This cell debris pellet (referenced hereafter 'pre-UC pellet') was stored at -80 °C. To isolate EVs from the epididymal fluid, 700 µl supernatant was transferred to polypropylene tubes. Using an ultracentrifuge with a TLA-55 rotor, the samples were centrifuged twice at 100,000 x g for 70 min at 4 °C by discarding the supernatant and resuspending the pellet until finally suspending the EVs in 100 µl filtered sterile H₂O. The isolated EVs (referenced as 'UC-EVs') were diluted for nanoparticle tracking analysis (NTA) or processed further for protein or RNA isolation.

2.1.3 Nanoparticle tracking analysis of UC-EVs

Nanoparticle tracking analysis was carried out using the Zetaview machine to measure the size and quantity of UC-EVs. Samples were diluted appropriately with H₂O for optimal particle measurement. Settings such as brightness (> 20), minimum (10 nm) and maximum (500 nm) size were set according to suggested ranges (Mehdiani et al., 2015). For comparability of samples, the sensitivity setting was identical within each experiment according to the optimal range of the scattering intensity of a control sample. Video acquisition and data analysis was carried out on 11 positions within the machine and with 3 cycles per sample. Particle sizes (peak, average, median and distribution), particle number and concentration were statistically analysed using unpaired, two tailed Student's T-test (ns > 0.05). Sample sizes for the NTA analysis were as follows: Rab35-het, n = 7; Rab35-control, n = 5; Rab27DKO, n = 4; WT, n = 3; Sytl4 ko/wt, n = 5; Sytl4 wt/wt n = 6.

2.2 Analysis of protein components of UC isolated epididymal EVs

2.2.1 Protein extraction

UC-EV pellets were resuspended in 100 μ l lysis buffer (50 mM HEPES (pH 7.4), 150 mM NaCl, 1 mM EDTA, 2 % SDS, 1 mM DTT, 1 \times protease and phosphatase inhibitor) and placed on ice. The samples were sonicated 6 times for 1 min (35 kHz) with 2 min incubation on ice in between to aid lysis. Following this, samples were incubated at 95 $^{\circ}$ C for 5 min at 500 rpm and centrifuged for 20 min at maximum speed. The supernatant containing the proteins was frozen at -80 $^{\circ}$ C until further use.

2.2.2 Western Blot

For Western Blot analysis, 4 \times SDS loading dye was added to the extracted protein, followed by 5 min at 95 $^{\circ}$ C, a brief incubation on ice and a short centrifugation step. Samples were run at 125 V for 1.5 hours on 12 % tris-glycine polyacrylamide gels (1.5 M Tris-HCl (pH 8.8), 0.5 M Tris-HCl (pH 6.8), 10 % SDS, 30 % Acrylamide solution, 10 % Ammonium persulfate, TEMED). Afterwards, the samples were transferred onto a nitrocellulose membrane in a wet chamber with 0.3 A for 1.5 hours. Membranes were placed in 10 % milk for 1 hour on a shaker to block unspecific antibody binding followed by an overnight incubation at 4 $^{\circ}$ C with the primary antibodies diluted in 1 % milk. After three consecutive washes with first 1 \times PBS and then 1 \times PBST at room temperature, membranes were incubated with the secondary antibody for 1.5 hours at room temperature. After an additional washing step, the membranes were developed using Western Bright (ECL and Peroxide) and imaged on a ChemiDoc Imaging System. Primary and secondary antibodies with their dilutions are listed in Tab. 2 and Tab. 3.

Tab. 2: List of primary antibodies used for either Western blot protein analysis of mice UC-EVs and antibodies used for fluorescence imaging of the male *Drosophila* AG.

Antigen	Host	Producer	Catalog No.	Dilution
CD9	Rabbit	Abcam	ab92726	1:1000
Flotillin 1	Rabbit	Cell Signaling	18634	1:1000
Calnexin	Rabbit	Santa Cruz	sc-11397	1:1000
Actin	Mouse	MP Biomedicals	691001	1:30000
Fasciclin III	Mouse	DSHB	7G10	1:10

Tab. 3: List of secondary antibodies used in either Western blot protein analysis of mice UC-EVs and antibodies used for fluorescence imaging of the male *Drosophila* AG.

Host	Reactivity	Conjugate	Producer	Catalog No.	Dilution
Mouse	Goat	HRP	Dako	P0447	1:10000
Rabbit	Goat	HRP	Promega	W401B	1:3000
Goat	Mouse	Alexa Fluor 594	Life Technologies	A11005	1:400

2.2.3 Mass spectrometry analysis of UC isolated epididymal EVs

Liquid-Chromatography-Mass spectrometry/Mass spectrometry (LC-MS/MS) was carried out on UC-EVs. Following protein extraction (as described above in the paragraph 'Protein extraction'), samples were heated at 95 °C for 5 min followed by a quick chill on ice and a spin down. UC-EV protein samples (10 µg) and BSA standards were mixed with 4 x SDS loading dye and run on a 12 % tris-glycine polyacrylamide gel (as described above in the paragraph 'Protein extraction') first for 15 min at 100 V and later for 75 min at 150 V. Protein concentrations were quantified by SilverQuest Silver Staining following manufacturer's instructions and gel images were analysed using the ChemiDoc to determine the protein concentration based on the BSA standard curve.

To generate tryptic peptides for LC-MS/MS, a modified Filter-aided-Sample-preparation (FASP) was carried out as follows. Protein samples were reduced and alkylated by incubating them with 10 mM DTT and 2 mM TCEP for 15 min at 60 °C, adding IAA and incubating them in the dark for 30 min. After adding 300 µl urea buffer, each sample was transferred to a filter column and centrifuged for 40 min at room temperature. Following this, the filter columns were washed 6 times using 300 µl urea buffer and centrifuged at 17,000 x g for 20 min. For sample digestion, trypsin (60 µl 100 mM ABC, 40 µl HPLC water and 40 µl Trypsin) was added to each filter column and incubated for 1 h at 37 °C and overnight at 30 °C. The columns were centrifuged at 17,000 x g for 20 min to collect the peptides and the flow through was stored at 4 °C. To remove the detergents from the peptide solution, an equal volume of 2 M KCl was mixed with the samples and incubated for 30 min at room temperature, followed by a centrifugation at maximum speed for 20 min to collect the supernatant. The peptides were cleaned using C18 Stage tips, resuspended in Formic Acid and stored at 4 °C until use. Dr. Enzo Scifo (Translational Biogerontology Lab, AG Ehninger, DZNE e.V. Bonn) carried out the quantification of the peptides on a Dionex Ultimate 3000 RSLC nanosystem coupled to an Orbitrap Exploris

480 MS and processed the data files with Proteome Discoverer™ software (v2.5.0.400, Thermo Scientific) using SEQUEST® HT search engine against the Swiss-Prot® Mus musculus database. Sample size for LC-MS/MS analysis of UC-EVs and epididymis using WT mice were as follows: UC-EVs, n = 3; epididymis, n = 3.

2.3 Analysis of RNA content within UC isolated epididymal EVs

2.3.1 RNase pre-treatment and RNA extraction from UC isolated epididymal EVs

UC-EVs samples were pre-treated with RNase before carrying out the RNA extraction protocol. For this, samples were incubated for 5 min at 37 °C with RNase H and RNase A and flash frozen using dry ice. Afterwards, RNA was extracted using the miRNeasy Mini Kit following manufacturer's instructions. DNA contamination was removed by incubating with DNase at 37 °C for 10 min. A Monarch RNA Cleanup Kit was used on samples following the manufacturer's instructions. Sample size and purity was analysed using the Agilent Small RNA kit on the Bioanalyzer as per manufacturer's instructions. Samples were stored at -80 °C until further processed.

2.3.2 Total RNA sequencing from UC isolated epididymal EVs

To analyse total RNA sequencing on UC-EVs RNA content, RNA samples were ligated with 3' Adapter and 5' Adapter before the LM-Seq library preparation protocol was carried out. In short, isolated UC-EV RNA samples were ligated with 3' Adapter using a reagent mixture of Ligation Buffer, RNase Inhibitor and T4 RNA Ligase for 1 h at 28 °C. Afterwards, the samples were cleaned using Ampure Clean Up beads as per manufacturer's recommendations. The RNA samples were then incubated with a mixture of RNA 5' Adapter, 10 mM ATP and T4 RNA Ligase for 1 h at 28 °C. The samples were then purified with Ampure Clean Up beads as before.

LM-Seq library preparation was carried out based on published protocols (Hou et al., 2015). In brief, RNA samples were fragmented at 85°C for 7 min, before cooling on ice. For cDNA synthesis, samples were incubated at 23 °C for 10 min then 42 °C for 30 min, followed by 10 min incubation at room temperature with SmartScribe Reverse Transcriptase (100 U) and random hexamer oligo primer. RNA was then removed by treating the samples with RNase A and RNase H for 15 min at 37 °C and 5 min at 95 °C. The cDNA was then purified using Ampure Clean Up beads as before and ligated with a

5' Illumina adaptor with an overnight incubation at 22 °C with T4 RNA ligase I. Samples were amplified by 24 PCR cycles using FailSafe PCR enzyme and oligos that contain Illumina adaptors and index primers with unique nucleotides for each sample. The cDNA samples were purified with Ampure Clean Up beads, selected by size using SPRIselect beads and quantified by a Qubit dsDNA High Sensitivity Assay Kit. To generate the library, 10 ng cDNA of each sample was pooled and the pooled library was then quantified for quality and average fragment size using an Agilent High Sensitivity DNA chip on a Bioanalyzer. Dr. Enzo Scifo (Translational Biogerontology Lab, AG Ehninger, DZNE e.V. Bonn) carried out the sequencing of the generated cDNA library on a Illumina NovaSeq 6000 system and processed the data as follows: fastq files were generated using bcl2fastq2 (v2.20); adaptor sequences were removed from the sequencing reads using CutAdapt (<https://usegalaxy.org/>); trimmed reads were mapped using HISAT2 (v2.1.0) in Galaxy (<https://usegalaxy.org/>); indexing was carried out using Samtools and count matrices were generated with Genomic Alignments in R; library normalisation and quantification of differentially expressed genes (DEG) between samples was carried out with the DESeq2 package (Love et al., 2014). The threshold for DEG was set at a false discovery rate (FDR) < 0.05. Sample size for RNA sequencing analysis of UC-EVs was as follows: Rab35-het and Rab35-control, n = 10; Rab27DKO and WT, n = 7.

2.4 Analysis of *Drosophila Melanogaster* model system of inhibited secretion of EVs from SCs within the AG and their offspring under paternal dietary interventions

2.4.1 Establishment of a *Drosophila Melanogaster* model system with decreased secretion of EVs from SCs within AG

The *UAS-Gal4* system was used to establish fly lines with a specific expression of CD63-GFP and various RNAi lines in secondary cells (SCs) of the reproductive tract. For this, the *dve-Gal4* line (RRID:BDSC_12859) was crossed with *UAS-CD63-GFP* line (donated by Dr. Suzanne Eaton, RRID:BDSC_91390) to establish a *dve-Gal4-UAS-CD63-GFP* stock, which expresses CD63-GFP in all cells that express *dve*. CD63 is a common EV component and used as a marker for EVs (Corrigan et al., 2014, Dar et al., 2021, Fan et al., 2020, Gross et al., 2012, Linnemannstöns et al., 2022, Sanchez-Lopez et al., 2022). All stock lines were crossed with *yw* double balancer to generate lines carrying comparable balancers. To generate a paternal F0 genotype with a decreased

EV secretion from SCs (F0 generation), the *dve-Gal4-UAS-CD63-GFP* line was crossed with the following stocks: *UAS-Luciferase-RNAi* (control, resulting line referred as '*Luciferase-RNAi*'), *UAS-Alix-RNAi* (resulting line named hereafter '*Alix-RNAi*'), *UAS-Hrs-RNAi* (resulting line referred as '*Hrs-RNAi*') and *UAS-Rab11-RNAi* (resulting line named hereafter '*Rab11-RNAi*'). The purchased and generated lines used in this thesis are listed in Tab. 4.

Tab. 4: Acquired and generated *Drosophila Melanogaster* lines used within this study.

Purchased lines	Source
w[1118]; P[w[+mGT]=GT1] dve[BG02382]/CyO	Bloomington (#12859)
y[1] v[1];; P[y[+t7.7] v[+t1.8]=UAS-LUC.VALIUM10]attP2	Bloomington (#35788)
y[1] sc[*] v[1]; P[y[+t7.7]v[+t1.8]=TRiP.HMS00298]attP2	Bloomington (#33417)
y[1] sc[*] v[1];; P[y[+t7.7] v[+t1.8]=TRiP.HMS00841]attP2	Bloomington (#33900)
y[1] v[1]; P[y[+t7.7] v[+t1.8]=TRiP.JF02812}attP2	Bloomington (#27730)
yw	Prof. Gaia Tavosanis, DZNE e.V., Bonn
w[*]; P[w[+mC]=UAS-EGFP.CD63]2; Dr[1]/TM3, Sb[1]	Suzanne Eaton, Max Planck Institute of Molecular Cell Biology and Genetics
Generated lines	
yw; IF/CyO;MKRS/TM6B	
yw; dveGal4-UAS-CD63-GFP/CyO; TM6B/MKRS	
yw; IF/CyO; UAS-Luciferase-RNAi/TM6B	
yw; IF/CyO; UAS-Alix-RNAi/TM6B	
yw; IF/CyO; UAS-Rab11-RNAi/TM6B	
yw; IF/CyO; UAS-Hrs-RNAi/TM6B	
Generated F0 Lines carrying Gal4 and UAS-RNAi components	Referred to in thesis as
yw;dveGal4-UAS-CD63-GFP/IF;UAS-Luciferase-RNAi/MKRS	<i>Luciferase-RNAi</i>
yw; dveGal4-UAS-CD63-GFP/IF; UAS-Rab11-RNAi/MKRS	<i>Rab11-RNAi</i>
yw; dveGal4-UAS-CD63-GFP/IF; UAS-Hrs-RNAi/MKRS	<i>Hrs-RNAi</i>
yw; dveGal4-UAS-CD63-GFP/IF; UAS-Alix-RNAi/MKRS	<i>Alix-RNAi</i>
Generated F1 line from paternal genotypes and paternal diets	Referred to in thesis as
yw; IF/+; MRKS/+	F1

2.4.2 Imaging of the AG within the male *Drosophila melanogaster* reproductive tract

Five-day-old male flies expressing *UAS-CD63-GFP* and *UAS-RNAis* under *dve-Gal4* control were anaesthetised on ice. In cold 0.03 % PBST, the male reproductive tract was dissected and fixed in 4 % PFA for 15 min. If staining was carried out, the tissue was permeabilised with 0.3 % Triton X-100 for 30 min and blocked with 10 % BSA for 1 hour, before the primary antibody Fascilin III (FasIII, Tab. 2) was incubated overnight at 4 °C. Following washing and incubation with secondary antibody for 2 hours at room temperature (Tab. 3), the tissue was mounted on microscope slides using VectorShield mounting medium with DAPI. Slides were stored at 4 °C prior to imaging. Images were acquired on a LSM700 confocal microscope with 20 x, 40 x, and 63 x objectives. Gain and laser intensity settings were optimised for representative images, but standardised between samples for quantification. Representative images are shown as maximum intensity projections.

2.4.3 Quantification of CD63-GFP puncta within the *Drosophila melanogaster* AG lumen

To quantify the number of CD63-GFP puncta within the AG lumen, confocal images were taken in 3 different sections of the AG of male flies expressing *UAS-CD63-GFP* and *UAS-RNAis* under *dve-Gal4* control. Images were acquired with 63x objective, 1 µm slice intervals, and taken from the top to the bottom epithelial cell layer of the AG, visible by the DAPI staining of the cell nucleus. Using ImageJ, below the first 10 confocal slice layers, the total GFP area of 20 slices was quantified in arbitrary units [a.u.] and averaged per section and AG. Normal distribution was determined using the Shapiro-Wilk test and statistical significance was tested by one-way ANOVA Kruskal-Wallis (Two-stage linear step-up procedure of Benjamini, Krieger and Yekutieli) with ns $p < 0.05$, **** $p < 0.0001$. Samples sizes for the quantification of CD63-GFP puncta within the AG lumen are as follows: *Luciferase-RNAi* n = 48, *Alix-RNAi* n = 30; *Hrs-RNAi* n = 38; *Rab11-RNAi* n = 35.

2.4.4 Food preparation and dietary exposures of male F0

The normal diet (ND) for flies was cooked by the technical assistant of Prof. Dr. Gaia Tavosanis, DZNE e.V. (Bonn), using a standard food recipe (Tab. 5). To make a high sugar diet (HSD) or a high fat diet (HFD), the food for the ND was reheated and supplemented with either sucrose or coconut oil to create a 30 % HSD or 30 % HFD, respectively. Male F0 flies (*Luciferase-RNAi*, *Rab11-RNAi* and *Hrs-RNAi*) were aged for 5 days post-eclosion and then fed a ND, HSD or HFD for 5 days.

Tab. 5: Ingredients for a normal diet and supplements for high sugar or high fat diets.

Ingredients	Amount	Dietary intervention (in 1 L)
Agar	11.7 g	Normal diet (ND)
Cornmeal	100 g	
Sojameal	10 g	
Yeast	18.5 g	
Diamalt	40 g	
Sugar syrup	40 g	
Nipagin salt	25 g	
H3PO4 (10 %)	100 ml	
+ Coconut Oil	300 g	High fat diet (HFD)
+ Sucrose	300 g	High sugar diet (HSD)

2.4.5 F1 Generation

Post dietary exposures, F0 males were placed with 3-5 day old *yw* wildtype females in single crosses on a ND. After 20 hours, the F0 males were removed and the females were placed in fresh food (ND) for egg laying and F1 generation. F1 flies used in this study were selected specifically to carry identical balancers and to not carry any of the paternal *dve-Gal4* or *UAS-RNAi* chromosomes. These flies were raised in ND and were never exposed to paternal dietary interventions (Tab. 4).

2.4.6 Fecundity analysis

After mating with F0 males, *yw* wildtype females were flipped onto fresh food on day 2 and day 4 and the numbers of eggs laid on the food were counted. Adult F1 eclosion from each vial was counted. Sample size for the fecundity analysis was as follows: n > 13 per genotype and dietary condition.

2.5 Metabolic analysis of *Drosophila Melanogaster* F0 models and their F1 offspring

For the following metabolic analysis, male F0 flies were 10 days old (post-dietary intervention) and their F1 offspring were 5 days old at the time of analysis.

2.5.1 Body weight measurement of male F0 flies and their F1 offspring

Flies were placed in an empty vial for 30 min to defecate. Afterwards, 5-10 flies were placed into pre-weighed 1.5 ml Eppendorf tubes and weighed on an ultra-sensitive scale with up to 0.01 mg precision. The tubes were then frozen in liquid nitrogen and stored at -80 °C until further processed. To determine the average fly weight, the weight of the tube containing flies was subtracted from the weight of the tube without flies and then divided by the number of flies in the tube. Sample size for the body weight analysis was as follows: male F0, n > 12 per genotype and dietary condition; female F1, n > 9 per paternal genotype and condition; male F1, n > 12 per paternal genotype and condition.

2.5.2 Triglyceride measurement of male F0 flies and their F1 offspring

To measure the triglyceride (TAG) content of flies, the procedure was followed previously described (Tennessen et al., 2014). In short, 5 flies were homogenised in 100 µl cold PBS + 0.05 % Tween 20 (PBST) and then heated for 10 min at 70 °C. Following this, 20 µl PBST and 20 µl triglyceride reagent were each added to 20 µl fly samples, glycerol standards and a PBST blank. The mixtures were incubated for 30 - 60 min at 37 °C. After centrifuging for 3 min at full speed, 30 µl of each sample was transferred to a 96-well plate. The samples were treated with 100 µl free glycerol reagent and the plate was incubated for 5 min at 37 °C. The absorbances of the sample mixtures were measured at 540 nm on a Tecan plate reader. To determine the TAG concentration for each sample, the absorbance of free glycerol in untreated samples was subtracted from the absorbance of samples treated with triglyceride reagent and then calculated using the standard curve from the glycerol standards. A Bradford assay was carried out as described by manufacturer's instructions to measure the protein amount for normalisation. Sample size for the TAG content quantification was as follows: F0, n > 13 per genotype and dietary condition; female F1, n > 12 per paternal genotype and condition; male F1, n > 13 per paternal genotype and condition.

2.5.3 Lifespan analysis of male F0 and F1 offspring

F1 flies were collected after eclosion with males and females being separated after 48 hours. Fly handling was followed as previously described (Linford et al., 2013). In short, flies were flipped into fresh vials every 2 - 3 days, with dead, escaped or stuck flies documented every 2 days. The sample size for all datasets was $n > 100$. Data was plotted using Kaplan-Meier survival curves and analysed with a Log-rank (Mantel-Cox) Test: ns $p > 0.05$, * $p < 0.05$, ** $p < 0.01$, *** $p < 0.001$, **** $p < 0.0001$.

2.5.4 RNA isolation and mRNA sequencing of F1 offspring

The gene expression profile in offspring generated from male F0 flies was analysed by mRNA sequencing in young adult F1 (5 days old) and aged F1 (males: 3 weeks; females: 4 weeks) flies. For each sample, 3 - 5 flies were homogenized in 400 μ l TRI Reagent and incubated at room temperature for 5 min. After centrifuging at 12,000 x g for 10 min at 4 °C, the supernatant was transferred into a new tube and 200 μ l chloroform was added. Samples were centrifuged at 12,000 x g for 15 min at 4 °C to separate the aqueous phase from the organic phase. The aqueous phase was mixed with 500 μ l isopropanol to precipitate the DNA. The samples were then incubated for 10 min at room temperature followed by centrifuging at 12,000 x g for 15 min at 4 °C to pellet the RNA. The pellet was washed with 1 ml 75 % ethanol and centrifuged at 7,500 x g for 5 min at 4 °C. The ethanol was removed and the pellet was dissolved in 30 μ l RNase free water. DNA was removed by incubating the RNA samples with DNase for 10 min at 37°C. A Monarch RNA Cleanup Kit was used following the manufacturer's instructions. Samples were stored at -80 °C until further processed. For RNA sequencing of samples, mRNA was isolated using NEBNext Poly(A) mRNA Magnetic Isolation Module (NEB #E7490) following manufacturer's instructions. LM-Seq library preparation and analysis was carried out as described above in the paragraph 'Total RNA sequencing from UC isolated epididymal EVs (UC-EVs)'. Sample sizes for the mRNA sequencing of F1 males and females were as follows: young adult F1 from paternal HFD, $n = 5$; young adult F1 from paternal HSD, $n = 7$; aged F1 from paternal HSD and HFD, $n = 5$.

2.6 Gene ontology analysis

To identify potential functions of differentially expressed genes and proteins, Gene Ontology (GO) analysis (GO Consortium, <http://geneontology.org/>) powered by PANTHER was carried out. The categories 'biological processes', 'molecular function' and 'cellular component' were selected and analysed separately for up- and down-regulated genes and proteins, with false discovery rate (FDR) < 0.05 threshold.

2.7 Statistical analysis

Unless otherwise specified, data was analysed in Microsoft Excel (2010) and GraphPad Prism (Version 9.3.1). Outliers were identified and removed using ROUT (Q = 1%). Statistical analysis was carried out by two-way ANOVA (with Fisher LSD Test): ns $p > 0.05$, * $p < 0.05$, ** $p < 0.01$, *** $p < 0.001$, **** $p < 0.0001$. Only statistical significances within genotype or within diet comparison are shown in the graphs.

2.8 Reagents and consumables

Reagents and consumables, as well as equipment and software used in this thesis are listed in Tab. 6 and Tab. 7, respectively.

Tab. 6: List of consumables and reagents used in the experiments of this thesis.

Consumables and Reagents		
Product	Manufacturer	Catalog no.
2-Propanol, min. 99,8 %	Carl Roth	6752.2
3' Adapter Primer	Sigma Aldrich	
5' Adapter Primer	Sigma Aldrich	
Acetic acid, optima™ LC/MS grade	Thermo Fisher Scientific	A113-50
Acetone	Thermo Fisher Scientific	10417440
Agilent High Sensitivity DNA Kit	Agilent	5067-4626
Amicon ultra-0.5 centrifugal filter uni , 10k mwco, 0.5 ml (96 pack)	Thermo Fisher Scientific	UFC501096
Ammonium bicarbonate (ABC)	Sigma	A6141-500g
Ammonium persulfate	Sigma	A3678-25g
Ampure Beads , 60ml	Agencourt	A63881
Bioanalyzer Small RNA Analysis	Agilent	5067-1548
Nitrocellulose Blotting Membrane (0.1µm)	Sigma Aldrich	GE10600000
Bond-Breaker TCEP	Thermo Fisher Scientific	77720
Bradford Dye Reagent Concentrate	Biorad	5000006
BSA	Sigma Aldrich	A9418-100g

Coconut oil	VWR	ACRO36547 1000
DTT (dithiothreitol)	Thermo Fisher Scientific	R0862
EDTA	Applichem	A11030500
Eppendorf™ protein LoBind	Thermo Fisher Scientific	10708704
Ethanol min. 99,8 %	Carl Roth	9065.2
FailSafe PCR Enzyme (2.5U/ul, 250U)	Epicentre	FS99250
Forene 100 % (Isoflurane)	Abbvie	B506
Formic acid (modifier), LC/MS grade	Thermo Fisher Scientific	15655840
Free Glycerol Reagent	Sigma	F6428
HEPES	Roth	HN78.1
HPLC water	Thermo Fisher Scientific	51140
Iodo acetic acid (iaa)	Thermo Fisher Scientific	35603
LC MS autosampler vials (100 pack)	Waters	186000384C
Microfuge Tube Polypropylene	Beckman Coulter	357448
Milk powder	Roth	T145.3
miRNeasy Mini Kit	Qiagen	217004
Monarch RNA Cleanup Kit (50 µg)	New England Biolabs	T2040L
NEBNext Single Cell/Low Input RNA Library Prep Kit for Illumina	NEB	E6420L
NovaSeq 6000 S1 Reagent Kit (100 cycles)	Illumina	20012865
Optima LC/MS acetonitrile with 0.1% (v/v) trifluoroacetic acid	Thermo Fisher Scientific	LS121-1, 1 L
Optima LC/MS acetonitrile with 0.1% (v/v) formic acid	Thermo Fisher Scientific	LS120-1, 1 L
Optima LC/MS water with 0.1% (v/v) formic acid	Thermo Fisher Scientific	LS118-1, 1 L
Optima LC/MS water with 0.1% (v/v) trifluoroacetic acid	Thermo Fisher Scientific	LS119-1, 1 L
PageRuler Plus Prestained Protein Ladder	Thermo Fisher Scientific	26619
Paraformaldehyde solution 4% in PBS (PFA)	Santa Cruz	sc-281692
Pierce C18 tips, 100 ul bed 96 tips	Thermo Fisher Scientific	87784
Pierce protease and phosphatase inhibitor mini tablets, EDTA-free	Thermo Fisher Scientific	A32961
Pierce trypsin protease MS grade	Thermo Fisher Scientific	90058
Potassium chloride (KCl)	Roth	6781.3
Qubit™ dsDNA HS Assay Kit	Thermo Fisher Scientific	Q32851
RNase A (50mg)	Epicentre	MRNA092
RNase H (250 U)	NEB	M0297S
RNase Inhibitor (2000 U)	Thermo Fisher Scientific	N8080119
SilverQuest Silver Staining Kit	Life Technologies	LC6070
Smartscribe Rev Trans (100 U/µl)	Clontech	639537

Sodium Chloride (NaCl)	Roth	3957.2
Sodium dodecyl sulfate (SDS)	Roth	2326.2-500g
Sodium hydroxide (NaOH)	Roth	9356.1
Sucrose	Serva	35580.03
T4 RNA Ligase 1 (10U/μl; 5000 U)	NEB	M0204L
Tetramethylethylenediamine (TEMED)	Roth	2367.3
TFA, LC/MS grade	Thermo Fisher Scientific	10723857
TRI Reagent	Sigma Aldrich	T9424-200ML
Trichlormethan/Chloroform	Carl Roth	3313.2
Triglyceride Reagent	Sigma	T2449
Tris-HCl	Thermo Fisher Scientific	15568025
Triton X-100	Sigma	X100-500
Tween 20	Sigma	274348-1L
Urea (Harnstoff)	Appllichem	A1360,1000
Vectashield with DAPI	Fisher Scientific	13273694
Western Bright Chemiluminescence Substrate Quantum	Biozyme	541010

Tab. 7: List of equipment and software used in the experiments and analysis of this thesis.

Equipment and Software		
Product	Manufactory/Creator	Specifications
Bioanalyzer	Agilent	2100 Bioanalyzer
Bioanalyzer Chip Vortexer	Agilent	MS 3 basic S36 Agilent
Centrifuge	Thermo Fisher Scientific	Heraeus Fresco 21
ChemiDoc	Biorad	ChemiDoc MP Imaging System
Confocal Microscope	Zeiss	LSM700
Excel	Microsoft	2010
Fixed-Angle Rotor	Beckman Coulter	TLA-55
GraphPad Prism	GraphPad Software, Inc	Version 9.3.1
ImageJ	Wayne Rasband (NIH)	
Plate reader	Tecan	Infinite M Plex
Spectrophotometer	Thermo Scientific	NanoDrop 2000c
Thermomixer	Eppendorf	Thermomixer comfort
Ultracentrifuge	Beckman Coulter	Optima Max-XP Biosafe Tabletop
Zetaview	Particle Metrix	Mono

3. Results

3.1 Evaluation of candidate mouse lines as *in vivo* loss of function models for EVs secreted by the epididymis into the epididymal fluid

We generated three candidate transgenic mouse lines with a knock down of proteins with published functions in the EV biogenesis or secretion pathway. The suitability of these candidate lines as *in vivo* loss of function models for EVs secreted by the epididymis into the epididymal fluid is analysed here.

3.1.1 Characterisation of EVs isolated from epididymal fluid using ultracentrifugation

Following the guidelines of the International Society of Extracellular Vesicles (Théry et al., 2018), EVs isolated by ultracentrifugation from the epididymal fluid (UC-EVs) were characterised by protein composition and size before the evaluation of the three mouse lines was carried out (Fig. 1).

Following ultracentrifugation isolation, approximately 60 µg proteins are extracted from UC-EVs of both epididymis sides of a WT mouse. Although there is currently no definitive EV marker, the representative Western blot comparing proteins extracted from epididymal fluid EVs (UC-EVs), cell debris pellet (pre-UC pellet) and epididymal tissue in Fig. 1 A demonstrates antibodies targeting proteins commonly used to determine the nature and purity of EV samples. CD9 and FLOT1 are well-described EV proteins and are present in the UC-EVs sample (Fig. 1 A). While the epididymal tissue and pre-UC pellet have much stronger antibody bands against FLOT1 than UC-EVs, the CD9 antibody band is most prominent in the UC-EV sample (Fig. 1 A). ACTIN is another common, though not specific EV protein, and is very weakly present in the UC-EV sample in comparison to the epididymal tissue (Fig. 1 A). As a component of the endoplasmic reticulum, the antibody against CALNEXIN is a common marker for non-EV structures and is not present in UC-EVs (Fig. 1 A).

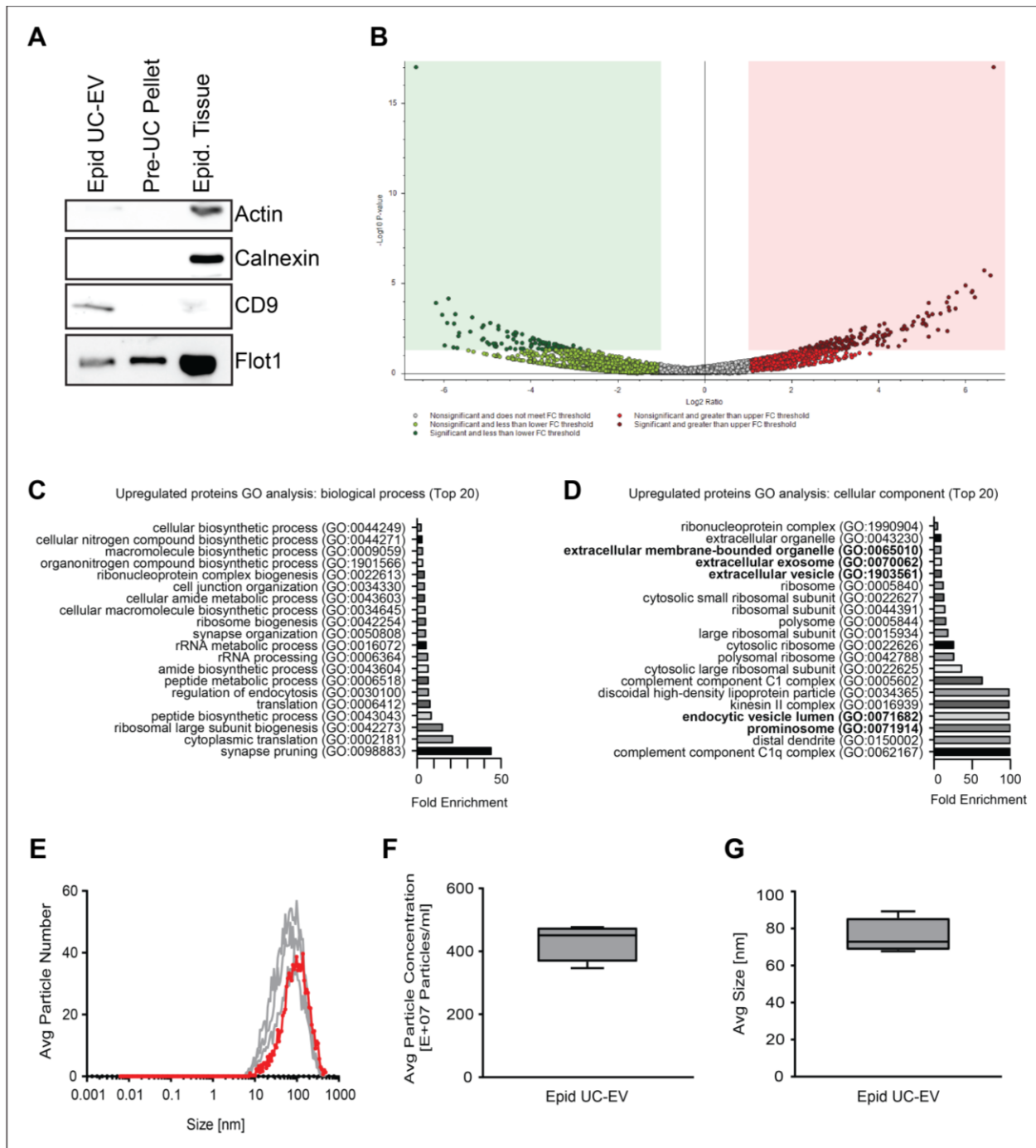


Fig. 1: Protein composition analysis and size quantification of EVs isolated from epididymal fluid from WT mice using ultracentrifugation. Representative Western blot membrane staining depicts antibodies targeting CD9, FLOT1, CALNEXIN and ACTIN from UC-EVs, pre-UC cell pellet and epididymal tissue protein samples (A). Significantly upregulated and downregulated proteins from UC-EV samples compared to epididymal tissue measured using LC-MS/MS are shown in a volcano plot (threshold: fold change 1.5, $p < 0.05$; $n = 3$) (B). For the significantly upregulated UC-EV proteins, top 20 biological processes (C) and cellular components (D) based on fold enrichment are predicted by gene ontology analysis (PANTHER; FDR < 0.05). Nanoparticle tracking analysis quantifies the size of UC-EVs (E-G). Average particle number vs size [nm] is

shown on a logarithmic scale (*E*) with the mean displayed in red. The mean particle concentration [$E+07$ particle/ml] (*F*) and mean particle size [nm] (*G*) are displayed with mean \pm SD ($n = 4$).

To determine the full protein composition of UC-EVs, LC-MS/MS was carried out comparing tryptic peptides of UC-EVs and epididymal tissue ($n = 3$). With medium-high confidence, a total of 4458 proteins are identified with 151 proteins in the UC-EVs upregulated compared to the epididymal tissue samples and 735 proteins downregulated (Fig. 1 *B*, fold change 1.5, p value < 0.05). Within the upregulated proteins in the UC-EVs samples, well-known EV markers are identified: CD63 (P41731), CD81 (P35762) and RAB35 (Q6PHN9). Other proteins, which are currently defined as non-EV proteins, are also upregulated in the UC-EV samples: APOLIPOPROTEIN A-I (Q00623), E (P08226), C-I (P34928) and Ribosomal proteins (60S ribosomal protein L7a (P12970), 40S ribosomal protein S19 (Q9CZX8)). Using gene ontology analysis (GO analysis, PANTHER, FDR < 0.05) to analyse the 151 significantly upregulated proteins, 38 enriched biological processes are predicted, with the top 20 according to fold enrichment reported here (Fig. 1 *C*). Some notable biological processes are 'cytoplasmic translation' (GO:0002181), 'peptide biosynthetic process' (GO:0043043) and 'peptide metabolic process' (GO:0006518). Furthermore, 37 enriched cellular components are identified from the upregulated UC-EV proteins with the top 20 displayed in Fig. 1 *D*, among them: 'extracellular vesicle' (GO:1903561) and 'extracellular exosome' (GO:0070062).

Nanoparticle tracking analysis (NTA) was carried out on UC-EV samples of 4-month old WT mice ($n = 4$) to determine their size (Fig. 1 *E*). Mean particle concentration for each UC-EV sample is $456.9 \pm 64.30 E+07$ Particles/ml (Fig. 1 *F*), with a mean particle size of 75.68 ± 9.60 nm and most particles having a diameter of 95.41 ± 9.20 nm (Fig. 1 *G*).

Based on the protein composition and size profile of UC-EVs, EVs can be isolated from the epididymal fluid of mice using UC, although potential impurities such as for example Apolipoproteins need to be considered.

3.1.2 NTA-based size characterisation of epididymis-derived UC-EVs from mouse lines carrying mutations within the EV biogenesis or secretion pathway

To determine if the mutations within the EV biogenesis or secretion pathway indeed lead to decreased EV amounts within the epididymal fluid, NTA was carried out to measure the number and size distribution of UC-EVs from the mutant mice lines and their respective controls.

The conditional knock out of *Rab35* (*Rab35*-het, n = 7) within the epididymis and kidney does not affect the amount or size of UC-EVs compared to their littermates (*Rab35*-control, n = 5) (Fig. 2 A and D). Between *Rab35*-het and *Rab35*-control, the concentration of particles ($493.6 \pm 139.1 \text{ E}+07$ particles/ml vs $504.5 \pm 110.8 \text{ E}+07$ particles/ml; unpaired two-tailed t-test: p = 0.8874) and mean particle size (87.34 ± 12.12 nm vs 87.99 ± 9.09 nm; unpaired two-tailed t-test: p = 0.9217) are not significantly different (Fig. 2 A and D).

The global knockout of *Rab27* (*Rab27*DKO) causes the reduced expression of both *Rab27a* and *Rab27b* within all tissue. Comparing the *Rab27*DKO mice (n = 4) and age matched WT controls (n = 3), no significant differences between the particle numbers ($361.3 \pm 69.45 \text{ E}+07$ particles/ml vs $447.5 \pm 131.3 \text{ E}+07$ particles/ml; unpaired two-tailed t-test: p = 0.3053) and the mean particle sizes (87.12 ± 9.536 nm vs 83.57 ± 10.10 nm; unpaired two-tailed t-test: p = 0.6543) are observed (Fig. 2 B and E).

Sytl4 knockout leads to a globally decreased expression of *Sytl4*. Between *Sytl4* ko/wt (n = 5) and their littermates *Sytl4* wt/wt (n = 6), no significant differences in particle number ($5323 \pm 2215 \text{ E}+07$ particles/ml vs $5664 \pm 2939 \text{ E}+07$ particles/ml; unpaired two-tailed t-test: p = 0.8361), nor mean particle size (81.49 ± 14.06 nm vs 83.48 ± 7.05 nm; unpaired two-tailed t-test: p = 0.7667) are measurable (Fig. 2 C and F).

The absence of significant changes to the size and amount of UC-EVs from any of the three mouse line candidates indicates that the mutations do not affect the EV secretion or biogenesis pathways in the epididymal cells in the same manner as published for other cell types (Hsu et al., 2010, Ostrowski et al., 2010). Consequently, these mouse lines cannot be utilised as absolute UC-EV depletion models.

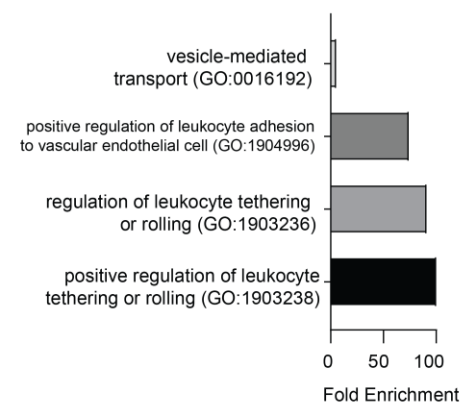
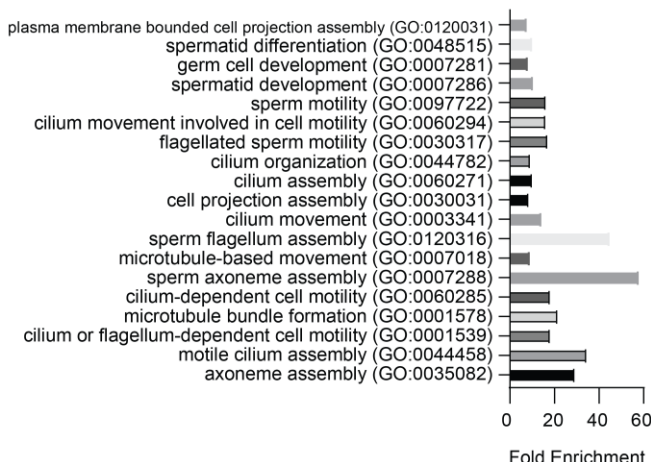
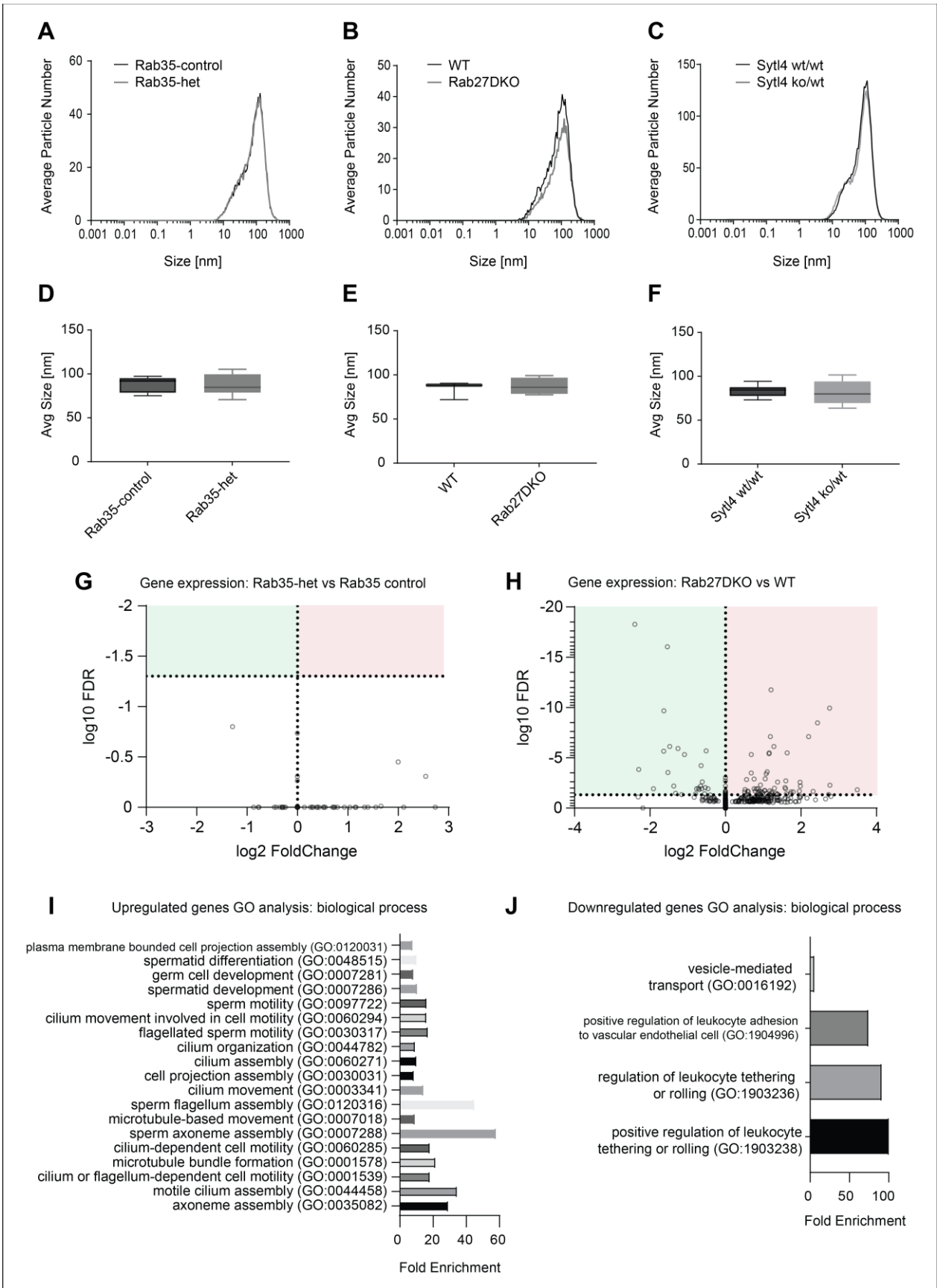


Fig. 2: Evaluation of candidate mouse lines with a knockout of proteins involved in EV biogenesis or secretion pathways by UC-EV size and RNA content. NTA analysis compares the size of UC-EVs from Rab35-control and Rab35-het mice (n = 5 and 7, respectively) (A and D), Rab27DKO and their WT control (n= 4 and 3, respectively) (B and E) and Sytl4 ko/wt and Sytl4 wt/wt mice (n = 5 and 6, respectively) (C and F). Average number of particles vs size [nm] is displayed on logarithmic scale (A, B and C). Average size of particles [nm] is shown as mean \pm SD (D, E and F). Statistical analysis: an unpaired two-tailed Student's t-test (ns p > 0.05). Volcano plots display gene expression of UC-EVs mRNA sequencing from Rab35-het vs Rab35-control (G; n = 10) and Rab27DKO vs WT mice (H; n = 7) (FDR < 0.05). Significantly enriched biological processes are identified using gene ontology analysis for the significant upregulated (I; top 20) and downregulated (J) differentially expressed genes of UC-EVs from Rab27DKO mice (Gene Ontology Resource – PANTHER; FDR < 0.05).

3.1.3 Characterisation of epididymis-derived UC-EV RNA content of the candidate mouse lines carrying mutations within the EV biogenesis or secretion pathway

Although no significant changes to both UC-EV size and numbers were identified in the three mouse model candidates, the gene deletion in these mutant lines could result in RNA cargo changes of UC-EVs. To address this possibility, RNA was extracted from the UC-EVs using an RNase pre-treatment and mRNA sequencing was carried out on the Cdh16-cre/Rab35-flox and Rab27DKO mouse lines.

RNA sequencing analysis reveals no significantly differentially expressed genes (DEG) between Rab35-het and Rab35-control mice (FDR < 0.05) (Fig. 2 G). Shifting the analysis thresholds to FDR > 0.05 and p-value < 0.05, 687 genes are differentially expressed in Rab35-het mice, with 295 upregulated and 392 downregulated genes (Tab. 1). Within the top 10 genes according to the p-value, *Rab27b* is downregulated in UC-EVs from Rab35-het mice compared to Rab35-control, indicating that *Rab35* may be involved in the regulation of *Rab27b* (Tab. 8).

In the Rab27DKO line, mRNA sequencing identifies 99 significantly DEG (FDR < 0.05) (Fig. 2 H). GO analysis (PANTHER, FDR < 0.05) predicts an enrichment in 19 biological processes for the 62 upregulated proteins, including: 'sperm axoneme assembly' (GO:0007288); 'sperm motility' (GO:0097722) and 'germ cell development' (GO:0007281) (Fig. 2 I). For the 37 downregulated genes, 4 significant biological processes have been identified with among them 'vesicle-mediated transport' (GO:0016192) (Fig. 2 J).

Tab. 8: Top 10 genes identified in UC-EV mRNA sequencing, sorted based on p-value.

Gene Name	log ₂ (Fold Change)	p-value	FDR
Rab27b	-1.29E+00	6.54E-06	1.58E-01
Pomp	-3.08E-05	1.52E-05	1.84E-01
Gm21738	2.00E+00	4.40E-05	3.55E-01
Akap2	-7.69E-06	8.15E-05	4.92E-01
Gm33838	2.54E+00	1.02E-04	4.92E-01
Btbd11	-1.10E-05	1.35E-04	5.44E-01
Gm10800	1.66E+00	3.05E-04	9.74E-01
Rhoh	-8.78E-06	3.22E-04	9.74E-01
Ddx19a	7.20E-01	4.69E-04	9.99E-01
Gm25650	-4.98E-06	5.61E-04	9.99E-01

In summary, EVs have been isolated using UC and were characterised according to current recommendation from the epididymal fluid of mice. Three candidate mouse lines, carrying mutations in genes coding for proteins involved in the EV biogenesis or secretion pathways, have been studied with none of these mouse lines showing a measurably decreased amount of EVs secreted into the epididymal fluid. Although some changes to the UC-EV mRNA content have been identified with the Rab27DKO line, the nature of the global knockout of *Rab27a* and *Rab27b* causes effects on tissue both inside and outside of the reproductive tract to be additionally contributing uncontrollable factors to consider in future intergenerational studies.

Therefore, the mouse lines analysed in this thesis cannot act as the loss of function model system to study the role of EVs from somatic cells of the reproductive tract as potential mediators of intergenerational effects *in vivo*. Yet, the findings suggest that epididymal-specific deletion of *Rab27a* and *Rab27b* could be explored in future studies to address whether this is sufficient to manipulate epididymal EV cargo *in vivo*.

3.2 Establishment of an *in vivo* loss of function model for EVs secreted by somatic cells within the male reproductive tract in *Drosophila melanogaster*

As establishing an *in vivo* loss of function model of EVs in the mouse has remained challenging, we aimed to generate a *Drosophila melanogaster in vivo* model with decreased secretion of EVs from somatic cells of the reproductive tract.

3.2.1 *Drosophila melanogaster* lines expressing RNAis in the secondary cells of the accessory gland under *dve-Gal4* control

Within the reproductive tract of the male *Drosophila melanogaster*, the accessory gland (AG) produces most of the components of the seminal fluid. A small subtype of AG cells known as secondary cells (SCs) have been shown to secrete EVs into the AG lumen.

With the *UAS-Gal4* system, a *Drosophila melanogaster* line expressing human CD63-GFP (green) (CD63 being a common EV component), specifically in SCs of the AG within the male reproductive system under *dve-Gal4* control has been generated (Fig. 3 A). FasIII antibody (red) and DAPI staining (blue) visualise the cell borders and nucleus respectively, in order to clearly differentiate the epithelial cell layer and the AG lumen containing the AG fluid in the AG tip (Fig. 3 B and C). In the top epithelial cell layer of the AG, CD63-GFP (green) expressed in SCs localises on intraluminal structures (Fig. 3 B). Outside of the SCs in the AG luminal space, small green GFP puncta are visible, indicating particles secreted by SCs (Fig. 3 C).

In order to study the impact of EVs on the phenotypic outcome of the next generation *in vivo*, we established a *Drosophila melanogaster* model with decreased secretion of CD63-GFP puncta from SCs into the AG lumen by expressing RNAi targeting common components of the EV biogenesis or secretion pathway in SCs under the same *dve-Gal4* control (Fig. 3 D-K). With *Luciferase-RNAi* as the reference condition (Fig. 3 D and E), changes to the SC intraluminal structures (Fig. 3, left column D, F, H, J) and the number of GFP puncta in the AG lumen (Fig. 3, right column E, G, I, K) can be observed in *Alix-*, *Hrs-* and *Rab11-RNAi* expressing flies. *Alix-RNAi* expression shows neither visual changes in the SC structure nor in the amount of GFP puncta within the AG lumen (Fig. 3 F-G). Similarly, *Hrs-RNAi* expression leads to no obvious changes to the SCs intraluminal structures, but observable changes in the amount of GFP puncta in the AG lumen are visible (Fig. 3 H-I). *Rab11-RNAi* expression under *dve-Gal4* control leads to a

similar decrease of GFP puncta in the AG lumen as *Hrs-RNAi*, but a more severe disruption of SC intraluminal structures than the other RNAis (Fig. 3 J-K). These observations within the AG lumen are confirmed by quantification of the GFP puncta area within defined sections of the AG lumen (Fig. 3 L). Non-parametric ANOVA Kruskal-Wallis test indicates a significant difference between all 4 genotypes, with Dunn's multiple comparisons showing no significant difference between the control genotype and *Alix-RNAi* ($p > 0.9999$), but a significant difference between *Luciferase-RNAi* and *Hrs-RNAi* ($p < 0.0001$), as well as *Luciferase-RNAi* and *Rab11-RNAi* ($p < 0.0001$) (Fig. 3 L). These findings indicate that expressing *Hrs-RNAi* and *Rab11-RNAi* under *dve-Gal4* control leads to a decreased secretion of CD63-GFP puncta from SCs into the AG lumen, although with different effects on the SC internal structure.

To test for possible effects of long-term RNAi expression on the overall health of the control and the two genotypes, a lifespan analysis was carried out (Fig. 3 M). Log-rank (Mantel-Cox) test shows a significant genotype effect on the lifespan curves ($p < 0.0001$) (Fig. 3 M), and a median survival of the *Luciferase-RNAi* for 38 days, *Hrs-RNAi* 36 days and *Rab11-RNAi* 30 days. No significant difference is observable between the lifespan curves of the *Luciferase-* (blue) and *Hrs-RNAi* (purple) genotypes ($p = 0.8979$). However, there is a significant difference in the survival curves of *Luciferase-RNAi* and *Rab11-RNAi* (green) ($p < 0.0001$), indicating that expression of *Rab11-RNAi* under the *dve-Gal4* driver control causes a detrimental effect on the male F0 lifespan (Fig. 3 M).

Although *Rab11-RNAi* expression causes the highest decrease CD63-GFP puncta within the AG lumen, the reduced lifespan compared to the other RNAi genotypes could lead to currently unclear effects on the next generation. For this reason and the fact that *Hrs-RNAi* expression under *dve-Gal4* control leads to similar significantly decreased secretion of CD63-GFP in SCs, both fly lines were utilised for the *in vivo* investigation of the impact of EVs from somatic cells within the reproductive tract on the phenotypic outcome of the next generation.

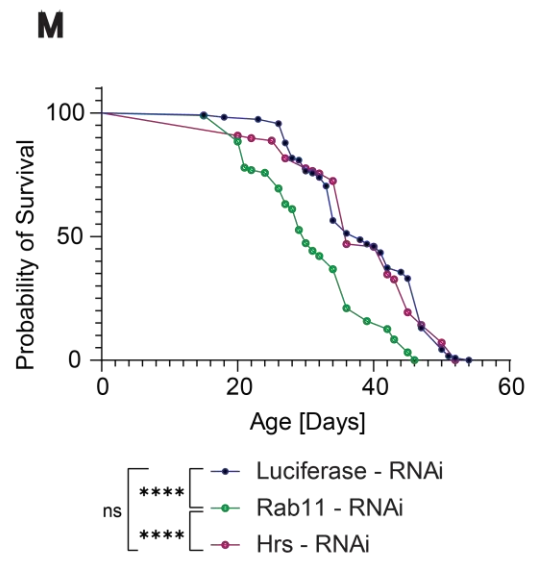
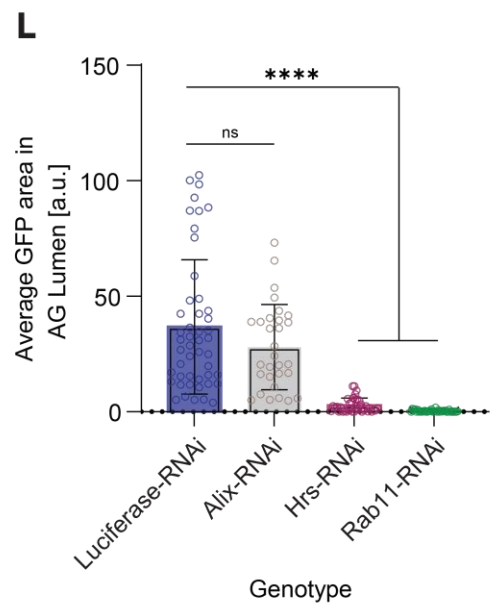
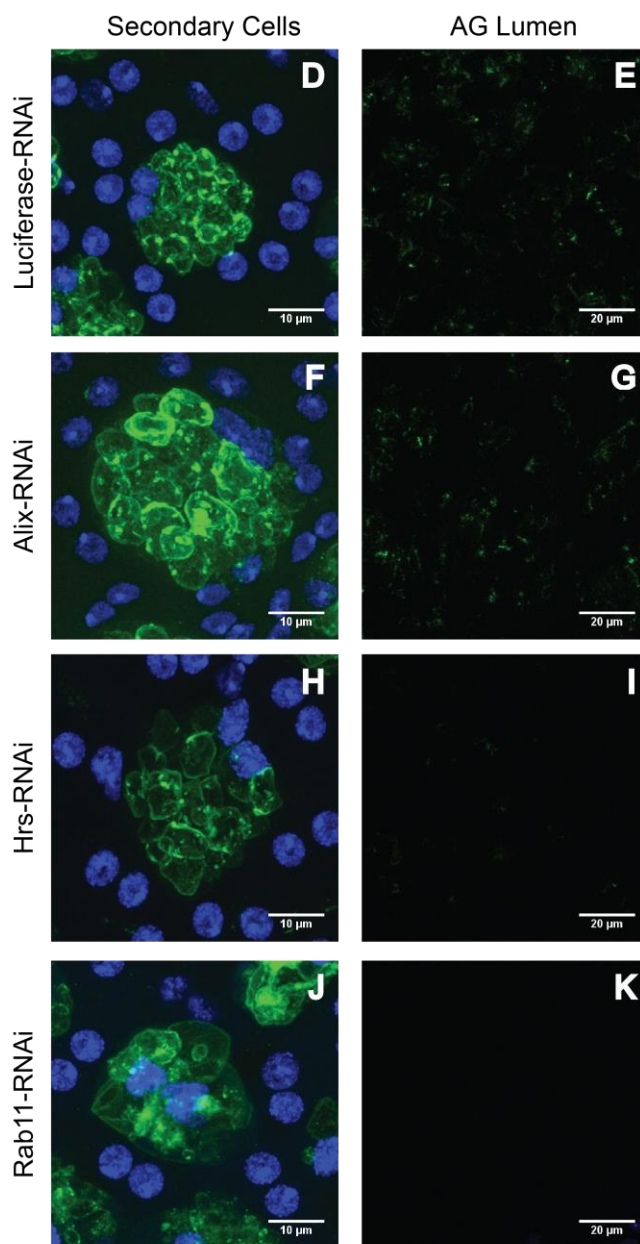
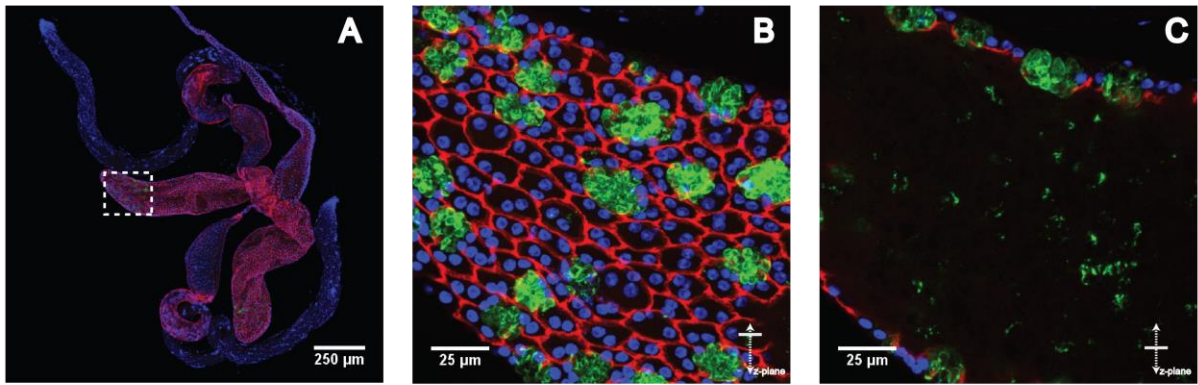


Fig. 3: Evaluation of CD63-GFP puncta secreted by SCs of male *Drosophila melanogaster* expressing RNAs under *dve-Gal4* control. Antibody staining of FasIII (red) and DAPI (blue) visualise the cell membrane and the nucleus, respectively (A-C). The male reproductive tract from 5-day old male flies with *CD63-GFP* expressed in SCs under *dve-Gal4* control is shown in a representative confocal image (20x, scale bar 250 μ m) (A). Endogenous CD63-GFP (green) within SCs is visible in the top confocal slice image of the AG (40x, scale bar 25 μ m) (B) and green CD63-GFP puncta are visible in the AG lumen within the middle confocal image slice of the AG (40x, scale bar 25 μ m) (C). Representative confocal images display the effect of expressing *Luciferase-RNAi* (D, E), *Alix-RNAi* (F, G), *Hrs-RNAi* (H, I) and *Rab11-RNAi* (J, K) under *dve-Gal4* control on SC intraluminal structures (left column, scale bar 10 μ m) and the CD63-GFP puncta within the AG lumen (right column, scale bar 20 μ m). Displayed images are maximum intensity z-projections. Average total area of GFP within defined spaces of the AG lumen from male flies expressing *Luciferase-RNAi* (n = 48), *Alix-RNAi* (n = 30), *Hrs-RNAi* (n = 38) or *Rab11-RNAi* (n = 35) under *dve-Gal4* control are quantified using ImageJ (L). Statistical analysis is carried out using one-way ANOVA (Kruskal-Wallis; ns p > 0.05, **** p < 0.0001) with bar graphs shown as mean \pm SD (L). Survival curves of male flies expressing *Luciferase-RNAi* (blue), *Rab11-RNAi* (green) and *Hrs-RNAi* (purple) under *dve-Gal4* control are displayed with the Kaplan-Meier method (M). Statistical significance data is analysed with the Log-rank (Mantel-Cox) test (ns p > 0.05, **** p < 0.0001; n > 100).

3.2.2 Body composition and fecundity analysis of male *Drosophila melanogaster* lines expressing RNAs under *dve-Gal4* control and exposed to dietary interventions

Male F0 *Drosophila melanogaster* expressing *Luciferase-RNAi*, *Hrs-RNAi* and *Rab11-RNAi* under *dve-Gal4* control were exposed to ND, HSD or HFD for 5 days prior to mating. To analyse the impact of the dietary exposures on the F0 males, body composition and fecundity changes were measured post dietary interventions (Fig. 4 A). All data were standardised, using z-transformations, to the *Luciferase-RNAi* under ND. Two-way ANOVA reveals an overall significant dietary effect on the body weight of male F0 flies after dietary exposure (F (2, 143) = 15.27; p < 0.0001), but no genotype effect (F (2, 143) = 1.950; p = 0.1461) (Fig. 4 B). Using Multiple Comparison Analysis (Fisher LSD Test), within genotype or within diet differences are identified. Comparing the dietary exposures within the F0 control genotype, there is a non-significant decrease in body weight under HSD (p = 0.0867), and a trending increase in body weight under HFD when compared to HSD (p = 0.0519) (Fig. 4 B). Similarly, a significant decrease in body weight after HSD is visible for both *Hrs-* and *Rab11-RNAi* (p = 0.0012 and p = 0.0359, respectively) (Fig. 4 B). HFD leads to a significant increase in body weight in male flies

expressing *Rab11-RNAi* under *dve-Gal4* control ($p = 0.0094$), but not in the *Hrs-RNAi* genotype ($p = 0.4657$) (Fig. 4 B). These findings indicate that the directionality of male F0 body weight changes are dependent on the dietary exposures, with the strength of these changes being possibly dependent on the F0 genotype.

With regards to the TAG content of male F0 flies exposed to dietary interventions, there is an overall effect caused by diet according to two-way ANOVA ($F(2, 192) = 24.15$; $p < 0.0001$), with a genotype effect trending but not significant ($F(2, 192) = 3.041$; $p = 0.0501$) (Fig. 4 C). Multiple Comparison Analysis (Fisher LSD Test) identifies within genotype or within diet changes, with only significant differences between diets or between genotypes shown in Fig. 4 C. Between F0 flies expressing *Luciferase-RNAi*, there is only a trending increase in TAG content when comparing ND and HSD, while HFD leads to an increased TAG content ($p < 0.0001$) (Fig. 4 C). HSD leads to a significant increase in TAG content in F0 males expressing *Rab11-* and *Hrs-RNAi* compared to ND ($p = 0.0345$ and $p = 0.0104$, respectively). Notably, after HFD exposure, *Hrs-RNAi* has a smaller increase in TAG compared to *Rab11-RNAi* ($p = 0.0343$ and $p = 0.0157$, respectively) and *Luciferase-RNAi* (Fig. 4 C). Overall, exposure to HSD and HFD causes increases in the TAG content of F0 male flies.

Investigation of fecundity under changing dietary conditions shows that there is no significant effect of either genotype or diet on the amount of eggs laid by female partners after mating with single F0 males post dietary exposure (Fig. 4 D).

Therefore, HSD and HFD dietary interventions on male F0 lead to differing changes in their body weight and TAG content, but have no effect on their fecundity. The dietary effects follow similar directions between the control and EV depleted models, with no strong genotype effect observable. Furthermore, under ND there are no significant changes between the three genotypes expressing RNAis under *dve-Gal4* control (Fig. 4).

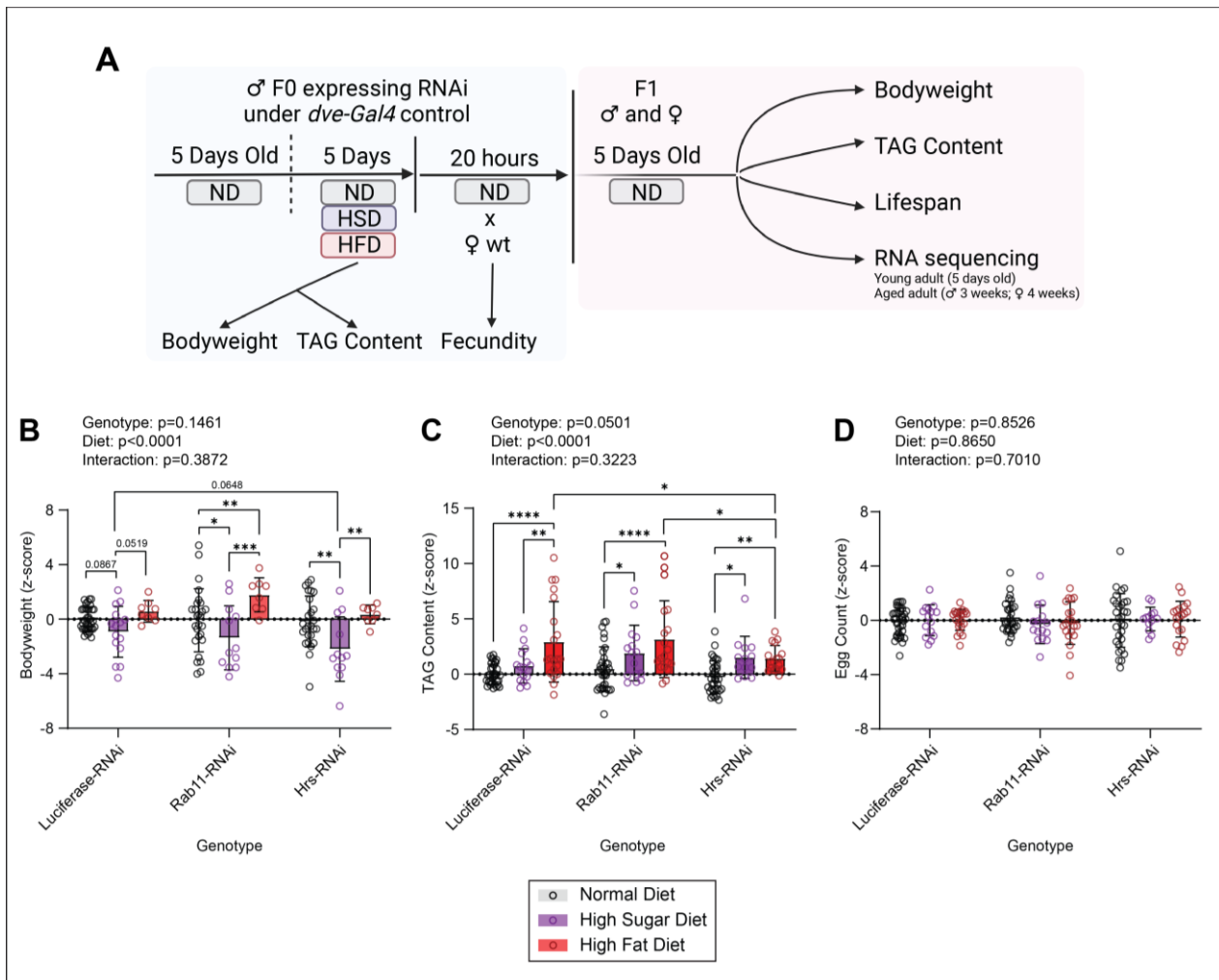


Fig. 4: Body composition and fecundity analysis of 10-day old adult male F0 flies expressing *Luciferase-RNAi*, *Rab11-RNAi* and *Hrs-RNAi* under *dve-Gal4* control post exposure to ND (black), HSD (purple) or HFD (red). Schematic diagram displays F0 dietary exposure, F1 generation and analysis procedures of this study (A). Z-standardised data of F0 body weight (B, $n > 12$), TAG content (C, $n > 13$), and number of eggs laid by female partners (D, $n > 13$) post dietary exposures are depicted in the bar graphs showing mean \pm SD (individual data points are superimposed). Statistical significance was calculated with a two-way ANOVA (Fisher LSD Test; ns $p > 0.05$, * $p < 0.05$, ** $p < 0.01$, *** $p < 0.001$, **** $p < 0.0001$), with the significance within-genotype or within-diet comparison shown here. ND = normal diet, HSD = high sugar diet, HFD = high fat diet. Schematic diagram (A) is created with Biorender.com

3.3 *In vivo* analysis of the impact of EVs secreted by somatic cells of the reproductive tract on offspring phenotypic outcome in *Drosophila melanogaster*

In order to analyse the impact of EVs secreted by somatic cells of the reproductive tract on the phenotypic changes in the next generation and the role of EVs as a potential mediator of intergenerational effects, male and female offspring were generated from the above established male F0 lines expressing RNAis under *dve-Gal4* control exposed to dietary interventions (Fig. 4 A).

3.3.1 Body composition analysis of F1 offspring derived from F0 male *Drosophila melanogaster* expressing RNAi under *dve-Gal4* control exposed to dietary interventions

Similar to their fathers, male and female F1 offspring of the *Drosophila melanogaster* expressing *Luciferase-RNAi*, *Rab11-RNAi* and *Hrs-RNAi* were analysed for effects on their body weight and TAG content as a readout for body composition (Fig. 5).

Two-way ANOVA shows an overall effect of paternal diet on the F1 female body weight ($F(2, 145) = 29.23$; $p < 0.0001$), with no observable effect from the paternal genotype ($F(2, 145) = 1.260$; $p = 0.2867$) (Fig. 5 A). Based on *post hoc* multiple comparison analysis (Fisher LSD test), female F1 offspring derived from F0 males expressing *Luciferase-RNAi* under *dve-Gal4* control have a trending increase in their body weight under paternal HSD ($p = 0.0518$) and a significant decrease in their body weight under paternal HFD ($p = 0.0183$) (Fig. 5 A). This pattern is also observed with the female F1 offspring derived from male F0 flies expressing *Rab11-* and *Hrs-RNAi* under *dve-Gal4* control. Under paternal HSD, the body weight of female F1 offspring from both *Rab11-* and *Hrs-RNAi* fathers increase significantly ($p = 0.0150$ and $p = 0.0010$, respectively), while under paternal HFD there is a significant decrease in body weight ($p = 0.0188$ and $p = 0.0070$, respectively) (Fig. 5 A). Of note, no significant difference is observable in the female offspring body weight between the paternal genotypes under any paternal dietary condition (Fig. 5 A).

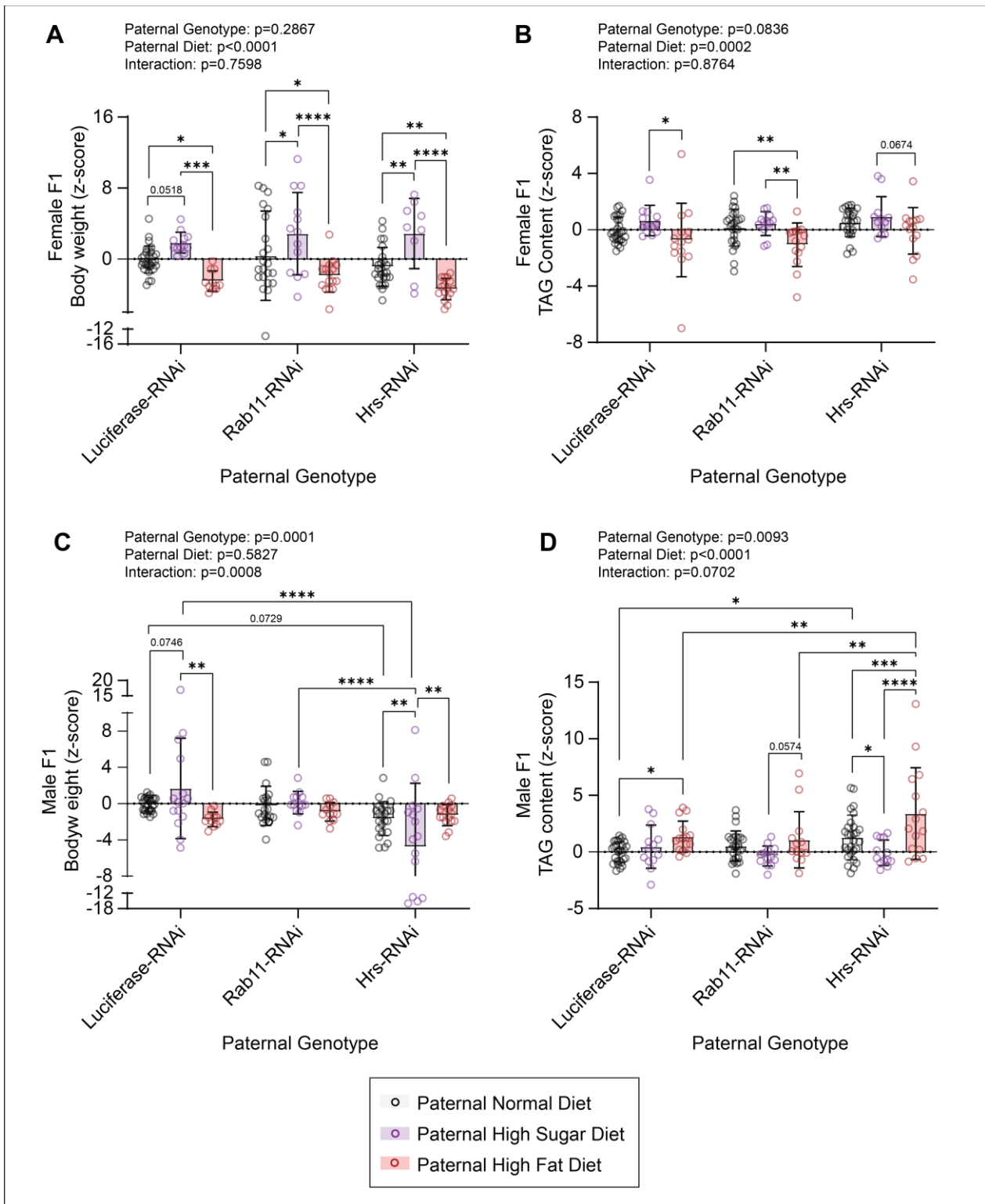


Fig. 5: Body composition of 5-day-old male and female F1 offspring derived from male F0 flies expressing *Luciferase-RNAi*, *Rab11-RNAi* and *Hrs-RNAi* under *dve-Gal4* control exposed to dietary interventions. Paternal dietary interventions include ND (black), HSD (purple) or HFD (red). Body weight and TAG content for F1 females (A ($n > 9$) and B ($n > 12$), respectively) and for F1 males (C ($n > 12$) and D ($n > 13$), respectively) are shown normalised to z-score. Graphs depict bar plots with mean \pm SD (individual data points

superimposed). Statistical significance is determined using two-way ANOVA (Fisher LSD Test: ns $p > 0.05$, * $p < 0.05$, ** $p < 0.01$, *** $p < 0.001$, **** $p < 0.0001$), with only the significance from within paternal genotype or within paternal diet comparison shown here.

TAG content from female F1 offspring is affected primarily by paternal diet as identified by two-way ANOVA ($F(2, 147) = 9.102$; $p = 0.0002$), with no significant effect coming from paternal genotype ($F(2, 147) = 2.524$; $p = 0.0836$) (Fig. 5 B). According to *post hoc* multiple comparison (Fisher LSD test), no significant differences are observed in the TAG content of the female F1 offspring between the three paternal genotypes under any dietary condition. *Post hoc* analysis within the paternal genotypes show no significant changes to the TAG content of female F1 offspring derived from F0 males expressing *Luciferase-RNAi* under *dve-Gal4* control caused by paternal HSD and HFD compared to paternal ND ($p = 0.1704$ and $p = 0.1120$, respectively) (Fig. 5 B). In contrast, the female F1 offspring from *Rab11-RNAi* fathers show a significant decrease in TAG content under paternal HFD when compared to both paternal ND and HSD ($p = 0.0097$ and $p = 0.0067$, respectively) (Fig. 5 B). The female F1 offspring derived from the *Hrs-RNAi* F0 genotype under paternal HSD and HFD lead to no significant changes in TAG content compared to paternal ND ($p = 0.4086$ and $p = 0.1957$) (Fig. 5 B). Although statistical significance is not reached, the pattern of these observations mirrors the findings in the female F1 body weight.

In summary, this data indicates that paternal diet causes an intergenerational effect on the body weight of their young adult female offspring, which is diet-dependent in its directionality, but not influenced by the paternal expression of *Rab11-RNAi* or *Hrs-RNAi* under *dve-Gal4* control (Fig. 5 A and B).

The body weight of F1 males indicates an interaction between paternal genotype and paternal diet by two-way ANOVA ($F(4, 143) = 5.072$; $p = 0.0008$) (Fig. 5 C). *Post hoc* multiple comparison analysis (Fisher LSD test) shows a trending decrease in body weight under paternal ND when comparing male F1 offspring from F0 males expressing *Luciferase-RNAi* and *Hrs-RNAi* under *dve-Gal4* control ($p = 0.0729$), suggesting an effect from the paternal expression of *Hrs-RNAi* under *dve-Gal4* (Fig. 5 C). No significant body weight differences are identified between male F1 offspring from *Luciferase-RNAi* and *Rab11-RNAi* fathers ($p = 0.6901$) (Fig. 5 C). Comparing the paternal dietary effects

within the individual paternal genotypes, *post hoc* analysis demonstrates that paternal HSD causes a trending increase in the body weight of young adult F1 males from fathers expressing *Luciferase-RNAi* under *dve-Gal4* control ($p = 0.0746$). In contrast, paternal HFD leads to a significant decrease in the body weight in male *Luciferase-RNAi* offspring when compared to paternal HSD ($p = 0.0059$) (Fig. 5 C). This observed pattern is similar to the female F1 body weight although much less prominent. Comparatively, the body weight of male F1 derived from F0 flies expressing *Rab11-RNAi* under *dve-Gal4* control shows no difference between the paternal dietary exposures (Fig. 5 C). In contrast, under paternal HSD the F1 males from *Hrs-RNAi* fathers show a significant decrease in body weight compared to paternal ND and paternal HFD ($p = 0.0026$ and $p = 0.0022$, respectively). This observed decrease is significantly different in both strength and directionality to the body weights of male F1 derived from F0 males expressing both *Luciferase-* and *Rab11-RNAi* under the same dietary regime (both $p < 0.0001$) (Fig. 5 C). These results indicate effects on the young adult male F1 body weight caused by the expression of *Hrs-RNAi* under *dve-Gal4* control in F0 males.

With regards to the male F1 TAG content, a notable trending interaction between paternal genotype and paternal diet is visible based on two-way ANOVA ($F(4, 155) = 2.212$; $p = 0.0702$) (Fig. 5 D). The effects of paternal genotype ($F(2, 155) = 4.820$; $p = 0.0093$) and paternal diet ($F(2, 155) = 11.34$; $p < 0.0001$) are significant for the male F1 TAG content (Fig. 5 D). Under paternal ND, *post hoc* multiple comparison analysis shows a significant increase in the TAG content of male F1 flies derived from F0 males expressing *Hrs-RNAi* under *dve-Gal4* control compared to the male F1 from *Luciferase-RNAi* fathers ($p = 0.0126$), suggesting an effect of the paternal expression of *Hrs-RNAi*. This pattern is similarly observed under paternal HFD with a significant increase seen in male offspring from *Hrs-RNAi* fathers compared to *Luciferase-* and *Rab11-RNAi* paternal genotypes ($p = 0.0044$ and $p = 0.0018$, respectively) (Fig. 5 D). When addressing the paternal dietary interventions within each paternal genotype, a significant increase in TAG content is seen in F1 males from *Luciferase-RNAi* expressing F0 under paternal HFD compared to the paternal ND condition ($p = 0.0276$) (Fig. 5 D). Although only trending, there is an increase in TAG content under paternal HFD in male F1 from fathers expressing *Rab11-RNAi* under *dve-Gal4* control, similar to *Luciferase-RNAi*, when compared to paternal HSD ($p = 0.0574$) (Fig. 5 D). Within the *Hrs-RNAi* paternal

genotype, male F1 show a significant increase in TAG content under paternal HFD compared to paternal ND ($p = 0.0008$) (Fig. 5 D). Additionally, paternal HSD leads to a significant decreased TAG content in male F1 from *Hrs-RNAi* when compared to paternal ND and HFD ($p = 0.0362$ and $p < 0.0001$, respectively) (Fig. 5 D).

In summary, body weight and TAG content changes in F1 males reveal diet specific intergenerational effects in both directionality and strength (Fig. 5 C and D). Notably, contrary to female F1, paternal genotype influences these phenotypic differences of the male F1 offspring, with the paternal expression of *Hrs-RNAi* under *dve-Gal4* control already leading to changes in body weight and TAG without paternal dietary interventions (Fig. 5 C and D).

3.3.2 Lifespan analysis of F1 offspring from male F0 expressing RNAi under *dve-Gal4* control exposed to dietary interventions

Lifespan analysis of male and female offspring was carried out to evaluate long-term paternal genotype effects on the offspring from male F0 expressing RNAis under *dve-Gal4* control exposed to dietary interventions.

Female F1 from *Luciferase-RNAi* fathers exposed to ND show a median survival of 49 days, while the female offspring from *Rab11-RNAi* and *Hrs-RNAi* expressing F0 males under the same paternal dietary condition have a median survival of 54 days and 56 days, respectively (Fig. 6 A). Log-rank (Mantel-Cox) test indicates a significant difference in the female F1 survival curves of the three paternal genotypes under paternal ND ($p < 0.0001$) (Fig. 6 A). A significant increase is identified in the curves when comparing female offspring of both *Rab11-RNAi* and *Hrs-RNAi* fathers to *Luciferase-RNAi* female offspring ($p = 0.0225$ and $p < 0.0001$, respectively). Investigation of paternal dietary effects shows that the median survival of female offspring from male F0 flies exposed to HSD is 49 days for *Luciferase-RNAi*, 48 days for female F1 from *Rab11-RNAi* and 47 days for female F1 from *Hrs-RNAi* fathers (Fig. 6 B), with no significant difference observable in the female offspring survival rate between any of the paternal genotypes exposed to HSD ($p = 0.1922$) (Fig. 6 B). Under paternal HFD, female F1 from F0 males expressing *Luciferase-RNAi* show a median survival of 52 days, while female F1 from *Rab11-RNAi* and *Hrs-RNAi* fathers show a median survival of 51 and 55 days, respectively (Fig. 6 C). Comparatively, there is a significant

Male offspring from male F0 flies expressing *Luciferase-RNAi* under *dve-Gal4* control exposed to ND have a median survival of 47 days, while male F1 from *Rab11-RNAi* and *Hrs-RNAi* fathers show a median survival of 43 days and 44 days, respectively (Fig. 6 D). Paternal ND leads to no significant difference in the lifespan curves of male F1 from the three F0 genotypes ($p = 0.1299$), with only a trending difference between *Luciferase-RNAi* and *Rab11-RNAi* offspring ($p = 0.0637$) (Fig. 6 D).

After paternal exposure to HSD, the median survival of the male F1 offspring from male F0 is 45 days for *Luciferase-RNAi*, 35 days for male F1 from *Rab11-RNAi* fathers and 46 days for male F1 from *Hrs-RNAi* fathers (Fig. 6 E). Paternal HFD leads to a median survival of 43 days in male F1 offspring from F0 males expressing *Luciferase-RNAi* under *dve-Gal4* control, 31 days in male F1 from *Rab11-RNAi* and 46 days in male F1 from *Hrs-RNAi* fathers (Fig. 6 F). Both paternal HSD (Fig. 6 E) and paternal HFD (Fig. 6 F) cause strong significant decreases in the survival curves of male F1 from male F0 expressing *Rab11-RNAi* under *dve-Gal4* control ($p < 0.0001$), with no significant differences observed between *Luciferase-RNAi* and *Hrs-RNAi* male offspring. Overall, the combination of paternal expression of *Rab11-RNAi* under *dve-Gal4* control and paternal dietary exposures causes a significant decrease in the male F1 lifespan.

3.3.3 Gene expression analysis of young and older adult F1 offspring from male F0 expressing *Hrs-RNAi* under *dve-Gal4* control

As changes to the phenotypic outcome of offspring have been indicated in male and female F1 from fathers expressing *Hrs-RNAi* under *dve-Gal4* control exposed to ND, whole body mRNA sequencing of young and older adult flies was carried out to analyse paternal genotype effects (Fig. 7). Gene expression analysis was carried out comparing offspring from male F0 expressing *Hrs-RNAi* and *Luciferase-RNAi* exposed to ND. Following the pattern observed in phenotypic findings, only 1 significantly downregulated DEG (FDR < 0.05) is identified in young adult female F1 offspring (Fig. 7 A), whereas older adult female F1 reveal 4 significant DEG (FDR < 0.05) and 21 genes with FDR < 0.1 (Fig. 7 B). As most of these genes are currently undescribed protein coding genes according to 'Flybase' (FB2022_05), no pathways or potential mechanisms can be currently identified (Gramates et al., 2022).

Young adult male F1 offspring from F0 males expressing *Hrs-RNAi* under *dve-Gal4* control reveal 145 significant DEG genes (FDR < 0.05) (Fig. 7 C), with older adult F1 males having no significant changes in their gene expression (Fig. 7 D). GO analysis (PANTHER, FDR < 0.05) identifies 5 enriched biological processes from the 81 significant upregulated genes of the young adult male offspring from *Hrs-RNAi* fathers, including 'cytoplasmic translation' (GO:0002181) and 'peptide biosynthetic process' (GO:0043043) (Fig. 7 E). For the 64 significantly downregulated genes, 95 biological processes were predicted, with 'axon extension' (GO:0048675) and 'neuron projection extension' (GO:1990138) among the highest fold enrichment (Fig. 7 F). These findings match the sex- and age-specific observations from the phenotypic data of both male and female offspring from F0 males expressing *Hrs-RNAi* exposed to ND.

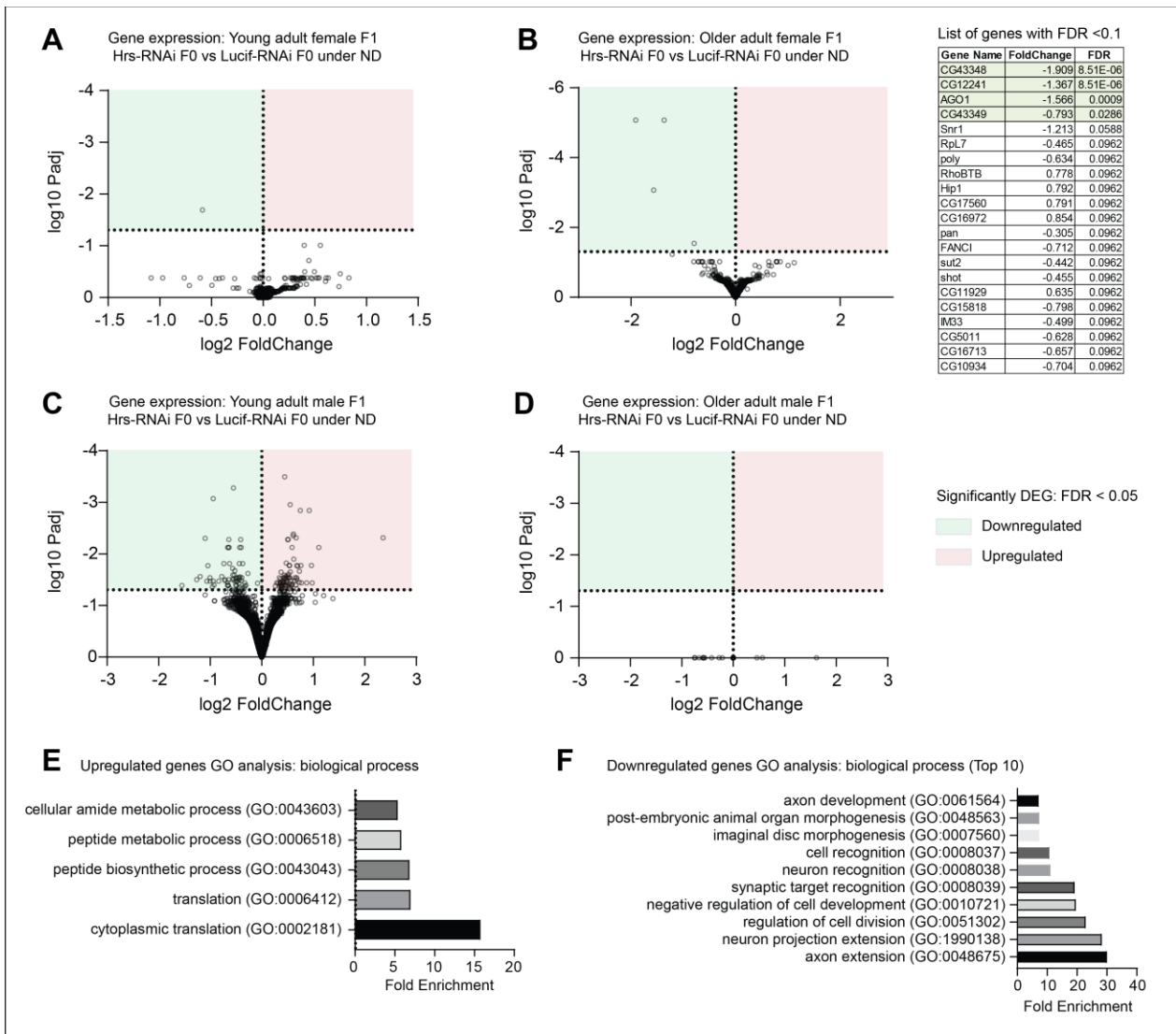


Fig. 7: mRNA sequencing analysis of young and older adult F1 from F0 males expressing *Hrs-RNAi* under *dve-Gal4* control exposed to ND. Gene expression of young (A) and older (B) adult female F1 from F0 fathers expressing *Hrs-RNAi* compared to *Luciferase-RNAi* under *dve-Gal4* control exposed to ND are shown. Genes with FDR < 0.1 of older adult female F1 are listed based on FDR (B). Differentially expressed genes in young (C) and older (D) adult male F1 flies from paternal genotypes expressing *Hrs-RNAi* are compared to *Luciferase-RNAi* under *dve-Gal4* control. Gene expression based on fold change and adjusted p-value is displayed in volcano plots on a logarithmic scale (FDR < 0.05). Significantly enriched biological processes are identified using GO analysis for the significant upregulated (E) and downregulated (F) DEG of young adult F1 males (PANTHER; FDR < 0.05). Young adult: 5 days old; Older adult: males, 3 weeks old and females, 4 weeks old. GO = gene ontology; DEG = differentially expressed genes; ND = normal diet.

3.3.4 Gene expression analysis of older adult male F1 offspring from male F0 expressing *Rab11-RNAi* under *dve-Gal4* control exposed to HSD and HFD

To investigate the paternal dietary effects observed in the male F1 lifespan from F0 fathers expressing *Rab11-RNAi* under *dve-Gal4* control, mRNA sequencing was carried out on older adult male F1 (3 weeks old) from *Rab11-RNAi* and *Luciferase-RNAi* fathers exposed to HSD and HFD (Fig. 8).

No significant DEG are identified in older adult male F1 offspring from *Rab11-RNAi* fathers under paternal ND (not shown here). Paternal HFD leads to 103 significant DEG in older adult *Rab11-RNAi* offspring compared to *Luciferase-RNAi* offspring, with 62 upregulated and 41 downregulated genes (FDR < 0.05) (Fig. 8 A). No biological processes are identified using GO analysis (PANTHER, FDR < 0.05), however 'ion binding' (GO:0043167) is predicted as an enriched molecular function.

Under paternal HSD, older adult male offspring from F0 males expressing *Rab11-RNAi* reveal 2304 significantly DEG (FDR < 0.05) (Fig. 8 B). GO analysis identified 531 significantly enriched biological processes from the 2178 upregulated genes, with 'synaptic target attraction' (GO:0016200), 'presynaptic membrane organization' (GO:0097090) and 'mannose metabolic process' (GO:0006013), among the top 10 based on fold enrichment (Fig. 8 C). For the 126 significantly downregulated genes, 6 significant biological processes are predicted including 'vitelline membrane formation involved in chorion-containing eggshell formation' (GO:0007305) with the highest fold enrichment (Fig. 8 D).

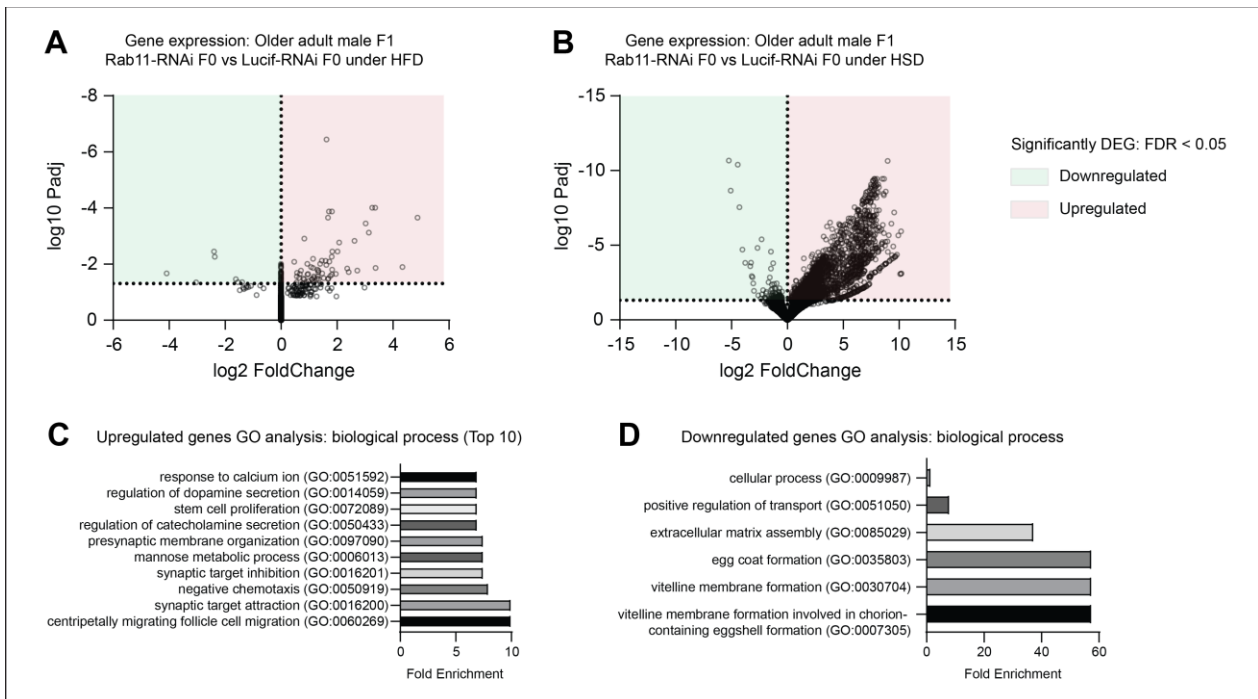


Fig. 8: mRNA sequencing analysis of older adult F1 males from F0 males expressing *Rab11-RNAi* under *dve-Gal4* control exposed to HFD and HSD. Gene expression of older adult F1 from F0 fathers expressing *Rab11-RNAi* is compared to F0 expressing *Luciferase-RNAi* under *dve-Gal4* control exposed to paternal HFD (A) and HSD (B). Gene expression based in fold change and adjusted p-value are shown in volcano plots on a logarithmic scale (FDR < 0.05). Significantly enriched biological processes are identified using GO analysis for the significant upregulated (C) and downregulated (D) DEG of older adult F1 males from F0 males expressing *Rab11-RNAi* under *dve-Gal4* control exposed HSD (PANTHER; FDR < 0.05). Older adult: males, 3 weeks. GO = gene ontology; DEG = differentially expressed genes; HFD = high fat diet; HSD = high sugar diet. Age of older adult males = 3 weeks (before lifespan drop off).

Of note, 35 significant DEG genes overlap between older adult male offspring from *Rab11-RNAi* exposed to HSD and HFD, with 27 similar in directionality (Tab. 9). As more than half of these overlapping genes are currently undescribed protein coding genes according to 'Flybase' (FB2022_05), no common pathways are currently identified (Gramates et al., 2022).

Tab. 9: List of overlapping significant DEG between older adult male F1 from F0 males expressing *Rab11-RNAi* under *dve-Gal4* control exposed to HSD and HFD. Red = upregulated; Green = downregulated.

Overlapping sigDEG	logFoldChange (FDR < 0.05)	
	HSD	HFD
CG14866	6.14949	-0.00035
Pkn	4.53384	2.62524
lncRNA:CR43652	4.46416	-0.00049
CG17107	3.71422	2.36264
bond	3.37836	1.83326
CG8303	3.03367	-3.03651
Nab2	2.56986	-4.08768
CG32023	2.56309	1.45554
CG16758	2.49347	1.39509
Lsp1beta	2.41667	3.02188
CG10934	2.37422	1.70919
Cyp309a1	2.35850	1.10157
Usp8	2.33063	1.69174
AANATL3	2.23986	1.28715
CG6218	2.22441	-0.00051
CG7296	2.15122	1.14424
CG45050	2.12492	-0.00047
CG34166	2.11214	1.80691
Dlish	2.02769	1.81898
Strn-Mlck	1.99379	-0.00057
LManIII	1.91538	1.67512
Cyp9b1	1.81597	1.10152
Gprk1	1.74306	1.67568
CG8468	1.70094	-0.00048
CG9498	1.53576	1.14463
CG15282	1.50497	1.34984
CG9331	1.49494	0.64831
Su(z)2	1.47397	0.97511
Psn	1.44311	0.96008
CG13905	1.41541	1.81815
Mcm3	1.30345	1.33832
hgo	1.22446	1.14279
Nacalpa	1.09782	0.55698
SNF4Agamma	1.08709	0.46731
Tep4	0.81356	0.56317

4. Discussion

The 'Weismann barrier' hypothesises that heritable information cannot be transmitted from somatic cells to germ cells, suggesting that paternal experiences do not change the phenotypic outcome of the next generation (Weismann, 1893). However, multiple human and animal studies show that paternal physiological and psychological conditions can affect not only the generation experiencing them, but also their descendants (Camilleri-Carter et al., 2019, Crean and Bonduriansky, 2014, Dimofski et al., 2021 and others given above in the Introduction). These intergenerational effects range from changes in body weight or reproductive success to increased risk of mortality from cancers, metabolic and cardiovascular disorders (Camilleri-Carter et al., 2019, Crean and Bonduriansky, 2014, Dimofski et al., 2021 and others given above in the Introduction). While changes to the sperm epigenome have been identified as one of the molecular mechanisms causing intergenerational effects (Champroux et al., 2018, Fitz-James and Cavalli, 2022, Ghai and Kader, 2022), how paternal experiences are transmitted from the somatic level to the germline is still unclear.

One hypothesis is that extracellular vesicles (EVs) transmit somatic cell-derived information to germ cells and cause the inherited characteristics in the next generations (Conine and Rando, 2022, Eaton et al., 2015, Smythies et al., 2014). These small membrane-bound particles act as communicators in both health and disease due to their capability to carry various cargos such as DNA, proteins and RNA species (Kalluri and LeBleu, 2020, Kalra et al., 2016, Maas et al., 2017). To date, only indirect evidence from mostly *in vitro* and a few *in vivo* studies suggest the role that EVs derived from somatic cells of the reproductive tract play in the transmission of paternal intergenerational effects (Al-Dossary et al., 2015, Chan et al., 2020, Foot et al., 2021, Martin-DeLeon, 2015, Nixon et al., 2019, Park et al., 2011, Schwarz et al., 2013, Sharma et al., 2018, Simon et al., 2018 and others as given above in the Introduction).

In this thesis, we aimed to generate an *in vivo* loss of function model by inhibiting EV secretion from a somatic cells source in the male reproductive tract. These somatic cell sources within the reproductive tract were selected in mouse and fly according to the current published literature (Corrigan et al., 2014, Hsu et al., 2010, Linnemannstöns et al., 2022, Ostrowski et al., 2010), although other somatic cell sources, even external of

the male reproductive tract, may play a role in intergenerational effects. For example, the study by Cossetti et al. (2014) demonstrated in a mouse model that EGFP RNA expressed in human melanoma cells xenografted into the brain could be found in blood-derived EVs and in the sperm of these mice. In a more recent study, O'Brien et al. (2020) similarly injected a virus expressing a specific RNA sequence into the brain of male mice, which was later detected in a third of the embryos from the fathers. Although both of these studies provide *in vivo* evidence for soma to germline communication, the experimental set-ups included viral injection and xenografting of metastatic cells, which may use other forms of intercellular communication that do not involve EVs or other forms of physiological cell-cell communication. This uncertainty is supported by a study in 2018 who demonstrated that unlike the testis and the epididymis, somatic cells of the liver did not deliver labelled RNAs to the sperm (Sharma et al., 2018). Therefore, follow up studies are recommended to repeat similar tracing procedures, but in a wider tissue range.

In this thesis, after the establishment of an *in vivo* model with inhibited EV secretion, we investigated if the inhibited secretion of somatic cell-derived EVs causes changes in the phenotypic fate of their offspring and, under paternal dietary interventions, if the inhibited secretion of these EVs leads to changes in the observed intergenerational effects.

4.1 Generation of an *in vivo* mouse model with inhibited secretion of EVs from the somatic cells of the male reproductive tract

The epididymis is a tubular tissue that connects the testis with the vas deferens. After spermatogenesis in the testis, immature spermatocytes travel through the epididymis, gaining their full functionality and motility during transit (Belleannée, 2015). Studies, mostly *in vitro* and a few *in vivo*, have shown that EVs secreted by epididymal cells interact with and transfer protein and RNA to them (Frenette et al., 2006, Griffiths et al., 2008, Martin-DeLeon, 2015, Nixon et al., 2019, Oh et al., 2009, Park et al., 2011, Reilly et al., 2016, Schwarz et al., 2013, Sharma et al., 2018, Suryawanshi et al., 2012). Furthermore, epididymal EVs are essential for sperm maturation (Foot et al., 2021) and both sperm RNA species and the content of EVs secreted by the epididymis have both been shown to change upon paternal dietary exposures (Alshanbayeva et al., 2021, Nätt et al., 2019). A recent study by Chan et al. (2020) demonstrated that incubation of sperm

with EVs from treated epididymal cell culture can mimic phenotypic changes in the offspring in mice through *in vitro* fertilisation. Due to the extensive research carried out with this mammalian model system, we aimed to establish a mouse model with decreased secretion of EVs from the epididymis into the epididymal fluid in order to investigate the impact of somatic cell-derived EVs on the phenotypic outcome on the next generation. For this purpose, three transgenic mouse lines with knockouts in protein targets known to be involved in the EV biogenesis or secretion pathway were characterised.

4.1.1 Establishment of the EV isolation method using ultracentrifugation

Within the field of EV research, many isolation and characterisation methods are currently accepted and expected (Théry et al., 2018). While some standardisation has been attempted with guidelines published by the International Society of Extracellular Vesicles, the variety of biological fluids, cell type or organism sources under investigation in EV studies lead to difficulties in establishing a uniform experimental and analysis pipeline in this field of research (Théry et al., 2018).

In this thesis, we followed the best practices as reviewed by Paul et al. (2021) to investigate EVs within the epididymal fluid, focusing on the size and protein composition as means to characterise the EVs. EVs were isolated from the epididymal fluid of mice using ultracentrifugation (UC) with pre-UC centrifugation steps to remove cell debris. While this technique has its disadvantages regarding the number and purity of EVs compared to other methods such as density gradient centrifugation, ultrafiltration or use of commercial kits (Théry et al., 2018), many published studies analysing EVs within the epididymal fluid have isolated UC-EVs using this method (Alshanbayeva et al., 2021, Caballero et al., 2013, Paul et al., 2021, Sharma et al., 2018).

With the protein composition of UC-EV samples containing well-known components of EVs (i.e., CD9, FLOT1, CD63, and CD81) and the particle size within expected ranges of EVs (i.e., approximately 100 nm in diameter) (Paul et al., 2021), the UC-EVs obtained in our study correspond with the current classifications to be identified as EVs. Of note, other non-classical EV components were also identified within the samples, leading to the conclusion that while we did indeed isolate EVs, contaminants of other non-EV structures cannot be ruled out. However, as the declaration of EV and non-EV proteins

continuously evolves, and proteins such as Apolipoproteins have been identified within the EV samples from other cell sources (Nikitidou et al., 2017, Pascua-Maestro et al., 2018), the purity of the UC-EV samples here needs to be additionally assessed using electron microscopy-based imaging.

For the purpose of this thesis, ultracentrifugation was used to isolate EVs from the mouse epididymal fluid (UC-EVs) and the analyses of UC-EVs from the mouse model candidates were carried out by comparing the candidate mouse lines with their respective controls under the same experimental conditions in order to control for non-EV contaminants.

4.1.2 Characterisation of three candidate transgenic mouse lines as *in vivo* models with inhibited secretion of EVs from the epididymis

To identify a transgenic mouse line with inhibited secretion of EVs from the epididymis into the epididymal fluid, three candidate mouse lines were investigated. Transgenic lines targeting *Rab35*, *Rab27a/b* and *Sytl4* were selected as these targets are known components of the EV biogenesis or secretion pathway and their knockout has been shown to lead to inhibited EV secretion in cell culture (Hsu et al., 2010, Ostrowski et al., 2010). In all three transgenic mouse lines, no differences were identified in UC-EV size or amounts in this study. There are many explanations for this with the first being that the endogenous expression level of the targets is not high in the epididymal tissue, hence, the KO of the target genes did not lead to an effect. However, according to the Expression Atlas from EMBL-EBI, both *Rab27a/b* and *Sytl4* are highly expressed in the epididymis (Papatheodorou et al., 2020). While *Rab35* is not highly expressed in the epididymis, but instead in the other organs such as the kidney (Papatheodorou et al., 2020), the homozygous *Rab35^{flox}-Cdh16^{cre}* mice were not viable, indicating that the KO did indeed work, although the lethality is potentially connected to the conditional expression of *Cdh16-cre* in the kidney.

The second probable reason why there are no changes in the amount of EVs within the epididymal fluid of the three transgenic mouse lines is that the selected KO targets are not essential for EV biogenesis or secretion within the epididymal tissue. The targets were selected based on published literature, which demonstrates that RAB proteins are involved in endocytosis and that SYTL4 modulates exocytosis (Hsu et al., 2010,

Ostrowski et al., 2010). In cell culture models, the KO of these targets inhibits EV secretion (Hsu et al., 2010, Ostrowski et al., 2010). As the same KO in the epididymis does not cause similar effects on the EV secretion, other proteins may be essential for the EV biogenesis or secretion pathways in the epididymis or there are pathways compensating for the loss of the targeted proteins (Colombo et al., 2014). The findings from this study highlight the complexity and transferability challenge within the EV field between cell types and model organisms.

Although the transgenic mouse lines do not show a significant change in the number or size of EVs, the KO of the targeted proteins could potentially change the EV content. It is known that EVs carry various RNA species, including mRNA and small non-coding RNA. In this study, the mRNA content of the UC-EVs from Rab35flox-Cdh16cre and Rab27DKO mice was analysed. Follow up studies are recommended to also investigate the small RNA, as this analysis was not within the scope of this study due to technical reasons.

While there were no significant differentially expressed genes (DEG) in the UC-EVs from Rab35-het mice, *Rab27b* was non-significantly downregulated indicating that there may be a connection between the expressed *Rab35* within epididymal cells and the packaging of *Rab27b* mRNA into EVs. Therefore, it is necessary to investigate this finding further for example by analysing changes in *Rab27b* expression in the epididymal tissue.

In the Rab27DKO mouse line, gene ontology analysis identified many biological processes connected with sperm motility in the significantly upregulated DEG of UC-EV samples. This is of interest as EVs have been suggested to play a role in the sperm maturation process based on mostly *in vitro* evidence (Al-Dossary et al., 2015, Chan et al., 2020, Foot et al., 2021, Griffiths et al., 2008, Martin-DeLeon, 2015, Nixon et al., 2019, Reilly et al., 2016, Sharma et al., 2018, Simon et al., 2018 and others given above in the Introduction). To date, only Foot et al. (2021) have shown evidence of this role of EVs in an *in vivo* environment by inhibiting the secretion of Arrdc4-dependent EVs from the epididymis disrupting sperm motility and fertilisation capabilities. In this thesis, we are the first to demonstrate that the mRNA content of EVs secreted by the epididymis may be one of the factors to influence the sperm maturation process, particularly sperm motility. It is important to note here that the Rab27DKO line remained fertile, indicating

that *Rab27a and b* KO in the epididymis did not cause pernicious effects to the germ cells. Follow up studies are recommended to investigate the sperm motility of this line.

As all three candidate mouse lines showed no decreased number of EVs in the epididymal fluid, these lines are not suitable as *in vivo* models for the inhibited secretion of EVs from somatic cells within the reproductive tract. Only the Rab27DKO line demonstrated changes to the mRNA content of EVs within the epididymal fluid. However, as this line contains a global KO of *Rab27a* and *Rab27b*, any experiments carried out investigating the phenotypic outcome of the next generation through paternal exposures, e.g. diets could be affected by the global system change (including *Rab27* in spermatogenic cell lineages).

Follow up studies are recommended to generate and investigate mouse lines targeting alternative EV pathway components, such as *Rab11*. For this purpose, a line with a KO of *Rab11* specifically in the epididymis needs to be established. This will ensure that future studies do not include confounding factors such as the influence of other organs and can include suitable corresponding controls.

4.2 Investigation of the impact of EVs secreted by somatic cells of the male reproductive tract on the phenotypic outcome of the next generation in *Drosophila melanogaster*

As establishing a mammalian model with inhibited secretion of EVs within the male reproductive tract remains challenging, we generated a *Drosophila melanogaster* model using the *UAS-Gal4* system. The accessory gland (AG) is a prostate-like secretory organ that produces most components of the seminal fluid (Wilson et al., 2017). Previous studies have demonstrated that EVs are secreted by secondary cells (SCs) within the AG and are transported to the female reproductive tract upon mating where they interact with sperm (Corrigan et al., 2014, Wilson et al., 2017). The conserved pathways between *Drosophila melanogaster* and mammals (Eickelberg et al., 2022), added to the number of published studies on EVs (Beckett et al., 2013, Beer and Wehman, 2017, Fan et al., 2020, Gross et al., 2012, van Niel and Théry, 2020) and paternal inter- and transgenerational effects in *Drosophila melanogaster* (Camilleri-Carter et al., 2019, Dew-Budd et al., 2016, Emborski and Mikheyev, 2019, Guida et al., 2019, Zajitschek et al., 2017), provided strong grounds to investigate the impact of EVs

from somatic cells on the phenotypic outcome of the next generation using the *Drosophila Melanogaster* model system.

4.2.1 CD63-GFP is used as a marker for EVs secreted by SCs in the *Drosophila melanogaster* AG lumen

CD63 is a well-known marker for EVs within many biological fluids and a variety of model organisms (Théry et al., 2018). In this thesis, human CD63-GFP was expressed within somatic cells of the male reproductive tract to label EVs using the *UAS-Gal4* system as described by Corrigan et al. (2014). The *Drosophila melanogaster* line expressing CD63-GFP was first published by Panáková et al. (2005) and has since been used in multiple studies to investigate the endosomal system (Ma et al., 2022, Mezzofanti et al., 2019, Shibata et al., 2017). Labelled expression of CD63 with GFP or other tags has been used as an EV marker in multiple studies in a variety of different *Drosophila melanogaster* tissues, such as the male reproductive tract (Corrigan et al., 2014, Dar et al., 2021, Fan et al., 2020), the female reproductive tract (Sanchez-Lopez et al., 2022), the adult wing (Gross et al., 2012) and larval fat body (Linnemannstöns et al., 2022). Corrigan et al. (2014) and this study show that targeting known components of the EV secretion or biogenesis pathway using genetic manipulations, such as RNAis, inhibit the secretion of CD63-GFP puncta visibility within a given biological fluid.

It is important to note here that *CD63* is not an endogenous gene in *Drosophila melanogaster*. In a study in 2013, Beckett et al. (2013) carried out mass spectrometry to identify the protein composition of EVs isolated from S2 tub-Wg cells. Within this *in vitro* dataset, 2 tetraspanins were identified: Tsp42Ee and Tsp42Ef (Beckett et al., 2013). The fly genetics database 'Flybase' (via DIOPT v8.0) describes Tsp42Ee as an orthologue of CD63 and TSPAN3 for human and other model organisms (Gramates et al., 2022). Furthermore, Ma et al. (2022) demonstrated that mammalian CD63 and fly Tsp29Fa are functionally conserved. Based on this information, CD63-GFP is a good candidate as a marker to visualise EVs within *Drosophila melanogaster*.

If technically possible, EV analysis in *Drosophila melanogaster* would follow the same guidelines as for other experimental organisms (Théry et al., 2018). This includes isolation of EVs from the AG lumen, visualisation and quantification by e.g. NTA and EM, and additional molecular characterisation by their protein or RNA composition. Due

to the minute amount of fluid obtainable from the AG lumen containing EVs, these recommended characterisation steps are technically challenging and therefore, were not possible at the time of this study.

Hence, two possible follow up studies are recommended here. The first is to isolate the seminal fluid containing CD63-GFP puncta within the AG lumen in the same way as sperm is isolated and analysed from the male *Drosophila melanogaster* reproductive tract. This would entail dissecting the AG tissue and collecting the AG fluid contents in PBS. However, this method is technically challenging since from the whole adult body only 1 µl hemolymph is attained from 50 to 100 flies (Piyankarage et al., 2012). Due to the small amount of fluid within the AG lumen and the fact that EVs only contribute a minor part to this luminal fluid, the number of flies needed for EV analysis would likely be in the thousands, which would probably make this invertebrate model not feasible.

The second recommended method to analyse the EVs within the AG lumen would be to characterise the seminal fluid protein composition. As described by Sepil et al. (2019), AG luminal fluid contents, such as EVs, can be analysed by comparing the proteome of the whole AG pre-mating (i.e. containing seminal fluid and EVs) and post-mating (i.e. empty of seminal fluid and EVs). Therefore, additional analysis can be carried out comparing this proteomic data to the female reproductive tract pre-mating (i.e., without seminal fluid) and post-mating (i.e., containing seminal fluid) (Sepil et al., 2019). Through this quantitative and qualitative comparative analysis, EVs and other seminal fluid protein components can be analysed in the AG lumen of *Drosophila melanogaster*. To express CD63-GFP specifically in SCs within the AG lumen, the *dve-Gal4* driver was selected as it is the least detrimental and most effective driver currently available. Although *dve* is expressed in both SCs and in the midgut (Krause et al., 2022), potentially causing confounding effects, other *gal4* lines used in other publications are unsuitable. Published SC-specific drivers such as *esg-Gal4*, *dsx-Gal4*, *iab-Gal4* and *prd-Gal4* either express in other organs such as the gut, brain, salivary gland, or the entire AG structure (Corrigan et al., 2014, Dar et al., 2021, Gligorov et al., 2013, Leiblich et al., 2012, Minami et al., 2012, Prince et al., 2019) and therefore, made them unsuitable for this particular study.

Under *dve-Gal4* control three selected RNAis targeting components known to be involved in the EV biogenesis or secretion pathway were expressed specifically in SCs

within the male reproductive tract. An RNAi line targeting Luciferase, a firefly gene, was used as the control. The expression of *Alix-RNAi*, *Rab11-RNAi* and *Hrs-RNAi* under *dve-Gal4* control resulted in varying changes in the number of CD63-GFP puncta secreted by SCs into the AG lumen. Previous publications have demonstrated that *Alix* is essential for the formation of ILVs and targeted inhibition of *Alix* leads to changes to the EV secretion (Baietti et al., 2012, Corrigan et al., 2014, Sanchez-Lopez et al., 2022). In this study the expression of *Alix-RNAi* in SCs did not lead to decreased amounts of CD63-GFP puncta in the AG lumen. This is possibly caused by basic experimental issues due to the functionality of the RNAi and the expression strength of the *gal4* driver component. Another cause could be the complexity and diversity of EV secretion and biogenesis pathways in different cell types, resulting in the lack of transferability between model organisms.

Expressing the other two selected RNAis targeting *Rab11* and *Hrs* under *dve-Gal4* control successfully decreased the number of CD63-GFP puncta secreted by SCs into the AG lumen, as previously published (Corrigan et al., 2014, Sanchez-Lopez et al., 2022). Although the expression of *Rab11-RNAi* under *dve-Gal4* control resulted in the highest decrease of CD63-GFP puncta within the AG lumen among the three RNAi candidates, other effects were observed in these flies. These included the disruption of the intraluminal space within the SCs and a significant decrease in lifespan, which were not seen in the line expressing *Hrs-RNAi* under *dve-Gal4* control.

Based on current literature, *Rab11* plays an essential role in EV secretion and biogenesis, particularly in the vesicle recycling pathway in multiple cell types, such as the *Drosophila* S2 cells (Beckett et al., 2013, Blanc and Vidal, 2018, Savina et al., 2002). As a component of ESCRT 0 complex, *Hrs* has been demonstrated to be required for EV biogenesis and secretion in both mammals and flies (Colombo et al., 2013, Corrigan et al., 2014, Gross et al., 2012, Tamai et al., 2010). The differing effects of the number of CD63-GFP puncta secreted by SCs into the AG lumen, on the SC intraluminal structure, and on the lifespan between the lines expressing *Rab11-RNAi* and *Hrs-RNAi* under *dve-Gal4* control may be explained by the fact that *Rab11* and *Hrs* are components of different EV pathways. This suggests that different EV biogenesis or secretion pathways may be affected by *Rab11-RNAi* and *Hrs-RNAi* expression under *dve-Gal4* control in the SCs.

Although the *Rab11-RNAi* flies are shown in this study to experience detrimental lifespan changes indicating potential confounding effects, the expression of *Rab11-RNAi* causes the strongest inhibited secretion of CD63-GFP puncta by SCs into the AG lumen. Therefore, in this study the investigation of the impact of EVs secreted by somatic cells of the male reproductive tract on the next generation was carried out with both *Rab11-RNAi* and *Hrs-RNAi* as both cause the inhibited secretion of CD63-GFP puncta by SCs into the AG lumen but to different levels and with possibly different EV pathways affected.

4.2.2 F0 body composition and fecundity are not changed by the expression of RNAi lines under *dve-Gal4* control, but by dietary exposures

Male F0 flies expressing *Rab11-RNAi*, *Hrs-RNAi*, and *Luciferase-RNAi* under *dve-Gal4* control were exposed to a 30 % high sugar diet (HSD) or a 30 % high fat diet (HFD). These diets have been shown in previous publications to cause phenotypic changes in the exposed animals and to cause intergenerational effects (Camilleri-Carter et al., 2019, Eickelberg et al., 2022).

Effects resulting from the genotype and dietary exposure were analysed for the F0 flies. Common readouts for body composition, body weight and TAG content demonstrated that the expression of *Rab11-RNAi* and *Hrs-RNAi* under *dve-Gal4* control do not cause overall genotype effects under the tested dietary conditions. Similar to previous publications, phenotypic changes to the male F0 flies are caused by dietary exposure (Eickelberg et al., 2022, Tennessen et al., 2014). The body weight of F0 flies is found to be changed in a diet-dependent way. Exposure to HSD causes a decrease in body weight in all three F0 lines. A possible explanation for this is dehydration, as a recent study published by van Dam et al. (2020) demonstrated that detrimental effects of HSD on the lifespan could be reversed if given access to water. Under HFD, body weight increases as previously described (Eickelberg et al., 2022, Tennessen et al., 2014). Some of the body weight changes may be explained by the increase in TAG content in all F0 genotypes after dietary exposure, indicating that the excess sugar and fat in the food is being stored in for example, the fat body (Chatterjee and Perrimon, 2021). Notably, the expression of *Rab11-RNAi* and *Hrs-RNAi* within somatic cells under *dve-*

Gal4 control and the exposure to diets with high sugar and high fat content do not cause any changes to the fecundity of the male F0 flies.

These findings lead to the conclusion that the expression of *Rab11-RNAi* and *Hrs-RNAi* under *dve-Gal4* control do not cause genotype effects in the body composition and fecundity as mainly dietary exposures lead to phenotypic changes in the F0.

4.2.3 Sex-specific phenotypic changes are observed in the offspring from male flies expressing RNAis under *dve-Gal4* control exposed to dietary interventions

To determine the role of somatic cell-derived EVs on the phenotypic outcome of the next generation, F1 offspring were generated from male F0 flies expressing *Rab11-RNAi* and *Hrs-RNAi* under *dve-Gal4* control exposed to dietary interventions. F1 offspring from male F0 flies expressing *Luciferase-RNAi* under *dve-Gal4* control acted as the controls. The variety of published intergenerational studies show no clear consensus on what phenotypic changes occur in the next generation as this is dependent on the type, concentration, and duration of paternal exposure (Dew-Budd et al., 2016, Emborski and Mikheyev, 2019, Guida et al., 2019, Öst et al., 2014, Teltumbade et al., 2020, Zajitschek et al., 2017). In this thesis, the body weight, TAG content, lifespan, and whole-body transcriptomics of adult male and female F1 were analysed to gain a wide overview of phenotypic readouts. It is important to note here that the selected F1 flies do not carry the paternal *dve-Gal4* and RNAis components and are exposed purely to ND and therefore, consequently any phenotypic changes observed in the F1 offspring are derived from paternal genotype and/or dietary effects.

Five-day old young adult female offspring derived from fathers expressing *Rab11-RNAi* and *Hrs-RNAi* under *dve-Gal4* control were taken and it was found that their body composition changes in a paternal diet dependent manner. Paternal HSD causes an increase in body weight and paternal HFD causes a decrease in body weight. Previous publications confirm the observed paternal diet dependent body weight changes in the female F1 (Emborski and Mikheyev, 2019, Guida et al., 2019). This paternal diet dependent directional change in the female F1 offspring body weight is not affected by the paternal expression of *Rab11-RNAi* and *Hrs-RNAi* under *dve-Gal4* control. This implies that somatic-cell-derived EVs (more specifically, secondary-cell-derived EVs) are not involved in the paternal-diet-mediated modification of phenotypic outcomes in young

adult female offspring. Although the female F1 fat content, assessed here by TAG content, corresponds with the paternal diet dependent directional changes observable in the body weight and are independent of the paternal genotype, the paternal diet directional effects appear less strong than for body weight. This finding suggests that other body composition modifications may be linked to the observable body weight changes. Body composition is determined by not only fat mass (here analysed by TAG content), but also factors including bone mass, muscle mass and water retention (Lemos and Gallagher, 2017). To address whether these factors contribute to the changing body weight, tissue specific analyses by either FACS analysis or histology are recommended in future studies to quantify for example, muscle mass.

Although intergenerational effects are caused primarily by paternal dietary interventions in young adult female flies independent of paternal EV secretion status, the paternal expression of *Rab11-RNAi* and *Hrs-RNAi* under *dve-Gal4* control does lead to changes in the lifespan of their female F1 offspring. This paternal genotype effect is also dependent on the paternal diet as female offspring of both *Rab11-RNAi* and *Hrs-RNAi* show an increased lifespan compared to female offspring from fathers expressing *Luciferase-RNAi* under *dve-Gal4* control exposed to ND. However, paternal HSD and HFD do not lead to major differences in the female F1 lifespan from the three F0 genotypes. RNA sequencing carried out on female F1 offspring from fathers expressing *Hrs-RNAi* under *dve-Gal4* control confirms these age-dependent observations in the female F1 *Hrs-RNAi* offspring. Young adult females from *Hrs-RNAi* fathers reveal no paternal genotype dependent gene expression changes under paternal ND, corresponding with the body composition findings.

To investigate the age-dependent observations, gene expression changes were also analysed in older female F1 flies (4 weeks old). This analysis time point, just before the lifespan drops, was selected to avoid survival bias within the dataset. Older female F1 from *Hrs-RNAi* fathers exposed to ND reveal some significant gene expression changes. Although only around 20 genes are differentially expressed and most are currently uncharacterised genes, these findings, added to the lifespan observations, indicate an age-dependent paternal genotype effect in female F1 offspring stemming from the paternal expression of RNAis targeting components of the EV pathway in SCs. Follow up studies are recommended to carry out phenotypic analysis of the older F1 females to

investigate, which mechanisms could be the cause of the lifespan changes and whether the observed paternal diet dependent intergenerational effects are long-term.

Young adult male offspring from male F0 flies expressing *Rab11-RNAi* and *Hrs-RNAi* reveal paternal diet and paternal genotype dependent phenotypic changes. Although the body composition changes in a paternal diet dependent manner, paternal genotype influences some of the observed phenotypic changes. Paternal HSD leads to an increase in body weight in the male F1 flies from the paternal *Luciferase* control genotype similar to the observed effect in the female F1. In comparison, the paternal expression of *Rab11-RNAi* under *dve-Gal4* control ameliorates this body weight change while *Hrs-RNAi* causes a decrease in body weight. The fat content (as assessed here by TAG content) under paternal HSD does not change in the young adult F1 offspring from any of the three paternal lines. This indicates that the phenotypic changes in the body weight are not caused by altered fat storage, but potentially by other contributing factors to the body composition such as muscle mass or water retention, as discussed similarly for the female F1 findings (Lemos and Gallagher, 2017). The differing body weight observations in the young adult male F1 may be explained by the targets of the RNAis in the fathers. As described above, Rab11 and Hrs are involved in different EV biogenesis and secretion pathways (Beckett et al., 2013, Blanc and Vidal, 2018, Colombo et al., 2013, Colombo et al., 2014, Gross et al., 2012, Savina et al., 2002, Tamai et al., 2010), consequently different EV types or other cellular mechanisms may be altered by the expression of the RNAis under *dve-Gal4* control. Notably, the observed paternal genotype effects are primarily diet dependent as they are only observed under paternal HSD, while paternal HFD causes the same body composition changes in the young adult male F1 offspring for all three paternal genotypes.

Under paternal ND, both the body weight and fat content of male F1 from *Hrs-RNAi* fathers are changed signifying a paternal genotype effect from the paternal expression of *Hrs-RNAi* in the fathers under *dve-Gal4* control. Gene expression analysis of young adult male F1 offspring derived from fathers expressing *Hrs-RNAi* exposed to ND also identified a number of paternal genotype effects with a significant overrepresentation of gene ontologies such as protein synthesis and neurogenesis among differentially expressed genes. Follow up studies are recommended to investigate in particular changes to the protein synthesis pathway to identify potential mechanisms behind the

phenotypic changes in the young adult male F1 from fathers expressing *Hrs-RNAi* under *dve-Gal4*. Notably, these effects are not long-term as no differentially expressed genes were identified in older adult male F1 flies (3 weeks old) from *Hrs-RNAi* fathers compared to *Luciferase-RNAi* fathers. This finding must be followed up with phenotypic analyses in order to confirm the absence of phenotypic changes.

Paternal genotypes effects are not observed under paternal ND on the lifespan of the male F1 offspring. Notably, a drastic decrease in lifespan is observed in male F1 offspring from *Rab11-RNAi* fathers exposed to HSD and HFD that is not seen in the female F1. As these sex-specific lifespan changes are not observed under paternal ND and the offspring from *Hrs-RNAi* fathers do not display the same lifespan changes under paternal dietary intervention, the phenotypic effects resulting from the expression of *Rab11-RNAi* under *dve-Gal4* control in the fathers combined with the dietary interventions cause the observed survival decreases in the male F1 flies.

Although RNA sequencing revealed no changes in the young adult male F1 from fathers expressing *Rab11-RNAi* under *dve-Gal4* control, older adult male offspring from *Rab11-RNAi* fathers revealed significant differentially expressed genes under both paternal HSD and HFD, corresponding with the lifespan findings. While no enriched biological process could be identified for the male F1 under paternal HFD, older adult male offspring from *Rab11-RNAi* fathers exposed to paternal HSD reveal a wide variety of predicted pathways, ranging from developmental to signal transduction processes. Notably, 35 genes are similarly differentially expressed between male F1 flies from *Rab11-RNAi* fathers exposed to HSD and HFD, with 27 genes following the same directionality. As many of the differentially expressed genes are currently undescribed protein coding genes (Gramates et al., 2022), it is challenging to identify potential molecular mechanisms or pathways that cause the paternal *Rab11-RNAi* genotype and diet effects on the male F1 lifespan.

In the F0 males, under *dve-Gal4* control, *Rab11-RNAi* is expressed specifically in SCs within the reproductive tract and also in the cardia, R1 and R4 regions of the *Drosophila melanogaster* midgut (Buchon et al., 2013). The expression of *Rab11-RNAi* in cells of the midgut could cause in a similar manner disruptions of the intraluminal structures and inhibited EV secretion as observed in the SCs. Previous publications have investigated the effects of *Rab11* expression and dietary changes in the midgut with a research focus

on gut microbiome, stem cells, cancers, and inflammation (Bonfini et al., 2021, Nie et al., 2019, von Frieling et al., 2020, Yu et al., 2014, Zhang et al., 2017). Owing to the observed findings in this thesis and the current literature, we hypothesise that under *dve-Gal4* control *Rab11-RNAi* causes disruptions to midgut cells that are exaggerated by exposure to HSD or HFD either directly or through the gut microbiome. These midgut modifications cause pernicious effects on the next generation in a sex specific manner. The findings in the thesis have not been shown by others and reveal another paternal condition that causes intergenerational effects. Follow up studies are recommended to repeat the F1 analysis pipeline from this thesis with an F0 *Drosophila melanogaster* line that expresses *Rab11-RNAi* specifically in the midgut in order to investigate this possible mechanism behind this sex-specific intergenerational effect.

Overall, sex-specific intergenerational effects are also well described in human, mammalian studies and invertebrate studies (Dew-Budd et al., 2016, Emborski and Mikheyev, 2019, Gong et al., 2021, Huypens et al., 2016, Ng et al., 2010, Pembrey et al., 2006, Vågerö et al., 2018). Currently, these sex-specific changes still remain to be elucidated, although hormonal differences have been hypothesised as the cause, as for example oestrogen has protective functions against cardiovascular and metabolic diseases (Dearden et al., 2018). Therefore, this is another area that should be investigated in future studies.

In general, relating to the findings here follow up studies are recommended to perform LC-MS/MS on both male and female F1 offspring from fathers expressing *Rab11-* and *Hrs-RNAi* under *dve-Gal4* control, as some insights may be gained into the offspring phenotypic changes from analysing the protein level that cannot be elucidated by RNA analysis, e.g. post-translational modifications.

4.3 Conclusion

In this thesis, the impact of EVs secreted by somatic cell sources of the male reproductive tract on the phenotypic outcome of the next generation was analysed.

Attempting to establish a mammalian *in vivo* loss of function model demonstrated the complexity and the lack of transferability between cell types and model organisms in the field of EV research. However, mRNA sequencing analysis of Rab27DKO mice revealed that the mRNA content of EVs within the epididymal fluid are potentially involved in sperm maturation, particularly the motility process.

Therefore, an *in vivo* model with inhibited secretion of CD63-GFP from somatic cells of the male reproductive tract was established in *Drosophila melanogaster* using the *UAS-Gal4* system to express RNAs targeting known components of the EV pathway. These male F0 were exposed to dietary interventions prior to mating. The generated offspring of these flies revealed paternal genotype and paternal dietary dependent phenotypic changes, gene expression changes and changes to the F1 lifespan. We are the first to demonstrate sex-specific and age-dependent paternal intergenerational effects in an *in vivo* depletion model of somatic cell-derived EVs.

5. Abstract

Evidence from both human and animal studies demonstrate that paternal experiences and exposures can cause phenotypic changes in the next generation. Extracellular vesicles (EVs) released by somatic cells are hypothesised to play a role in these paternal effects by acting as a messenger between somatic cells, including those of the male reproductive tract, and germ cells. To date, evidence acquired mainly from *in vitro* and a few *in vivo* studies confirm this EV-sperm interaction and information transfer. In this thesis, we aimed to establish an *in vivo* model system, in the mouse and in the fly, with inhibited secretion of EVs from somatic cells of the male reproductive tract, with the intention to utilise this model to study the impact of EVs on phenotypic outcomes in the next generation and their role as potential mediators of paternal intergenerational effects.

Within the epididymis of the male mouse reproductive tract, the knock-out of three different genes encoding proteins shown in *in vitro* studies to be involved in EV secretion or biogenesis did not change the number or size of EVs isolated from the epididymal fluid. This finding demonstrates the difficulty of transferability between model organisms in the EV field. Notably, mRNA sequencing analysis of the epididymal EVs from *Rab27*-DKO mice suggests a potential involvement of the EV mRNA in the sperm maturation process.

Using the UAS-Gal4 system, we established a *Drosophila melanogaster* model with an inhibited secretion of CD63-GFP from secondary cells, by expressing RNAis against known components of the EV pathway. Prior to mating, these F0 flies were exposed to dietary interventions. Phenotypic and transcriptomic analyses of the generated F1 flies demonstrate paternal genotype and paternal diet dependent changes. These paternal intergenerational effects are firstly sex-specific and age-dependent, and secondly influenced by somatic cell-derived EVs. Furthermore, we are the first to observe that the exposure of male flies expressing *Rab11-RNAi* under *dve-Gal4* control to high sugar and high fat diet cause pernicious sex-specific intergenerational effects. This finding is suggested to be caused by the combined vulnerability of paternal midgut cells and the exposure to energy dense foods, a so far unexplored paternal condition that causes phenotypic changes to the next generation.

6. List of figures

- Fig. 1: Protein composition analysis and size quantification of EVs isolated from epididymal fluid from WT mice using ultracentrifugation. 34
- Fig. 2: Evaluation of candidate mouse lines with a knockout of proteins involved in EV biogenesis or secretion pathways by UC-EV size and RNA content. 38
- Fig. 3: Evaluation of CD63-GFP puncta secreted by SCs of male *Drosophila melanogaster* expressing RNAis under *dve-Gal4* control. 43
- Fig. 4: Body composition and fecundity analysis of 10-day old adult male F0 flies expressing *Luciferase-RNAi*, *Rab11-RNAi* and *Hrs-RNAi* under *dve-Gal4* control post exposure to ND, HSD or HFD. 45
- Fig. 5: Body composition of 5-day-old male and female F1 offspring derived from male F0 flies expressing *Luciferase-RNAi*, *Rab11-RNAi* and *Hrs-RNAi* under *dve-Gal4* control exposed to dietary interventions. 47
- Fig. 6: F1 offspring survival curves from F0 fathers expressing *Luciferase-RNAi*, *Rab11-RNAi* and *Hrs-RNAi* under *dve-Gal4* control exposed to dietary interventions. 51
- Fig. 7: mRNA sequencing analysis of young and older adult F1 from F0 males expressing *Hrs-RNAi* under *dve-Gal4* control exposed to ND. 54
- Fig. 8: mRNA sequencing analysis of older adult F1 males from F0 males expressing *Rab11-RNAi* under *dve-Gal4* control exposed to HFD and HSD. 56

7. List of tables

Tab. 1: Genotype, strain, sex and age of the lines analysed as candidate models of mice with decreased amount of EVs within the epididymal fluid.	19
Tab. 2: List of primary antibodies used for either Western blot protein analysis of mice UC-EVs and antibodies used for fluorescence imaging of the male <i>Drosophila</i> AG.	21
Tab. 3: List of secondary antibodies used in either Western plot protein analysis of mice UC-EVs and antibodies used for fluorescence imaging of the male <i>Drosophila</i> AG.	22
Tab. 4: Acquired and generated <i>Drosophila Melanogaster</i> lines used within this study.	25
Tab. 5: Ingredients for a normal diet and supplements for high sugar or high fat diets.	27
Tab. 6: List of consumables and reagents used in the experiments of this thesis.	30
Tab. 7: List of equipment and software used in the experiments and analysis of this thesis.	32
Tab. 8: Top 10 genes identified in UC-EV mRNA sequencing, sorted based on p-value.	39
Tab. 9: List of overlapping significant DEG between older adult male F1 from F0 males expressing <i>Rab11-RNAi</i> under <i>dve-Gal4</i> control exposed to HSD and HFD.	57

8. References

Al-Dossary AA, Bathala P, Caplan JL and Martin-DeLeon PA. Oviductosome-Sperm Membrane Interaction in Cargo Delivery: Detection of fusion and underlying molecular players using three-dimensional super-resolution structured illumination microscopy (SR-SIM). *J Biol Chem*, 2015; 290: 17710-17723

Alshanbayeva A, Tanwar DK, Roszkowski M, Manuella F and Mansuy IM. Early life stress affects the miRNA cargo of epididymal extracellular vesicles in mouse†. *Biol Reprod*, 2021; 105: 593-602

Alvarez-Erviti L, Seow Y, Yin H, Betts C, Lakhai S and Wood MJ. Delivery of siRNA to the mouse brain by systemic injection of targeted exosomes. *Nat Biotechnol*, 2011; 29: 341-345

Baietti MF, Zhang Z, Mortier E, Melchior A, Degeest G, Geeraerts A, Ivarsson Y, Depoortere F, Coomans C, Vermeiren E, Zimmermann P and David G. Syndecan-syntenin-ALIX regulates the biogenesis of exosomes. *Nat Cell Biol*, 2012; 14: 677-685

Becker A, Thakur BK, Weiss JM, Kim HS, Peinado H and Lyden D. Extracellular Vesicles in Cancer: Cell-to-Cell Mediators of Metastasis. *Cancer Cell*, 2016; 30: 836-848

Beckett K, Monier S, Palmer L, Alexandre C, Green H, Bonneil E, Raposo G, Thibault P, Le Borgne R and Vincent JP. *Drosophila* S2 cells secrete wingless on exosome-like vesicles but the wingless gradient forms independently of exosomes. *Traffic*, 2013; 14: 82-96

Beer KB and Wehman AM. Mechanisms and functions of extracellular vesicle release in vivo-What we can learn from flies and worms. *Cell Adh Migr*, 2017; 11: 135-150

Belleannée C. Extracellular microRNAs from the epididymis as potential mediators of cell-to-cell communication. *Asian J Androl*, 2015; 17: 730-736

Belleannée C, Calvo É, Caballero J and Sullivan R. Epididymosomes convey different repertoires of microRNAs throughout the bovine epididymis. *Biol Reprod*, 2013; 89: 30

Beylerli O, Gareev I, Sufianov A, Ilyasova T and Guang Y. Long noncoding RNAs as promising biomarkers in cancer. *Noncoding RNA Res*, 2022; 7: 66-70

Blanc L and Vidal M. New insights into the function of Rab GTPases in the context of exosomal secretion. *Small GTPases*, 2018; 9: 95-106

Bodden C, Pang TY, Feng Y, Mridha F, Kong G, Li S, Watt MJ, Reichelt AC and Hannan AJ. Intergenerational effects of a paternal Western diet during adolescence on offspring gut microbiota, stress reactivity, and social behavior. *Faseb j*, 2022; 36: e21981

Bohacek J, Farinelli M, Mirante O, Steiner G, Gapp K, Coiret G, Ebeling M, Durán-Pacheco G, Iniguez AL, Manuella F, Moreau JL and Mansuy IM. Pathological brain plasticity and cognition in the offspring of males subjected to postnatal traumatic stress. *Mol Psychiatry*, 2015; 20: 621-631

Bohacek J and Mansuy IM. Molecular insights into transgenerational non-genetic inheritance of acquired behaviours. *Nat Rev Genet*, 2015; 16: 641-652

Bonfini A, Dobson AJ, Duneau D, Revah J, Liu X, Houtz P and Buchon N. Multiscale analysis reveals that diet-dependent midgut plasticity emerges from alterations in both stem cell niche coupling and enterocyte size. *Elife*, 2021; 10

Brandao BB, Lino M and Kahn CR. Extracellular miRNAs as mediators of obesity-associated disease. *J Physiol*, 2022; 600: 1155-1169

Buchon N, Osman D, David FP, Fang HY, Boquete JP, Deplancke B and Lemaitre B. Morphological and molecular characterization of adult midgut compartmentalization in *Drosophila*. *Cell Rep*, 2013; 3: 1725-1738

Busatto S, Morad G, Guo P and Moses MA. The role of extracellular vesicles in the physiological and pathological regulation of the blood-brain barrier. *FASEB Bioadv*, 2021; 3: 665-675

Caballero JN, Frenette G, Belleannée C and Sullivan R. CD9-positive microvesicles mediate the transfer of molecules to Bovine Spermatozoa during epididymal maturation. *PLoS One*, 2013; 8: e65364

Camilleri-Carter TL, Dowling DK, R LR and Piper MDW. Transgenerational Obesity and Healthy Aging in *Drosophila*. *J Gerontol A Biol Sci Med Sci*, 2019; 74: 1582-1589

Carone BR, Fauquier L, Habib N, Shea JM, Hart CE, Li R, Bock C, Li C, Gu H, Zamore PD, Meissner A, Weng Z, Hofmann HA, Friedman N and Rando OJ. Paternally induced transgenerational environmental reprogramming of metabolic gene expression in mammals. *Cell*, 2010; 143: 1084-1096

César H, Sertorio MN, de Souza EA, Jamar G, Santamarina A, Jucá A, Casagrande BP and Pisani LP. Parental high-fat high-sugar diet programming and hypothalamus adipose tissue axis in male Wistar rats. *Eur J Nutr*, 2022; 61: 523-537

Champroux A, Cocquet J, Henry-Berger J, Drevet JR and Kocer A. A Decade of Exploring the Mammalian Sperm Epigenome: Paternal Epigenetic and Transgenerational Inheritance. *Front Cell Dev Biol*, 2018; 6: 50

Chan JC, Morgan CP, Adrian Leu N, Shetty A, Cisse YM, Nugent BM, Morrison KE, Jašarević E, Huang W, Kanyuch N, Rodgers AB, Bhanu NV, Berger DS, Garcia BA, Ament S, Kane M, Neill Epperson C and Bale TL. Reproductive tract extracellular vesicles are sufficient to transmit intergenerational stress and program neurodevelopment. *Nat Commun*, 2020; 11: 1499

Chatterjee N and Perrimon N. What fuels the fly: Energy metabolism in *Drosophila* and its application to the study of obesity and diabetes. *Sci Adv*, 2021; 7

Chen Q, Yan M, Cao Z, Li X, Zhang Y, Shi J, Feng GH, Peng H, Zhang X, Zhang Y, Qian J, Duan E, Zhai Q and Zhou Q. Sperm tsRNAs contribute to intergenerational inheritance of an acquired metabolic disorder. *Science*, 2016; 351: 397-400

Chen Y, Zhao Y, Yin Y, Jia X and Mao L. Mechanism of cargo sorting into small extracellular vesicles. *Bioengineered*, 2021; 12: 8186-8201

Chleilat F, Schick A, Deleemans JM, Ma K, Alukic E, Wong J, Noye Tuplin EW, Nettleton JE and Reimer RA. Paternal high protein diet modulates body composition, insulin sensitivity, epigenetics, and gut microbiota intergenerationally in rats. *Faseb j*, 2021; 35: e21847

Colombo M, Moita C, van Niel G, Kowal J, Vigneron J, Benaroch P, Manel N, Moita LF, Théry C and Raposo G. Analysis of ESCRT functions in exosome biogenesis, composition and secretion highlights the heterogeneity of extracellular vesicles. *J Cell Sci*, 2013; 126: 5553-5565

Colombo M, Raposo G and Théry C. Biogenesis, secretion, and intercellular interactions of exosomes and other extracellular vesicles. *Annu Rev Cell Dev Biol*, 2014; 30: 255-289

Conine CC and Rando OJ. Soma-to-germline RNA communication. *Nat Rev Genet*, 2022; 23: 73-88

Cornwall GA. New insights into epididymal biology and function. *Hum Reprod Update*, 2009; 15: 213-227

Corrigan L, Redhai S, Leiblich A, Fan SJ, Perera SM, Patel R, Gandy C, Wainwright SM, Morris JF, Hamdy F, Goberdhan DC and Wilson C. BMP-regulated exosomes from *Drosophila* male reproductive glands reprogram female behavior. *J Cell Biol*, 2014; 206: 671-688

Cossetti C, Lugini L, Astrologo L, Saggio I, Fais S and Spadafora C. Soma-to-germline transmission of RNA in mice xenografted with human tumour cells: possible transport by exosomes. *PLoS One*, 2014; 9: e101629

Crean AJ and Bonduriansky R. What is a paternal effect? *Trends Ecol Evol*, 2014; 29: 554-559

Crisóstomo L, Videira RA, Jarak I, Starčević K, Mašek T, Rato L, Raposo JF, Batterham RL, Oliveira PF and Alves MG. Inherited Metabolic Memory of High-Fat Diet Impairs Testicular Fatty Acid Content and Sperm Parameters. *Mol Nutr Food Res*, 2022; 66: e2100680

da Cruz RS, Clarke J, Curi ACP, Al-Yawar A, Jin L, Baird A, Cruz MI, Kallakury B and de Assis S. Parental obesity programs pancreatic cancer development in offspring. *Endocr Relat Cancer*, 2019; 26: 511-523

Dar GH, Mendes CC, Kuan WL, Speciale AA, Conceição M, Görgens A, Uliyakina I, Lobo MJ, Lim WF, El Andaloussi S, Mäger I, Roberts TC, Barker RA, Goberdhan DCI, Wilson C and Wood MJA. GAPDH controls extracellular vesicle biogenesis and enhances the therapeutic potential of EV mediated siRNA delivery to the brain. *Nat Commun*, 2021; 12: 6666

Darwin C. *On the Origin of Species*. London: John Murray, 1859; 488:

Dasgupta P, Sarkar S, Das AA, Verma T and Nandy B. Intergenerational paternal effect of adult density in *Drosophila melanogaster*. *Ecol Evol*, 2019; 9: 3553-3563

Dashorst P, Mooren TM, Kleber RJ, de Jong PJ and Huntjens RJC. Intergenerational consequences of the Holocaust on offspring mental health: a systematic review of associated factors and mechanisms. *Eur J Psychotraumatol*, 2019; 10: 1654065

de Sousa Neto IV, Tibana RA, da Silva LGO, de Lira EM, do Prado GPG, de Almeida JA, Franco OL, Durigan JLQ, Adesida AB, de Sousa MV, Ricart CAO, Damascena HL,

Castro MS, Fontes W, Prestes J and Marqueti RC. Paternal Resistance Training Modulates Calcaneal Tendon Proteome in the Offspring Exposed to High-Fat Diet. *Front Cell Dev Biol*, 2020; 8: 380

Dearden L, Bouret SG and Ozanne SE. Sex and gender differences in developmental programming of metabolism. *Mol Metab*, 2018; 15: 8-19

Denomme MM, Haywood ME, Parks JC, Schoolcraft WB and Katz-Jaffe MG. The inherited methylome landscape is directly altered with paternal aging and associated with offspring neurodevelopmental disorders. *Aging Cell*, 2020; 19: e13178

Dew-Budd K, Jarnigan J and Reed LK. Genetic and Sex-Specific Transgenerational Effects of a High Fat Diet in *Drosophila melanogaster*. *PLoS One*, 2016; 11: e0160857

Dias BG and Ressler KJ. Parental olfactory experience influences behavior and neural structure in subsequent generations. *Nature Neuroscience*, 2013; 17: 89-96

Dietz DM, Laplant Q, Watts EL, Hodes GE, Russo SJ, Feng J, Oosting RS, Vialou V and Nestler EJ. Paternal transmission of stress-induced pathologies. *Biol Psychiatry*, 2011; 70: 408-414

Dimofski P, Meyre D, Dreumont N and Leininger-Muller B. Consequences of Paternal Nutrition on Offspring Health and Disease. *Nutrients*, 2021; 13: 2818

Eaton SA, Jayasooriah N, Buckland ME, Martin DI, Cropley JE and Suter CM. Roll over Weismann: extracellular vesicles in the transgenerational transmission of environmental effects. *Epigenomics*, 2015; 7: 1165-1171

Eickelberg V, Lüersen K, Staats S and Rimbach G. Phenotyping of *Drosophila Melanogaster*-A Nutritional Perspective. *Biomolecules*, 2022; 12

Emborski C and Mikheyev AS. Ancestral diet transgenerationally influences offspring in a parent-of-origin and sex-specific manner. *Philos Trans R Soc Lond B Biol Sci*, 2019; 374: 20180181

Fan SJ, Kroeger B, Marie PP, Bridges EM, Mason JD, McCormick K, Zois CE, Sheldon H, Khalid Alham N, Johnson E, Ellis M, Stefana MI, Mendes CC, Wainwright SM, Cunningham C, Hamdy FC, Morris JF, Harris AL, Wilson C and Goberdhan DC. Glutamine deprivation alters the origin and function of cancer cell exosomes. *Embo j*, 2020; 39: e103009

Fennell KA, Busby RGG, Li S, Bodden C, Stanger SJ, Nixon B, Short AK, Hannan AJ and Pang TY. Limitations to intergenerational inheritance: subchronic paternal stress preconception does not influence offspring anxiety. *Sci Rep*, 2020; 10: 16050

Fitz-James MH and Cavalli G. Molecular mechanisms of transgenerational epigenetic inheritance. *Nat Rev Genet*, 2022; 23: 325-341

Foot NJ, Gonzalez MB, Gembus K, Fonseka P, Sandow JJ, Nguyen TT, Tran D, Webb AI, Mathivanan S, Robker RL and Kumar S. Arrdc4-dependent extracellular vesicle biogenesis is required for sperm maturation. *J Extracell Vesicles*, 2021; 10: e12113

Frenette G, Girouard J and Sullivan R. Comparison between epididymosomes collected in the intraluminal compartment of the bovine caput and cauda epididymidis. *Biol Reprod*, 2006; 75: 885-890

Fullston T, McPherson NO, Owens JA, Kang WX, Sandeman LY and Lane M. Paternal obesity induces metabolic and sperm disturbances in male offspring that are exacerbated by their exposure to an "obesogenic" diet. *Physiol Rep*, 2015; 3

Gáliková M and Klepsatel P. Obesity and Aging in the *Drosophila* Model. *Int J Mol Sci*, 2018; 19

Gao M, Brown MA, Neff D, Crowell SE and Conradt E. Prenatal paternal stress predicts infant parasympathetic functioning above and beyond maternal prenatal stress. *J Reprod Infant Psychol*, 2021; 1-14

Gapp K, Jawaid A, Sarkies P, Bohacek J, Pelczar P, Prados J, Farinelli L, Miska E and Mansuy IM. Implication of sperm RNAs in transgenerational inheritance of the effects of early trauma in mice. *Nature Neuroscience*, 2014; 17: 667-669

Garcia-Martin R, Wang G, Brandão BB, Zanotto TM, Shah S, Kumar Patel S, Schilling B and Kahn CR. MicroRNA sequence codes for small extracellular vesicle release and cellular retention. *Nature*, 2022; 601: 446-451

Ghai M and Kader F. A Review on Epigenetic Inheritance of Experiences in Humans. *Biochem Genet*, 2022; 60: 1107-1140

Gligorov D, Sitnik JL, Maeda RK, Wolfner MF and Karch F. A novel function for the Hox gene *Abd-B* in the male accessory gland regulates the long-term female post-mating response in *Drosophila*. *PLoS Genet*, 2013; 9: e1003395

Golding J, Gregory S, Northstone K, Pembrey M, Watkins S, Iles-Caven Y and Suderman M. Human transgenerational observations of regular smoking before puberty on fat mass in grandchildren and great-grandchildren. *Sci Rep*, 2022; 12: 1139

Gong P, Bailbé D, Bianchi L, Pommier G, Liu J, Tolu S, Stathopoulou MG, Portha B, Grandjean V and Movassat J. Paternal High-Protein Diet Programs Offspring Insulin Sensitivity in a Sex-Specific Manner. *Biomolecules*, 2021; 11

Gramates LS, Agapite J, Attrill H, Calvi BR, Crosby MA, Dos Santos G, Goodman JL, Goutte-Gattat D, Jenkins VK, Kaufman T, Larkin A, Matthews BB, Millburn G and Strelets VB. Fly Base: a guided tour of highlighted features. *Genetics*, 2022; 220

Grandjean V, Fourré S, De Abreu DA, Derieppe MA, Remy JJ and Rassoulzadegan M. RNA-mediated paternal heredity of diet-induced obesity and metabolic disorders. *Sci Rep*, 2015; 5: 18193

Gray J, Sokolowski B and Simpson J. *Drosophila* as a useful model for understanding the evolutionary physiology of obesity resistance and metabolic thrift. *Fly (Austin)*, 2021; 15: 47-59

Griffiths GS, Galileo DS, Reese K and Martin-Deleon PA. Investigating the role of murine epididymosomes and uterosomes in GPI-linked protein transfer to sperm using SPAM1 as a model. *Mol Reprod Dev*, 2008; 75: 1627-1636

Gross JC, Chaudhary V, Bartscherer K and Boutros M. Active Wnt proteins are secreted on exosomes. *Nat Cell Biol*, 2012; 14: 1036-1045

Guida MC, Birse RT, Dall'Agnese A, Toto PC, Diop SB, Mai A, Adams PD, Puri PL and Bodmer R. Intergenerational inheritance of high fat diet-induced cardiac lipotoxicity in *Drosophila*. *Nat Commun*, 2019; 10: 193

Hopkins BR, Sepil I, Bonham S, Miller T, Charles PD, Fischer R, Kessler BM, Wilson C and Wigby S. BMP signaling inhibition in *Drosophila* secondary cells remodels the seminal proteome and self and rival ejaculate functions. *Proc Natl Acad Sci U S A*, 2019; 116: 24719-24728

Hou Z, Jiang P, Swanson SA, Elwell AL, Nguyen BK, Bolin JM, Stewart R and Thomson JA. A cost-effective RNA sequencing protocol for large-scale gene expression studies. *Sci Rep*, 2015; 5: 9570

Hsu C, Morohashi Y, Yoshimura S, Manrique-Hoyos N, Jung S, Lauterbach MA, Bakhti M, Grønberg M, Möbius W, Rhee J, Barr FA and Simons M. Regulation of exosome secretion by Rab35 and its GTPase-activating proteins TBC1D10A-C. *J Cell Biol*, 2010; 189: 223-232

Huypens P, Sass S, Wu M, Dyckhoff D, Tschop M, Theis F, Marschall S, Hrabe de Angelis M and Beckers J. Epigenetic germline inheritance of diet-induced obesity and insulin resistance. *Nat Genet*, 2016; 48: 497-499

Janas T, Janas MM, Sapoń K and Janas T. Mechanisms of RNA loading into exosomes. *FEBS Lett*, 2015; 589: 1391-1398

Kaati G, Bygren LO and Edvinsson S. Cardiovascular and diabetes mortality determined by nutrition during parents' and grandparents' slow growth period. *Eur J Hum Genet*, 2002; 10: 682-688

Kalluri R and LeBleu VS. The biology, function, and biomedical applications of exosomes. *Science*, 2020; 367

Kalra H, Drummen GP and Mathivanan S. Focus on Extracellular Vesicles: Introducing the Next Small Big Thing. *Int J Mol Sci*, 2016; 17: 170

Kanmiki EW, Fatima Y and Mamun AA. Multigenerational transmission of obesity: A systematic review and meta-analysis. *Obes Rev*, 2022; 23: e13405

Kawai K, Harada T, Ishikawa T, Sugiyama R, Kawamura T, Yoshida A, Tsutsumi O, Ishino F, Kubota T and Kohda T. Parental age and gene expression profiles in individual human blastocysts. *Sci Rep*, 2018; 8: 2380

Kong X, Yang Z, Zhang B, Chen X, Yu L, Zhu H, Xing X and Yang W. Maternal and paternal histories differentially influence risks for diabetes, insulin secretion and insulin resistance in a Chinese population. *J Diabetes Investig*, 2021; 12: 434-445

Krause SA, Overend G, Dow JAT and Leader DP. FlyAtlas 2 in 2022: enhancements to the *Drosophila melanogaster* expression atlas. *Nucleic Acids Res*, 2022; 50: D1010-d1015

Leiblich A, Marsden L, Gandy C, Corrigan L, Jenkins R, Hamdy F and Wilson C. Bone morphogenetic protein- and mating-dependent secretory cell growth and migration in the *Drosophila* accessory gland. *Proc Natl Acad Sci U S A*, 2012; 109: 19292-19297

Lemos T and Gallagher D. Current body composition measurement techniques. *Curr Opin Endocrinol Diabetes Obes*, 2017; 24: 310-314

Lin Y, Lu Y, Huang Z, Wang Y, Song S, Luo Y, Ren F and Guo H. Milk-Derived Small Extracellular Vesicles Promote Recovery of Intestinal Damage by Accelerating Intestinal Stem Cell-Mediated Epithelial Regeneration. *Mol Nutr Food Res*, 2022; 66: e2100551

Linford NJ, Bilgir C, Ro J and Pletcher SD. Measurement of lifespan in *Drosophila melanogaster*. *J Vis Exp*, 2013

Linnemannstöns K, Karuna MP, Witte L, Choezom D, Honemann-Capito M, Lagurin AS, Schmidt CV, Shrikhande S, Steinmetz LK, Wiebke M, Lenz C and Gross JC. Microscopic and biochemical monitoring of endosomal trafficking and extracellular vesicle secretion in an endogenous in vivo model. *J Extracell Vesicles*, 2022; 11: e12263

Ma J, Zhang Z, Wang Y and Shen H. Investigation of miR-126-3p loaded on adipose stem cell-derived exosomes for wound healing of full-thickness skin defects. *Exp Dermatol*, 2022; 31: 362-374

Maas SLN, Breakefield XO and Weaver AM. Extracellular Vesicles: Unique Intercellular Delivery Vehicles. *Trends Cell Biol*, 2017; 27: 172-188

Machtiger R, Laurent LC and Baccarelli AA. Extracellular vesicles: roles in gamete maturation, fertilization and embryo implantation. *Hum Reprod Update*, 2016; 22: 182-193

Martin-DeLeon PA. Epididymosomes: transfer of fertility-modulating proteins to the sperm surface. *Asian J Androl*, 2015; 17: 720-725

Mehdiani A, Maier A, Pinto A, Barth M, Akhyari P and Lichtenberg A. An innovative method for exosome quantification and size measurement. *J Vis Exp*, 2015: 50974

Meldolesi J. Exosomes and Ectosomes in Intercellular Communication. *Curr Biol*, 2018; 28: R435-r444

Meldolesi J. Extracellular vesicles (exosomes and ectosomes) play key roles in the pathology of brain diseases. *Mol Biomed*, 2021; 2: 18

Merrill SM, Moore SR, Gladish N, Giesbrecht GF, Dewey D, Konwar C, MacIssac JL, Kobor MS and Letourneau NL. Paternal adverse childhood experiences: Associations with infant DNA methylation. *Dev Psychobiol*, 2021; 63: e22174

Mezzofanti E, Ignesti M, Hsu T, Gargiulo G and Cavaliere V. Vps28 Is Involved in the Intracellular Trafficking of Awd, the Drosophila Homolog of NME1/2. *Front Physiol*, 2019; 10: 983

Minami R, Wakabayashi M, Sugimori S, Taniguchi K, Kokuryo A, Imano T, Adachi-Yamada T, Watanabe N and Nakagoshi H. The homeodomain protein defective proventriculus is essential for male accessory gland development to enhance fecundity in *Drosophila*. *PLoS One*, 2012; 7: e32302

Morgan CP and Bale TL. Early prenatal stress epigenetically programs dysmasculinization in second-generation offspring via the paternal lineage. *J Neurosci*, 2011; 31: 11748-11755

Musselman LP, Fink JL, Narzinski K, Ramachandran PV, Hathiramani SS, Cagan RL and Baranski TJ. A high-sugar diet produces obesity and insulin resistance in wild-type *Drosophila*. *Dis Model Mech*, 2011; 4: 842-849

Musselman LP and Kühnlein RP. *Drosophila* as a model to study obesity and metabolic disease. *J Exp Biol*, 2018; 221:

Nätt D, Kugelberg U, Casas E, Nedstrand E, Zalavary S, Henriksson P, Nijm C, Jäderquist J, Sandborg J, Flinke E, Ramesh R, Örkenby L, Appelkvist F, Lingg T, Guzzi N, Bellodi C, Löf M, Vavouri T and Öst A. Human sperm displays rapid responses to diet. *PLoS Biol*, 2019; 17: e3000559

Ng SF, Lin RC, Laybutt DR, Barres R, Owens JA and Morris MJ. Chronic high-fat diet in fathers programs beta-cell dysfunction in female rat offspring. *Nature*, 2010; 467: 963-966

Nie Y, Yu S, Li Q, Nirala NK, Amcheslavsky A, Edwards YJK, Shum PW, Jiang Z, Wang W, Zhang B, Gao N and Ip YT. Oncogenic Pathways and Loss of the Rab11 GTPase Synergize To Alter Metabolism in *Drosophila*. *Genetics*, 2019; 212: 1227-1239

Nikitidou E, Khoonsari PE, Shevchenko G, Ingelsson M, Kultima K and Erlandsson A. Increased Release of Apolipoprotein E in Extracellular Vesicles Following Amyloid- β Protofibril Exposure of Neuroglial Co-Cultures. *J Alzheimers Dis*, 2017; 60: 305-321

Nixon B, De Iuliis GN, Dun MD, Zhou W, Trigg NA and Eamens AL. Profiling of epididymal small non-protein-coding RNAs. *Andrology*, 2019; 7: 669-680

Nixon B, De Iuliis GN, Hart HM, Zhou W, Mathe A, Bernstein IR, Anderson AL, Stanger SJ, Skerrett-Byrne DA, Jamaluddin MFB, Almazi JG, Bromfield EG, Larsen MR and Dun MD. Proteomic Profiling of Mouse Epididymosomes Reveals their Contributions to Post-testicular Sperm Maturation. *Mol Cell Proteomics*, 2019; 18: S91-s108

Nixon B, Stanger SJ, Mihalas BP, Reilly JN, Anderson AL, Tyagi S, Holt JE and McLaughlin EA. The microRNA signature of mouse spermatozoa is substantially modified during epididymal maturation. *Biol Reprod*, 2015; 93: 91

O'Brien EA, Ensbey KS, Day BW, Baldock PA and Barry G. Direct evidence for transport of RNA from the mouse brain to the germline and offspring. *BMC Biol*, 2020; 18: 45

Oh JS, Han C and Cho C. ADAM7 is associated with epididymosomes and integrated into sperm plasma membrane. *Mol Cells*, 2009; 28: 441-446

Öst A, Lempradl A, Casas E, Weigert M, Tiko T, Deniz M, Pantano L, Boenisch U, Itskov PM, Stoeckius M, Ruf M, Rajewsky N, Reuter G, Iovino N, Ribeiro C, Alenius M, Heyne S, Vavouri T and Pospisilik JA. Paternal diet defines offspring chromatin state and intergenerational obesity. *Cell*, 2014; 159: 1352-1364

Ostrowski M, Carmo NB, Krumeich S, Fanget I, Raposo G, Savina A, Moita CF, Schauer K, Hume AN, Freitas RP, Goud B, Benaroch P, Hacohen N, Fukuda M, Desnos C, Seabra MC, Darchen F, Amigorena S, Moita LF and Thery C. Rab27a and Rab27b control different steps of the exosome secretion pathway. *Nat Cell Biol*, 2010; 12: 19-30; sup pp 11-13

Panáková D, Sprong H, Marois E, Thiele C and Eaton S. Lipoprotein particles are required for Hedgehog and Wingless signalling. *Nature*, 2005; 435: 58-65

Papatheodorou I, Moreno P, Manning J, Fuentes AM, George N, Fexova S, Fonseca NA, Füllgrabe A, Green M, Huang N, Huerta L, Iqbal H, Jianu M, Mohammed S, Zhao L, Jarnuczak AF, Jupp S, Marioni J, Meyer K, Petryszak R, Prada Medina CA, Talavera-López C, Teichmann S, Vizcaino JA and Brazma A. Expression Atlas update: from tissues to single cells. *Nucleic Acids Res*, 2020; 48: D77-d83

Park KH, Kim BJ, Kang J, Nam TS, Lim JM, Kim HT, Park JK, Kim YG, Chae SW and Kim UH. Ca²⁺ signaling tools acquired from prostasomes are required for progesterone-induced sperm motility. *Sci Signal*, 2011; 4: ra31

Pascua-Maestro R, González E, Lillo C, Ganfornina MD, Falcón-Pérez JM and Sanchez D. Extracellular Vesicles Secreted by Astroglial Cells Transport Apolipoprotein D to Neurons and Mediate Neuronal Survival Upon Oxidative Stress. *Front Cell Neurosci*, 2018; 12: 526

Paul N, Talluri TR, Nag P and Kumaresan A. Epididymosomes: A potential male fertility influencer. *Andrologia*, 2021; 53: e14155

Pembrey ME, Bygren LO, Kaati G, Edvinsson S, Northstone K, Sjöström M, Golding J and Team AS. Sex-specific, male-line transgenerational responses in humans. *Eur J Hum Genet*, 2006; 14: 159-166

Piyankarage SC, Featherstone DE and Shippy SA. Nanoliter hemolymph sampling and analysis of individual adult *Drosophila melanogaster*. *Anal Chem*, 2012; 84: 4460-4466

Polga N, Macul Ferreira de Barros P, Farhat LC, de Almeida KM, Bloch MH and Lafer B. Parental age and the risk of bipolar disorder in the offspring: A systematic review and meta-analysis. *Acta Psychiatr Scand*, 2022; 145: 568-577

Prince E, Kroeger B, Gligorov D, Wilson C, Eaton S, Karch F, Brankatschk M and Maeda RK. Rab-mediated trafficking in the secondary cells of *Drosophila* male accessory glands and its role in fecundity. *Traffic*, 2019; 20: 137-151

Qi Z, Zhao Y, Su Y, Cao B, Yang JJ and Xing Q. Serum Extracellular Vesicle-Derived miR-124-3p as a Diagnostic and Predictive Marker for Early-Stage Acute Ischemic Stroke. *Front Mol Biosci*, 2021; 8: 685088

Raad G, Serra F, Martin L, Derieppe MA, Gilleron J, Costa VL, Pisani DF, Amri EZ, Trabucchi M and Grandjean V. Paternal multigenerational exposure to an obesogenic diet drives epigenetic predisposition to metabolic diseases in mice. *Elife*, 2021; 10

Ragusa M, Barbagallo C, Cirnigliaro M, Battaglia R, Brex D, Caponnetto A, Barbagallo D, Di Pietro C and Purrello M. Asymmetric RNA Distribution among Cells and Their Secreted Exosomes: Biomedical Meaning and Considerations on Diagnostic Applications. *Front Mol Biosci*, 2017; 4: 66

Raposo G and Stahl PD. Extracellular vesicles: a new communication paradigm? *Nat Rev Mol Cell Biol*, 2019; 20: 509-510

Rastogi S, Rani K and Kumar S. Progression of Cognitive Impairment to Alzheimer's Disease: Through the Lens of Salivary Extracellular Vesicles. *Neurosci Insights*, 2021; 16: 26331055211058687

Razoux F, Russig H, Mueggler T, Balthes C, Dikaiou K, Rudin M and Mansuy IM. Transgenerational disruption of functional 5-HT(1A)R-induced connectivity in the adult mouse brain by traumatic stress in early life. *Mol Psychiatry*, 2017; 22: 519-526

Reilly JN, McLaughlin EA, Stanger SJ, Anderson AL, Hutcheon K, Church K, Mihalas BP, Tyagi S, Holt JE, Eamens AL and Nixon B. Characterisation of mouse epididymosomes reveals a complex profile of microRNAs and a potential mechanism for modification of the sperm epigenome. *Sci Rep*, 2016; 6: 31794

Rodgers AB, Morgan CP, Bronson SL, Revello S and Bale TL. Paternal stress exposure alters sperm microRNA content and reprograms offspring HPA stress axis regulation. *J Neurosci*, 2013; 33: 9003-9012

Rodgers AB, Morgan CP, Leu NA and Bale TL. Transgenerational epigenetic programming via sperm microRNA recapitulates effects of paternal stress. *Proc Natl Acad Sci U S A*, 2015; 112: 13699-13704

Ryan DP, Henzel KS, Pearson BL, Siwek ME, Papazoglou A, Guo L, Paesler K, Yu M, Muller R, Xie K, Schroder S, Becker L, Garrett L, Holter SM, Neff F, Racz I, Rathkolb B, Rozman J, Ehninger G, Klingenspor M, Klopstock T, Wolf E, Wurst W, Zimmer A, Fuchs H, Gailus-Durner V, Hrabe de Angelis M, Sidiropoulou K, Weiergraber M, Zhou Y and Ehninger D. A paternal methyl donor-rich diet altered cognitive and neural functions in offspring mice. *Mol Psychiatry*, 2018; 23: 1345-1355

Sahoo S and Losordo DW. Exosomes and cardiac repair after myocardial infarction. *Circ Res*, 2014; 114: 333-344

Salomão R, Neto IVS, Ramos GV, Tibana RA, Durigan JQ, Pereira GB, Franco OL, Royer C, Neves FAR, de Carvalho ACA, Nóbrega OT, Haddad R, Prestes J and Marqueti RC. Paternal Resistance Exercise Modulates Skeletal Muscle Remodeling Pathways in Fathers and Male Offspring Submitted to a High-Fat Diet. *Front Physiol*, 2021; 12: 706128

Sanchez-Lopez JA, Twena S, Apel I, Kornhaeuser SC, Chasnitsky M, Miklosi AG, Vega-Dominguez PJ, Shephard A, Hefetz A and Heifetz Y. Male-female communication enhances release of extracellular vesicles leading to high fertility in *Drosophila*. *Commun Biol*, 2022; 5: 815

Savina A, Vidal M and Colombo MI. The exosome pathway in K562 cells is regulated by Rab11. *J Cell Sci*, 2002; 115: 2505-2515

Schellong K, Melchior K, Ziska T, Rancourt RC, Henrich W and Plagemann A. Maternal but Not Paternal High-Fat Diet (HFD) Exposure at Conception Predisposes for 'Diabesity' in Offspring Generations. *Int J Environ Res Public Health*, 2020; 17

Schwarz A, Wennemuth G, Post H, Brandenburger T, Aumüller G and Wilhelm B. Vesicular transfer of membrane components to bovine epididymal spermatozoa. *Cell Tissue Res*, 2013; 353: 549-561

Seong KH, Ly NH, Katou Y, Yokota N, Nakato R, Murakami S, Hirayama A, Fukuda S, Kang S, Soga T, Shirahige K and Ishii S. Paternal restraint stress affects offspring metabolism via ATF-2 dependent mechanisms in *Drosophila melanogaster* germ cells. *Commun Biol*, 2020; 3: 208

Sepil I, Hopkins BR, Dean R, Thézénas ML, Charles PD, Konietzny R, Fischer R, Kessler BM and Wigby S. Quantitative Proteomics Identification of Seminal Fluid Proteins in Male *Drosophila melanogaster*. *Mol Cell Proteomics*, 2019; 18: S46-s58

Sharma U, Conine CC, Shea JM, Boskovic A, Derr AG, Bing XY, Belleannee C, Kucukural A, Serra RW, Sun F, Song L, Carone BR, Ricci EP, Li XZ, Fauquier L, Moore MJ, Sullivan R, Mello CC, Garber M and Rando OJ. Biogenesis and function of tRNA fragments during sperm maturation and fertilization in mammals. *Science*, 2016; 351: 391-396

Sharma U, Sun F, Conine CC, Reichholf B, Kukreja S, Herzog VA, Ameres SL and Rando OJ. Small RNAs Are Trafficked from the Epididymis to Developing Mammalian Sperm. *Dev Cell*, 2018; 46: 481-494 e486

Shibata T, Hadano J, Kawasaki D, Dong X and Kawabata SI. *Drosophila* TG-A transglutaminase is secreted via an unconventional Golgi-independent mechanism involving exosomes and two types of fatty acylations. *J Biol Chem*, 2017; 292: 10723-10734

Simon C, Greening DW, Bolumar D, Balaguer N, Salamonsen LA and Vilella F. Extracellular Vesicles in Human Reproduction in Health and Disease. *Endocr Rev*, 2018; 39: 292-332

Sitnik JL, Gligorov D, Maeda RK, Karch F and Wolfner MF. The Female Post-Mating Response Requires Genes Expressed in the Secondary Cells of the Male Accessory Gland in *Drosophila melanogaster*. *Genetics*, 2016; 202: 1029-1041

Smythies J, Edelstein L and Ramachandran V. Molecular mechanisms for the inheritance of acquired characteristics-exosomes, microRNA shuttling, fear and stress: Lamarck resurrected? *Front Genet*, 2014; 5: 133

Sullivan R. Epididymosomes: a heterogeneous population of microvesicles with multiple functions in sperm maturation and storage. *Asian J Androl*, 2015; 17: 726-729

Sullivan R and Saez F. Epididymosomes, prostasomes, and liposomes: their roles in mammalian male reproductive physiology. *Reproduction*, 2013; 146: R21-35

Sun W, Dong H, Becker AS, Dapito DH, Modica S, Grandl G, Opitz L, Efthymiou V, Straub LG, Sarker G, Balaz M, Balazova L, Perdikari A, Kiehlmann E, Bacanovic S, Zellweger C, Peleg-Raibstein D, Pelczar P, Reik W, Burger IA, von Meyenn F and Wolfrum C. Cold-induced epigenetic programming of the sperm enhances brown adipose tissue activity in the offspring. *Nat Med*, 2018; 24: 1372-1383

Suryawanshi AR, Khan SA, Joshi CS and Khole VV. Epididymosome-mediated acquisition of MMSDH, an androgen-dependent and developmentally regulated epididymal sperm protein. *J Androl*, 2012; 33: 963-974

Tamai K, Tanaka N, Nakano T, Kakazu E, Kondo Y, Inoue J, Shiina M, Fukushima K, Hoshino T, Sano K, Ueno Y, Shimosegawa T and Sugamura K. Exosome secretion of dendritic cells is regulated by Hrs, an ESCRT-0 protein. *Biochem Biophys Res Commun*, 2010; 399: 384-390

Teltumbade M, Bhalla A and Sharma A. Paternal inheritance of diet induced metabolic traits correlates with germline regulation of diet induced coding gene expression. *Genomics*, 2020; 112: 567-573

Tennessen JM, Barry WE, Cox J and Thummel CS. Methods for studying metabolism in *Drosophila*. *Methods*, 2014; 68: 105-115

Teves ME and Roldan ERS. Sperm bauplan and function and underlying processes of sperm formation and selection. *Physiol Rev*, 2022; 102: 7-60

Théry C, Witwer KW, Aikawa E, Alcaraz MJ, Anderson JD, Andriantsitohaina R, Antoniou A, Arab T, Archer F, Atkin-Smith GK, Ayre DC, Bach JM, Bachurski D, Baharvand H, Balaj L, Baldacchino S, Bauer NN, Baxter AA, Bebawy M, Beckham C, Bedina Zavec A, Benmoussa A, Berardi AC, Bergese P, Bielska E, Blenkiron C, Bobis-Wozowicz S, Boilard E, Boireau W, Bongiovanni A, Borràs FE, Bosch S, Boulanger CM, Breakefield X, Breglio AM, Brennan M, Brigstock DR, Brisson A, Broekman ML, Bromberg JF, Bryl-Górecka P, Buch S, Buck AH, Burger D, Busatto S, Buschmann D, Bussolati B, Buzás EI, Byrd JB, Camussi G, Carter DR, Caruso S, Chamley LW, Chang YT, Chen C, Chen S, Cheng L, Chin AR, Clayton A, Clerici SP, Cocks A, Cocucci E, Coffey RJ, Cordeiro-da-Silva A, Couch Y, Coumans FA, Coyle B, Crescitelli R, Criado MF, D'Souza-Schorey C, Das S, Datta Chaudhuri A, de Candia P, De Santana EF, De Wever O, Del Portillo HA, Demaret T, Deville S, Devitt A, Dhondt B, Di Vizio D, Dieterich LC, Dolo V, Dominguez Rubio AP, Dominici M, Dourado MR, Driedonks TA, Duarte FV, Duncan HM, Eichenberger RM, Ekström K, El Andaloussi S, Elie-Caille C, Erdbrügger U, Falcón-Pérez JM, Fatima F, Fish JE, Flores-Bellver M, Försönits A, Frelet-Barrand A, Fricke F, Fuhrmann G, Gabrielsson S, Gámez-Valero A, Gardiner C, Gärtner K, Gaudin R, Gho YS, Giebel B, Gilbert C, Gimona M, Giusti I, Goberdhan DC, Görgens A, Gorski SM, Greening DW, Gross JC, Gualerzi A, Gupta GN, Gustafson D, Handberg A, Haraszti RA, Harrison P, Hegyesi H, Hendrix A, Hill AF, Hochberg FH, Hoffmann KF, Holder B, Holthofer H, Hosseinkhani B, Hu G, Huang Y, Huber V, Hunt S, Ibrahim AG, Ikezu T, Inal JM, Isin M, Ivanova A, Jackson HK, Jacobsen S, Jay SM, Jayachandran M, Jenster G, Jiang L, Johnson SM, Jones JC, Jong A, Jovanovic-Talisman T, Jung S, Kalluri R, Kano SI, Kaur S, Kawamura Y, Keller ET, Khamari D, Khomyakova E, Khvorova A, Kierulf P, Kim KP, Kislinger T, Klingeborn M, Klinke DJ, 2nd, Kornek M, Kosanović MM, Kovács Á F, Krämer-Albers EM, Krasemann S, Krause M, Kurochkin IV, Kusuma GD, Kuypers S, Laitinen S, Langevin SM, Languino LR, Lannigan J, Lässer C, Laurent LC, Lavieu G, Lázaro-Ibáñez E, Le Lay S, Lee MS, Lee YXF, Lemos DS, Lenassi M, Leszczynska A, Li IT, Liao K, Libregts SF, Ligeti E, Lim R, Lim SK, Linē A, Linnemannstöns K, Llorente A, Lombard CA, Lorenowicz MJ, Lörincz Á M, Lötvall J, Lovett J, Lowry MC, Loyer X, Lu Q, Lukomska B, Lunavat TR, Maas SL, Malhi H, Marcilla A, Mariani J, Mariscal J, Martens-Uzunova ES, Martin-Jaular L, Martinez MC, Martins VR, Mathieu M, Mathivanan S, Maugeri M, McGinnis LK, McVey MJ, Meckes

DG, Jr., Meehan KL, Mertens I, Minciacchi VR, Möller A, Møller Jørgensen M, Morales-Kastresana A, Morhayim J, Mullier F, Muraca M, Musante L, Mussack V, Muth DC, Myburgh KH, Najrana T, Nawaz M, Nazarenko I, Nejsum P, Neri C, Neri T, Nieuwland R, Nimrichter L, Nolan JP, Nolte-'t Hoen EN, Noren Hooten N, O'Driscoll L, O'Grady T, O'Loghlen A, Ochiya T, Olivier M, Ortiz A, Ortiz LA, Osteikoetxea X, Østergaard O, Ostrowski M, Park J, Pegtel DM, Peinado H, Perut F, Pfaffl MW, Phinney DG, Pieters BC, Pink RC, Pisetsky DS, Pogge von Strandmann E, Polakovicova I, Poon IK, Powell BH, Prada I, Pulliam L, Quesenberry P, Radeghieri A, Raffai RL, Raimondo S, Rak J, Ramirez MI, Raposo G, Rayyan MS, Regev-Rudzki N, Ricklefs FL, Robbins PD, Roberts DD, Rodrigues SC, Rohde E, Rome S, Rouschop KM, Rughetti A, Russell AE, Saá P, Sahoo S, Salas-Huenuleo E, Sánchez C, Saugstad JA, Saul MJ, Schiffelers RM, Schneider R, Schøyen TH, Scott A, Shahaj E, Sharma S, Shatnyeva O, Shekari F, Shelke GV, Shetty AK, Shiba K, Siljander PR, Silva AM, Skowronek A, Snyder OL, 2nd, Soares RP, Sódar BW, Soekmadji C, Sotillo J, Stahl PD, Stoorvogel W, Stott SL, Strasser EF, Swift S, Tahara H, Tewari M, Timms K, Tiwari S, Tixeira R, Tkach M, Toh WS, Tomasini R, Torrecilhas AC, Tosar JP, Toxavidis V, Urbanelli L, Vader P, van Balkom BW, van der Grein SG, Van Deun J, van Herwijnen MJ, Van Keuren-Jensen K, van Niel G, van Royen ME, van Wijnen AJ, Vasconcelos MH, Vechetti IJ, Jr., Veit TD, Vella LJ, Velot É, Verweij FJ, Vestad B, Viñas JL, Visnovitz T, Vukman KV, Wahlgren J, Watson DC, Wauben MH, Weaver A, Webber JP, Weber V, Wehman AM, Weiss DJ, Welsh JA, Wendt S, Wheelock AM, Wiener Z, Witte L, Wolfram J, Xagorari A, Xander P, Xu J, Yan X, Yáñez-Mó M, Yin H, Yuana Y, Zappulli V, Zarubova J, Žėkas V, Zhang JY, Zhao Z, Zheng L, Zheutlin AR, Zickler AM, Zimmermann P, Zivkovic AM, Zocco D and Zuba-Surma EK. Minimal information for studies of extracellular vesicles 2018 (MISEV2018): a position statement of the International Society for Extracellular Vesicles and update of the MISEV2014 guidelines. *J Extracell Vesicles*, 2018; 7: 1535750

Trigg NA, Skerrett-Byrne DA, Xavier MJ, Zhou W, Anderson AL, Stanger SJ, Katen AL, De Iuliis GN, Dun MD, Roman SD, Eamens AL and Nixon B. Acrylamide modulates the mouse epididymal proteome to drive alterations in the sperm small non-coding RNA profile and dysregulate embryo development. *Cell Rep*, 2021; 37: 109787

Twenter H, Klohonatz K, Davis K, Bass L, Coleman SJ, Bouma GJ and Bruemmer JE. Transfer of MicroRNAs From Epididymal Epithelium to Equine Spermatozoa. *J Equine Vet Sci*, 2020; 87: 102841

Vågerö D, Pinger PR, Aronsson V and van den Berg GJ. Paternal grandfather's access to food predicts all-cause and cancer mortality in grandsons. *Nat Commun*, 2018; 9: 5124

Valadi H, Ekström K, Bossios A, Sjöstrand M, Lee JJ and Lötvall JO. Exosome-mediated transfer of mRNAs and microRNAs is a novel mechanism of genetic exchange between cells. *Nat Cell Biol*, 2007; 9: 654-659

van Dam E, van Leeuwen LAG, Dos Santos E, James J, Best L, Lennicke C, Vincent AJ, Marinos G, Foley A, Buricova M, Mokochinski JB, Kramer HB, Lieb W, Laudes M, Franke A, Kaleta C and Cochemé HM. Sugar-Induced Obesity and Insulin Resistance Are Uncoupled from Shortened Survival in *Drosophila*. *Cell Metab*, 2020; 31: 710-725.e717

van Niel G and Théry C. Extracellular vesicles: eat glutamine and spit acidic bubbles. *Embo j*, 2020; 39: e105119

Veenendaal MV, Painter RC, de Rooij SR, Bossuyt PM, van der Post JA, Gluckman PD, Hanson MA and Roseboom TJ. Transgenerational effects of prenatal exposure to the 1944-45 Dutch famine. *BJOG*, 2013; 120: 548-553

Villarroya-Beltri C, Baixauli F, Gutiérrez-Vázquez C, Sánchez-Madrid F and Mittelbrunn M. Sorting it out: regulation of exosome loading. *Semin Cancer Biol*, 2014; 28: 3-13

Villarroya-Beltri C, Gutierrez-Vazquez C, Sanchez-Cabo F, Perez-Hernandez D, Vazquez J, Martin-Cofreces N, Martinez-Herrera DJ, Pascual-Montano A, Mittelbrunn M and Sanchez-Madrid F. Sumoylated hnRNP A2B1 controls the sorting of miRNAs into exosomes through binding to specific motifs. *Nat Commun*, 2013; 4: 2980

von Frieling J, Faisal MN, Sporn F, Pfefferkorn R, Nolte SS, Sommer F, Rosenstiel P and Roeder T. A high-fat diet induces a microbiota-dependent increase in stem cell activity in the *Drosophila* intestine. *PLoS Genet*, 2020; 16: e1008789

Weismann A. *The Germ-Plasm: a Theory of Heredity*. NY, USA; Translated by W. Newton Parker and Harriet Rönnfeldt 1893

Wilson C, Leiblich A, Goberdhan DC and Hamdy F. The *Drosophila* Accessory Gland as a Model for Prostate Cancer and Other Pathologies. *Curr Top Dev Biol*, 2017; 121: 339-375

Xie K, Ryan DP, Pearson BL, Henzel KS, Neff F, Vidal RO, Hennion M, Lehmann I, Schleif M, Schroder S, Adler T, Rathkolb B, Rozman J, Schutz AL, Prehn C, Mickael ME, Weiergraber M, Adamski J, Busch DH, Ehninger G, Matynia A, Jackson WS, Wolf E, Fuchs H, Gailus-Durner V, Bonn S, Hrabe de Angelis M and Ehninger D. Epigenetic alterations in longevity regulators, reduced life span, and exacerbated aging-related pathology in old father offspring mice. *Proc Natl Acad Sci U S A*, 2018; 115: E2348-E2357

Yu S, Nie Y, Knowles B, Sakamori R, Stypulkowski E, Patel C, Das S, Douard V, Ferraris RP, Bonder EM, Goldenring JR, Ip YT and Gao N. TLR sorting by Rab11 endosomes maintains intestinal epithelial-microbial homeostasis. *Embo j*, 2014; 33: 1882-1895

Zajitschek F, Zajitschek S and Manier M. Paternal diet affects differential gene expression, but not sperm competition, in sons. *Biol Lett*, 2017; 13:

Zhang X, Jin Q and Jin LH. High sugar diet disrupts gut homeostasis through JNK and STAT pathways in *Drosophila*. *Biochem Biophys Res Commun*, 2017; 487: 910-916

Zhang Y, Zhang X, Shi J, Tuorto F, Li X, Liu Y, Liebers R, Zhang L, Qu Y, Qian J, Pahima M, Liu Y, Yan M, Cao Z, Lei X, Cao Y, Peng H, Liu S, Wang Y, Zheng H, Woolsey R, Quilici D, Zhai Q, Li L, Zhou T, Yan W, Lyko F, Zhang Y, Zhou Q, Duan E

and Chen Q. Dnmt2 mediates intergenerational transmission of paternally acquired metabolic disorders through sperm small non-coding RNAs. *Nat Cell Biol*, 2018; 20: 535-540

Zheng X, Li Z, Wang G, Wang H, Zhou Y, Zhao X, Cheng CY, Qiao Y and Sun F. Sperm epigenetic alterations contribute to inter- and transgenerational effects of paternal exposure to long-term psychological stress via evading offspring embryonic reprogramming. *Cell Discov*, 2021; 7: 101

Zhou W, Stanger SJ, Anderson AL, Bernstein IR, De Iuliis GN, McCluskey A, McLaughlin EA, Dun MD and Nixon B. Mechanisms of tethering and cargo transfer during epididymosome-sperm interactions. *BMC Biol*, 2019; 17: 35

Zhou Y, Zhu H, Wu HY, Jin LY, Chen B, Pang HY, Ming ZH, Cheng Y, Zhou CL, Guo MX, Huang YT, Yu DQ, Sheng JZ and Huang HF. Diet-Induced Paternal Obesity Impairs Cognitive Function in Offspring by Mediating Epigenetic Modifications in Spermatozoa. *Obesity (Silver Spring)*, 2018; 26: 1749-1757